INTERFACIAL TENSION AND PHASE BEHAVIOR OF OIL/AQUEOUS SYSTEMS WITH APPLICATIONS TO ENHANCED OIL RECOVERY

by

Jaeyub Chung

A Dissertation

Submitted to the Faculty of Purdue University

In Partial Fulfillment of the Requirements for the degree of

Doctor of Philosophy

Charles D. Davidson School of Chemical Engineering

West Lafayette, Indiana

December 2020

THE PURDUE UNIVERSITY GRADUATE SCHOOL
STATEMENT OF COMMITTEE APPROVAL

Dr. Bryan W. Boudouris, Co-chair

Charles D. Davidson School of Chemical Engineering

Dr. Elias I. Franses, Co-chair

Charles D. Davidson School of Chemical Engineering

Dr. David S. Corti

Charles D. Davidson School of Chemical Engineering

Dr. Osman A. Basaran

Charles D. Davidson School of Chemical Engineering

Dr. Ganesan Narsimhan

Agricultural & Biological Engineering

Approved by:

Dr. John Morgan

To the love of my life, Seulgi

ACKNOWLEDGMENTS

I am sincerely grateful to my academic advisors, Professor Bryan W. Boudouris and Professor Elias I. Franses. With their professional and wholehearted guidance, I was able to develop critical skill sets to be an independent researcher. Especially, I am thankful for their patience during my confrontation against multifaceted challenges of Ph.D. programs including self-motivation, language barriers, and the endless stress of writing. Instead of providing full answers for me to overcome such challenges, they gave me an optimized amount of guidance so that I could get through by myself while I was pioneering my own ways to foster my educational growth. I would also like to express my gratitude to my thesis committee members, Professor David S. Corti, Professor Osman A. Basaran, and Professor Ganesan Narsimhan. Their sincere comments and advice have constantly tested my knowledge and have stimulated me to maintain the attitude of a learner.

I wish to thank all the members of Boudouris Group, Franses Group, and the Enhanced Oil Recovery Lab at Purdue University. From small talks to heated discussions, I have experienced and witnessed the power of collaboration and the synergy of interdisciplinary contributions. Some people would say that finishing a Ph.D. program is similar to running a marathon, because both challenges test one's perseverance and determination toward a goal. However, based on what I have experienced over the past five years, a Ph.D. program is not like running a marathon, but like writing a series of small chapters for an encyclopedia. Each chapter of an encyclopedia has individual value by itself, and the collection of those chapters generates a trend of a philosophy that nurtures the collective intelligence of human being; I felt that finishing a Ph.D. is similar to finishing such processes. While sharing intellectual joys and sorrows with all the colleagues, I felt grateful that I have been a Ph.D. student with all of them.

Moreover, I would like to express sincere gratitude to the Korean Chemical Engineer community members. Specifically, I would like to thank Professor You-Yeon Won (Purdue University), Dr. Kyusoon Shin (Seoul National University), Professor Young-Sun Kim (Dong-Ah University), Professor Jaehong Kim (Yale University), Professor Jong-Chan Lee (Seoul National University), Professor Ki Bong Lee (Korea University), Professor Hyun Wook Jung (Korea University), Professor Joona Bang (Korea University), Professor Hyunmin Yi (Tufts University), Professor Sung Ho Yeom (Gangneung-Wonju National University), Professor Jae-hyuk Kim

(Busan University), Professor Suk Ho Bang (Sungkyunkwan University), Professor Jong Suk Lee (Sogang University), and Professor Jung-Hyun Lee (Korea University) for providing myriad advice as Korean scientists who have become competent researcher in their fields.

Finishing my Ph.D. program would be impossible without my wife, Seulgi Choi. As my life partner, she provided unconditional support that could not be quantified by any characterization technique. No matter what our life will be after we leave West Lafayette, I will remember all the eureka moments after numerous heated late-night discussions, and I will cherish every single moment that lies ahead of us.

TABLE OF CONTENTS

LIST OF TABLES

LIST OF FIGURES

ABSTRACT

Chemical enhanced oil recovery (cEOR) aims to increase the oil recovery of mature oil fields, using aqueous solutions of surfactants and polymers, to mobilize trapped oil and maintain production. The interfacial tensions (IFTs) between the injected aqueous solution, the oil droplets in reservoirs, and other possible phases formed (e.g., a "middle phase" microemulsion) are important for designing and assessing a chemical formulation. Ultralow IFTs, less than 10^{-2} $mN \cdot m^{-1}$, are needed to increase the capillary number and help mobilize trapped oil droplets. Despite this fact, phase behavior tests have received more attention than IFTs for designing and evaluating surfactant formulations that result in high oil recovery efficiencies, because incorporating reliable IFTs into such evaluation process is avoided due to difficulties in obtaining reliable values. Hence, the main thrusts of this dissertation are to: (a) develop robust IFT measurement protocols for obtaining reliable IFTs regardless of the complexity of water and oil phase constituents and (b) improve the existing surfactant polymer formulation evaluation and screening processes by successfully incorporating the IFT as one of the critical parameters.

First, two robust tensiometry protocols using the known emerging bubble method (EBM) and the spinning bubble method (SBM) were demonstrated, for determining accurately equilibrium surface tensions (ESTs) and equilibrium IFTs (EIFTs). The protocols are used for measuring the dynamic surface tensions (DSTs), determining the steady state values, and establishing the stability of the steady state values by applying small surface area perturbations by monitoring the ST or IFT relaxation behavior. The perturbations were applied by abruptly expanding or compressing surface areas by changing the bubble sizes with an automated dispenser for the EBM, and by altering the rotation frequency of the spinning tube for the SBM. Such robust tension measurement protocols were applied for Triton X-100 aqueous solutions at a fixed concentration above its critical micelle concentration (CMC). The EST value of the model solution was 31.5 ± 0.1 $mN \cdot m^{-1}$ with the EBM and 30.8 ± 0.2 $mN \cdot m^{-1}$ with the SBM. These protocols provide robust criteria for establishing the EST values.

Second, the EIFTs of a commercial single chain anionic surfactant solution in a synthetic brine against a crude oil from an active reservoir were determined with the new protocol described earlier. The commercial surfactant used here has an oligopropoxy group between a hydrophobic chain and a sulfate head group. The synthetic brine has 9,700 ppm of total dissolved salts, which

are a mixture of sodium chloride (NaCl), potassium chloride (KCl), manganese (II) chloride tetrahydrate ($MnCl_2 \cdot 4H_2O$), magnesium (II) chloride hexahydrate ($MgCl_2 \cdot 6H_2O$), barium chloride dihydrate ($BaCl_2 \cdot 2H_2O$), sodium sulfate decahydrate ($Na_2SO_4 \cdot 10H_2O$), sodium bicarbonate ($NaHCO_3$), and calcium chloride dihydrate ($CaCl_2 \cdot 2H_2O$). The DSTs curves of the surfactant concentrations from 0.1 ppm to 10,000 ppm by weight had a simple adsorption/desorption equilibrium at air/water surface with surfactant diffusion from bulk aqueous phase. Such a mechanism was also observed from the tension relaxation behavior after area perturbations for the oil/water interfaces while DIFT measurements. The CMC of the commercial surfactant was determined to be 12 ppm in water and 1 ppm in the synthetic brine used. From the initial tension reduction curves from DST and DIFT measurements, the equilibrium timescales were shorter with brine than with water, because the adsorbed surfactant on the oil/water interfaces were partitioned into oil phases. For both DST and DIFT results suggest that the adsorbed surfactant layer at interfaces were typical adsorbed soluble monolayers.

Third, the phase and rheological behavior of a commercial anionic surfactant in water and in brine are important for large scale applications. A phase map of the surfactant at 25 ℃ at full range of surfactant concentration was obtained. The supramolecular structures of the various phases were characterized by dynamic light scattering (DLS), cryogenic transmission electron microscopy (cryo-TEM), conductimetry, densitometry, and x-ray scattering. The identified phases evolved as the surfactant concentration was increased; they were a micellar solution phase, a hexagonal liquid crystalline phase, and a lamellar liquid crystalline phase. In addition, the characterization results provided detailed information about supramolecular structure parameters such as micellar sizes and their aggregation numbers, and liquid crystal spacings. The phase and rheological behavior trends identified here were of great importance because the trend was similar to that of single chain monoisomeric surfactant. Thus, this study provides a potential universality of phase behavior trends of surfactant-water systems despite of the multicomponent nature of surfactants.

Fourth, the EIFTs of the pre-equilibrated mixtures of surfactant, brine, and oil were determined and compared to the EIFTs prior to pre-equilibration, in order to systematically identify the most relevant IFT for oil recovery. The EIFT between surfactant solutions and oil without any pre-equilibration prior to tension measurements is defined as the un-pre-equilibrated EIFT ($EIFT_{up}$). The EIFT between oil and water phases after the pre-equilibration of surfactant, brine, and oil is defined as pre-equilibrated EIFT ($EIFT_p$). The $EIFT_p$'s were generally higher than

$EIFT_{up}$'s. In addition, the effects of three mixing methods and the water-to-oil volume ratio (WOR) on the $EIFT_p$ were evaluated. Out of three mixing methods, (A) mild mixing, (B) magnetic stirring, and (C) shaking vigorously by hand, method C produced mixtures which are the closest to the equilibrium state. The mixtures produced by method C had the largest decrease of the surfactant concentration during pre-equilibration due to the surfactant partitioning into oil phases. Moreover, the WOR affects the $EIFT_p$ significantly due to the preferential partitioning of surfactant components into oil phases. More specifically, the WOR and the $EIFT_p$ were found to be inversely correlated, because the amount of partitioned surfactant increased as the oil volume fraction increased. The $EIFT_p$'s were different from the $EIFT_{up}$'s at the same total surfactant concentrations in the aqueous layer evidently because of preferential partitioning of the various surfactant components.

Finally, the effect of surfactant losses due to adsorption into the rock surface on the pre-equilibrated EIFT ($EIFT_p$) were evaluated to improve surfactant formulation protocols. Here, five types of EIFTs were identified, along with robust protocols for determining them. These are: (I) the un-pre-equilibrated equilibrium IFT ($EIFT_{up}$); (II) the un-pre-equilibrated EIFTs in the presence of rock ($EIFT_{up,rock}$); (III) the pre-equilibrated EIFTs ($EIFT_p$) in the presence of oil; (IV) the pre-equilibrated EIFT in the presence of rock and oil ($EIFT_{p,rock}$); and (V) the effluent EIFT ($EIFT_{eff}$). The $EIFT_{up}$ is the EIFT of the aqueous surfactant/brine solution against an oil drop without any pre-equilibration. The $EIFT_{up,rock}$ is the EIFT between an oil drop and the surfactant solution after pre-equilibration with a rock sample to account for adsorption losses. The $EIFT_p$ is the EIFT between the pre-equilibrated water and the oil phases from surfactant/brine/oil mixtures. The $EIFT_{p,rock}$ is the EIFT between the pre-equilibrated water and the oil phases from surfactant/brine/oil/rock mixtures. The $EIFT_{eff}$ is the EIFT from an effluent sample mixture of a laboratory-scale core flood test. Among the five types of EIFTs, the $EIFT_{p,rock}$ was found to be the most important for the highest oil recovery performance in core flood tests, because it captures the most important surfactant partition processes, the partitioning to the oil phase and the partitioning by adsorption on the rock surface. Among three surfactant formulations tested with core flood experiments, the one with the lowest $EIFT_{p,rock}$ (~0.01 $mN \cdot m^{-1}$) had the highest oil recovery ratio (78%), and the one with the highest $EIFT_{p,rock}$ (~0.2 $mN \cdot m^{-1}$) had the lowest oil recovery ratio (55%). The other EIFTs correlated less with the oil recovery performance. Identifying surfactant formulations that have low or ultralow EIFTs, especially ultralow $EIFT_{p,rock}$'s, are critical for

screening formulations appropriate for core flood tests and target field applications, and for predicting oil recovery performance. These works are a significant contribution for improving (a) the surfactant formulation evaluation protocols, and (b) the utilization of reliable IFTs and phase behavior test protocols for oil recovery and many other surfactant and colloid sciences applications.

1. INTRODUCTION

1.1 Motivation

The initial stage of oil production from a reservoir, or primary recovery, is accomplished by spontaneous flow of oil along with some gas. The oil flow is driven by a naturally occurring high pressure in the reservoir. When the pressure-driven flow stops, additional oil can be recovered by injecting fluids, usually salt-containing aqueous solutions such as ground water or sea water. This process is termed secondary recovery. In most cases, significant amounts of crude oil are left unrecovered, even after extensive use of secondary recovery processes. Tertiary or enhanced oil recovery (EOR) processes were developed for applications in which the secondary processes had become inefficient or were inapplicable after the primary recovery processes.[1,2]

EOR processes can be classified into four categories. These are: (1) miscible flooding processes, in which a solvent that is fully miscible with the crude oil is used; (2) chemical flooding processes in which the oil remains in a separate phase throughout the process; (3) thermal flooding processes for reducing the oil viscosity and improving its flowability; and (4) microbial flooding processes, aimed at solubilizing some oil, and possibly mobilizing some oil drops after producing some surfactant with microbial processes. The focus of this research is chemical flooding, also known as a chemical EOR process, in which surfactants and often polymers are added to the aqueous brine solution. The surfactants are used to lower the interfacial tension (IFT) between the trapped crude oil drops and the injected fluid, to allow some oil drops to be displaced. The polymers are used to increase the aqueous solution viscosity above the oil viscosity, thus preventing a process called "viscous fingering", where the aqueous solution flows pass the oil.

In order to facilitate the mobilization of oil drops trapped in the porous reservoir rocks, it is critical to have low (< 1 mN·m^{-1}) or ultralow ($< 10^{-2}$ mN·m^{-1}) IFT values between the crude oil and the surfactant aqueous solution.[3–8] In order for the oil to be mobilized, the viscous forces of the flowing water stream need to overcome the IFT-based capillary forces, which often tend to keep the crude oil drops from being mobilized.. The capillary number value is a good measure to predict such oil mobilization. [5,9–14] It is defined as $N_c = \mu U/\gamma$, where the U is the characteristic velocity of the displacing liquid, μ is its viscosity (if it is Newtonian), and γ is the oil/aqueous IFT. Because of practical economic considerations in chemical EOR processes involving the use of

surfactants, it is important to achieve low IFTs at low surfactant concentrations (i.e., at < 1 wt%). Moreover, the surfactant formulation under consideration needs to be tailored to be effective at the salt concentrations ("salinity"), temperature, oil type, and other reservoir-specific conditions.[5,15–18]

A widely used screening method for selecting surfactants and their concentrations involves the phase behavior of mixtures of brine surfactant solutions and crude oil. Another method, sometimes used along with the first method, involves IFT measurements.[17,19–25] The IFT values are often measured either when there are two equilibrium phases, an oil and an aqueous phase, or when the system at equilibrium splits into three phases. The third, or "middle" phase may be a so-called "middle-phase microemulsion phase;" It contains most of the surfactant and has high oil and water mass fractions.[26,27] The other two phases are a "residual "aqueous brine phase and a "residual" oil phase, both of which contain some surfactant. Then, three IFT values exist, oil/water (O/W), oil/microemulsion (O/ME), and water/microemulsion (W/ME). The latter two IFT values are measured and reported in most reports, O/ME and ME/W. At certain salinities, temperatures, and surfactant concentrations, these IFT values are often ultralow and, for a specific salinity, called "optimal salinity", equal to each other.[18,28,29] In addition, at the conditions of three phases and ultralow IFTs, the solubilization ratios, in grams of oil or water per gram of surfactant, are high and, at the optimal salinity, equal to each other. The above results help define either the "pre-equilibrated" IFT value in two-phase systems or a pair of "pre-equilibrated" IFT values in three phase systems. Such experiments are usually done for water to oil volume ratio (WOR) of one. [5,15–18] Currently, selecting a surfactant in practice for favorable EOR performance is mostly empirical, and is often primarily based on a combination of phase behavior observations and actual or estimated IFT values based on measured solubilization data and empirical or semi-empirical correlations.[7,11,17,18,23,28,30–32] No firm guidelines on the relationships between the surfactant molecular structures and the IFT values have been reported in the open literature, except for some systems where pure hydrocarbons were studied as model oils.[33] Thus, a critical need exists for developing methods for screening surfactants properly by using reliable equilibrium interfacial tension (EIFT) values, and also, dynamic (time-dependent) IFTs (DIFTs).

Sometimes, in surfactant screening processes the "un-pre-equilibrated" IFT is measured between an aqueous surfactant solution and a small oil drop which has not been pre-mixed or pre-equilibrated with the aqueous solution. [21] Then the WOR ranging from 100 to 300, depending on

the volume of the drop used. These "un-pre-equilibrated" EIFT values are expected to be relevant at the initial stages of chemical flooding processes. The processes of the oil partitioning to the aqueous phase are anticipated to be slow due to low molecular solubilities and low mass transfer rates of the oil components in water and water and its components in the oil phase. Thus, long-term observations of phases and dispersions, centrifugation of oil and aqueous surfactant solution mixtures, and analysis of the surfactant concentrations in the aqueous phase after pre-mixing are also necessary to probe the phase behavior and surfactant partitioning and determine the approach to a possible equilibrium phase behavior.

IFT values between the aqueous phase and the oil phase after pre-mixing processes can be quite different from "un-pre-equilibrated" EIFT values because of the partitioning of chemicals between the aqueous and oil phase. The pre-mixed IFT value is defined as that between a layer of an aqueous surfactant solution and a layer of an oil after vigorous pre-mixing processes, designed to ensure or promote phase equilibration of all components. Combination of phase behavior studies of oil-water mixtures and the corresponding pre-mixed EIFT values should have a significant impact for understanding the fundamental physics of the later stages of the chemical flooding processes. The primary goal of this dissertation is to find the relative importance of un-pre-equilibrated and pre-mixed EIFT values and of the effects of key parameters (e.g., the water-to-oil ratio, the surfactant concentration, polymer concentration, and the salinity). Such studies shed light on establishing the physical chemistry of "un-pre-equilibrated" and "pre-mixed" systems and establishing more rigorous criteria for evaluating surfactant/polymer formulations for the EOR applications.

1.2 Thesis Overview

The main focuses of the dissertation is (a) to focus on a couple of parameters that have received little attention, such as equilibrium interfacial tension values between a crude oil sample and a commercial multicomponent surfactant solution; (b) to improve surfactant evaluation process; and (c) to advance the surfactant design paradigm for EOR applications. As emphasized in Section 1.1, the importance of how the capillary number represents the efficiency of the oil mobilization process, as is widely and intuitively accepted. There is a significant knowledge gap, on the several types of EIFT, and on the choice of the most relevant to oil mobilization and recovery. In this dissertation, a robust protocol for determining accurate and reliable tension values

was developed and is described in Chapter 3. This effort was published in 2019 in the *Journal of Visualized Experiments*.[34]

The first study of characterizing mixtures of a commercial surfactant, synthetic brine, and crude oil, for un-pre-equilibrated states was described in Chapter 4. A new concept of equilibrium interfacial tension was introduced, that of the "un-pre-equilibrated, but equilibrium, interfacial tension ($EIFT_{up}$). This is the equilibrium interfacial tension of a water/oil interface where the surfactant components have reached a local equilibrium across the interface, due to their substantial solubilities and fast transport, but the water and oil components have not yet done so, due to their much slower transport. The $EIFT_{up}$ was used for determining critical micelle concentration (CMC) and surface density (Γ) for a commercial multicomponent surfactant and for establishing that there is only monolayer adsorption behavior of the surfactant components on the O/W interface. This work was published in 2018 at *Colloids and Surfaces A: Physicochemical and Engineering Aspects*.[35]

In Chapter 5, the phase behavior of an aqueous commercial anionic extended surfactant solutions is described in detail. It was established that some extended anionic commercial surfactant mixture follows a similar phase behavior trend upon concentration increase compared to typical non-extended single-chain monoisomeric surfactants. Several liquid and liquid crystalline phases were characterized by various techniques, including small angle X-ray scattering (SAXS), polarizing microscopy (POM), and electrical conductimetry. This work, in collaboration with several colleagues, was published in 2019 at *Colloids and Surfaces A: Physicochemical and Engineering Aspects*.[36]

In Chapter 6, the significance of the mixing methods and robust interfacial tension protocols for surfactant formulation evaluation process is demonstrated by comparing the IFT and phase behavior of un-pre-equilibrated and pre-equilibrated mixtures of a surfactant, brine, and a crude oil. Here, the pre-equilibrated equilibrium interfacial tensions ($EIFT_p$) are defined to represent the interfacial tension values of water/oil interfaces after all the surfactant, water, and oil components have equilibrated across the phases This work was published in 2019 at *Colloids and Surfaces A: Physicochemical and Engineering Aspects*.[37]

In Chapter 7, yet another equilibrium interfacial tension is introduced, the effluent EIFT ($EIFT_{eff}$). In combination with the $EIFT_{up}$ and $EIFT_p$, it is used to develop an even more comprehensive surfactant evaluation protocol. Both laboratory-scale phase behavior tests of

surfactant, brine, and oil mixtures and core flood tests with a model sandstone core material are used to establish and evaluate a robust protocol for identifying promising surfactant formulations at specific oil and rock reservoir conditions.

In Chapter 8, preliminary results and recommendations for future research are presented. The EIFT determination protocol for the three phase systems generated by mixing surfactant, brine, and oil is suggested. Preliminary results for identifying critical micelle concentration or critical aggregation concentration of didodecyldimethylammonium bromide (DDAB) using emerging bubble method (EBM) along with area perturbation tests are presented.

2. LITERATURE REVIEW

2.1 Enhanced Oil Recovery (EOR) Fundamentals

To substantially lower the IFT values of injecting solutions against remaining crude oil, it is necessary to add surfactant.[3–8] Also, minor IFT changes can occur by adding electrolytes that may interact with certain amphiphilic oil components. The choice of surfactant can be determined not only from IFT values against crude oil, but also from other parameters such as the rate of tension lowering, the extent of adsorption on the reservoir rock, and the degree of partitioning to the oil phase. Three types of surfactant molecular structures are available: cationic, anionic, and nonionic. Cationic surfactants are sometimes avoided because of relatively higher fractions of adsorption losses to the negatively charged reservoir rock surfaces. Anionic surfactants are favored over cationic and nonionic surfactants because they are expected to have lower adsorption losses. Various types of anionic surfactants with different types of hydrophobic chains have been tested, internal olefin sulfonates, alkyl aryl sulfonates, ethoxylated sulfates, propoxylated sulfates, and many others.[24,31,38–40] The apparent logic in the development of such surfactant formulations was driven to yield high oil recoveries by generating low IFT values against crude oil and high solubilities in the specific brines. Such characteristics were targeted for improving oil mobilization and for avoiding precipitation in solution and removal by filtration during flow in porous rocks. Nonetheless, systematic approaches of establishing correlations between the surfactant structure and the overall performance of the surfactant are limited. Here, we have chosen to use a commercial anionic surfactant from Stepan Company based on the preliminary data from a company hired by the project sponsor.

In many cases, low or ultralow IFT values for both un-pre-equilibrated systems and pre-mixed systems may not be sufficient for a successful EOR process. The viscosity of the injected fluids must also be considered to suppress bypassing of the oil by the injected fluids, which is sometimes called “viscous fingering”. One of the ways to avoid or to suppress this undesired phenomenon is to have a displacing fluid with a viscosity larger than that of the oil which can be achieved by the addition of polymers.[15,41–43] If a continuous oil mass, or “oil bank”, is formed by the displacing liquid, it is followed by a surfactant/polymer solution and then by a polymer solution. The viscosity of the surfactant/polymer solution should be larger than that of the oil in the oil bank,

and smaller than that of the polymer solution that follows, in order to minimize viscous fingering phenomena between the aqueous surfactant/polymer solution and the polymer solution. The polymer type and concentration should be chosen carefully, not only to control the viscosity but also to minimize potential adverse effects on the surfactant phase behavior and the IFT. Ultralow IFT values between injected fluids against crude oil in the reservoir are necessary, but probably not sufficient for improving the EOR recovery process efficiency. The phase behavior of the surfactant/polymer solutions with crude oil should also be considered, as explained above. The number of phases remaining after vigorous mixing of surfactant/polymer solutions and crude oil is important. Mixing is essential to promote equilibration, which often cannot be totally assured, unless various tests are done. If three phases, including a ME phase, form upon rigorous phase equilibration in laboratory tests, at specific oil/water volume ratios, then such phase may also form when the aqueous solution contacts the oil phase in the porous media during EOR processes.[44] This behavior is not easy to define or predict, because the effective oil/water ratio in a flow test is not fixed or well defined due to the continually changing throughout the EOR process and nonhomogeneous conditions across the reservoir. In case that a ME phase forms, the viscosity of the third phase and the two additional IFT values must be considered in the interpretation of the oil recovery results.

2.2 Interfacial Tension Fundamentals

IFT values of surfactant/polymer solutions against crude oil are quite important for evaluating surfactant/polymer formulations for possible EOR applications. They should be determined with high accuracy and reliability. Generally, IFT values are measured with a force method or based on a shape of a drop or a bubble. Use of force-based methods, such as the Du-Noüy ring or the Wilhelmy plate, involves the use of a solid material, and hence requires knowledge of certain solid/liquid/liquid contact angle values, which are difficult to determine reliably and may introduce large errors. Several methods based on the shapes of drop or bubble interfaces, such as the emerging drop method or the spinning drop method, are quite reliable and can also be used to determine dynamic interfacial tension (DIFT) and then EIFT values. The latter method can be used for very low IFTs, less than 0.1 $mN \cdot m^{-1}$.

The emerging bubble/drop method is based on having hydrostatic equilibrium between the surface/interfacial tension forces and the gravity forces.[45–48] Then the bubble/drop shape is

determined from the solution of the Young-Laplace equation and the density difference of the two fluid phases in contact.[49,50] In the spinning bubble/drop method, there is gyrostatic equilibrium, which is a balance between surface or interfacial tension forces and centripetal forces.[47,51–53] At large spinning speeds, gravitational forces are negligible compared to the centripetal forces. When gyrostatic equilibrium is achieved, the corresponding tension values are determined based on the drop shapes, by using either the solution of the Young-Laplace equation for the drop shape[49,50] or the simpler Vonnegut equation[54].

2.3 Mechanisms of Surface Tension and Interfacial Tension Equilibration

After an air/liquid surface is created, surfactant diffuses, by stagnant diffusion or convective diffusion, towards the surface, where adsorption/desorption, and a net rate of adsorption occur. Thus, the surface tension (ST) depends on time, and is called dynamic (time-dependent) surface tension (DST). For oil/water interfaces, the interfacial tension (IFT) is dynamic also, because the surfactant adsorbs at the oil/water interface and may desorb toward the oil phase and then diffuse into it. Thus, the mechanism of the DIFT is more complex than the mechanism of DST. If there is no solubilization of the oil into the aqueous phase, or of water and its other components into the oil phase, there is no other relevant phenomenon that may affect the DIFT.[35] This condition may occur when the surfactant concentration in each liquid phase is below its respective CMC. If the surfactant is above its CMC, either in the aqueous or in the oil phase, then there will be some micellar solubilization, or enhanced equilibrium dissolution of the water in the oil phase, or oil in the water phase, or both. The enhancement is due to the presence of the surfactant micelles and the additional water (brine) or oil contained within the micelles. This process will complicate the tension equilibration mechanism, and possibly delay the equilibration. Hence, the first stage of the DIFT occurs when the aqueous solution phase contacts an oil drop for the first time. This DIFT may reach a steady-state value (SIFT), or even an equilibrium value, called the "un-pre-equilibrated-phases equilibrium IFT" ($EIFT_{up}$), which can be defined before any effects of solubilization may become important. This may occur when the timescale of the solubilization and of the IFT equilibration at the second stage upon solubilization are much larger than the that of the first stage of the IFT equilibration.[35] As solubilization proceeds, the compositions and microstructures of the oil and water phases start changing. Then the IFT may change again, from a local equilibrium state to a global equilibrium state. After the solubilization of each species in

each phase has reached an equilibrium state, the surfactant chemical potentials at each phase have changed significantly from those at the local equilibrium state. Therefore, a different EIFT, or pre-equilibrated EIFT ($EIFT_p$), is defined, and may be quite different from the $EIFT_{up}$. The EIFT value of the second stage can also be determined with a different procedure. After the oil and aqueous phases at a given volume ratio have been thoroughly mixed, and probably completely pre-equilibrated with each other, the EIFT is measured for a drop of the pre-equilibrated oil phase brought into contact with the pre-equilibrated aqueous phase.[28,55–57] The timescale for the second-stage equilibration with this procedure is expected to be shorter than that for the first-stage equilibration, because surfactant diffusion over only a short length scale is needed. Few such DIFT data for pre-equilibrated phases have been found in the literature, and have been determined in this thesis. Moreover, because the WOR is usually of the order of 1 for the procedure with the pre-equilibrated phases, and of the order of 300 for the procedure with the un-pre-equilibrated phases with an oil drop, the $EIFT_p$ values for the two cases could be quite different from each other. Such $EIFT_p$ values may be quite different from $EIFT_{up}$. Hence, several types of EIFT values, obtained in the laboratory-scale, should be collectively evaluated to characterize the interfacial tension equilibration mechanisms for the highly multicomponent mixture systems.

3. ACCURATE DETERMINATION OF EQUILBRIUM SURFACE TENSION VALUES WITH AREA PERTURBATION TESTS

3.1 Overview

In this chapter, we demonstrate two robust protocols for determining the equilibrium surface tension (EST) values with area perturbation tests. The EST values should be indirectly determined from the dynamic surface tension (DST) values when surface tension (ST) values are at steady-state and stable against perturbations. The emerging bubble method (EBM) and the spinning bubble method (SBM) were chosen, because, with these methods, it is simple to introduce area perturbations while continuing dynamic tension measurements. Abrupt expansion or compression of an air bubble was used as a source of area perturbation for the EBM. For the SBM, changes in the rotation frequency of the sample solution were used to produce area perturbations. A Triton X-100 aqueous solution of a fixed concentration above its critical micelle concentration (CMC) was used as a model surfactant solution. The determined EST value of the model air/water interface from the EBM was 31.5 ± 0.1 $mN \cdot m^{-1}$ and that from the SBM was 30.8 ± 0.2 $mN \cdot m^{-1}$. The two protocols described in this chapter provide robust criteria for establishing the EST values.

3.2 Introduction

The determination of the equilibrium surface tension (EST), or the equilibrium interfacial tension (EIFT), of a given air/water or oil/water interface is a critical step for applications in a wide range of industrial areas such as detergency, enhanced oil recovery, consumer products, and pharmaceutics.[47,58–60] Such tension values should be determined indirectly from the dynamic surface tension (DST) or the dynamic interfacial tension (DIFT), because only dynamic tension values are directly measurable. Dynamic surface tension values (i.e., measuring tension values as a function of time) are determined at regular time intervals. Equilibrium tension values are deemed to be determined when the DST values are at steady state. True equilibrium surface tension values are better established when they are stable against perturbations.[35] Several observations of the tension relaxation after surface area compression have been previously reported by Miller and Lunkenheimer, who used two classical tensiometry methods, the Du Noüy ring and the Wilhelmy plate methods.[61–63] Those methods are less accurate than the ones used in this study, and those

DSTs were measured every few minutes. Numerous techniques have been developed for measuring the surface tension (ST) or interfacial tension (IFT) values of interfaces, but there are only a handful of techniques that can be used to measure DST or DIFT values and allow one to apply perturbations to test the stability of the acquired steady-state tension values.[64] If the aqueous solution contains surfactant mixtures, and when one of the components adsorbs much faster than the others, then there may be a temporary plateau in the DST curves[65]. Then the presented methods may not work well in the short timescales as for one component surfactants, but they still may work if the procedures are extended slightly to cover longer timescales.

The protocols described here show representative data only for surface tension values of an air/aqueous solution. However, these protocols also apply for the IFT of an aqueous solution against a second liquid, such as an oil, which is immiscible with the aqueous solution and has a smaller density than that of the aqueous solution. Here, we present two robust methods that satisfy these criteria, the emerging bubble method (EBM) and the spinning bubble method (SBM). In both methods, one determines ST values that are based on bubble shapes and do not require contact angle information, which can introduce significant uncertainties and errors to the measurements. For the EBM, area perturbations are introduced by abruptly changing the volume of the bubble emerging from a syringe needle tip. For the SBM, changes in the rotation frequency of the samples are used for area perturbations. The detailed protocols are aimed to guide researchers in the field, such that they can avoid common mistakes or errors in dynamic and equilibrium tensiometry and help prevent inaccurate interpretations of the acquired data.

3.3 Surface and Interfacial Tensiometry

Two types of tensiometry techniques were used for measuring surface and interfacial tension values: the emerging bubble/drop method (EBM/EDM) and the spinning bubble/drop method (SBM/SDM). For the EBM or EDM, a Ramé-Hart Model 790 instrument was used. Prior to the measurements, a 4.00 mm steel ball was used as a standard for the scale of the camera image. For measuring surface tension values with the EBM, a liquid was placed in a quartz cell. An inverted stainless-steel syringe (usually with an inner diameter of 0.84 mm) was inserted into the liquid. Several air bubbles (with a total air volume of about 1 mL) were first purged through the syringe, in order to remove impurities possibly present on the tip of the syringe. This procedure was used to improve the surface chemical purity of the air/liquid interfaces. Then, an air bubble with $V_1 = 5$

μL was injected into the syringe tip. The axisymmetric drop shape analysis method, with the numerical solution of the Laplace-Young (LY) equation, was used to calculate the surface or interfacial tension and the interfacial area as a function of time.[49,66] It was assumed that the LY equation was also valid while the ST or IFT was changing with time. The assumption was confirmed at each measurement, because the optimal bubble or drop boundary profiles calculated from the LY equation fit well the observed profiles. The surface tension (ST) was calculated from the bubble shape once per second (or less frequently).[66] The same algorithm was used for calculating the surface area of the bubble or drop as a function of time. The "dead time", where no measurements could be obtained as the bubble volume and area expanded from the syringe tip, was about 1 s. The surface tension was measured as a function of time.

For the SBM or SDM, a DataPhysics SVT 20 instrument was used. Prior to the measurements, the SVTS 20 software was used to calibrate the scale of the image by recording the location of a bubble boundary before and after the camera was moved by a pre-determined distance. In order to measure dynamic surface tension with SBM, for instance, a glass tube filled with a liquid sample was first spun at a low rate of 500 rpm to prevent the injected bubble or drop from migrating upward and attaching to the tube wall. Then an air bubble or oil drop of about V_1 = 2.0 μL, or less for the low IFTs, was introduced into the spinning tube by having a syringe pierce through a septum sealing the spinning tube. The rotation frequency was then increased to v_1 such that the bubble or drop was deformed to reach an L/R ratio of over 8. It took about 3 minutes of "dead time" to reach an acceptable gyrostatic equilibrium (i.e., when there was no bubble or drop motion). Such a long dead time may limit the estimation of t_{95} values smaller than 10 minutes. The tension value was determined from the density difference $\rho_1 - \rho_2$, where ρ_1 and ρ_2 are the densities of the dense phase and the light phase, the rotation frequency (v), and the maximum radius R and the length L of the drop. Generally,

$$\gamma = \frac{(\rho_1 - \rho_2)\omega^2 R^3}{4} f\left(\frac{L}{R}\right) \tag{1}$$

where ω is a circular frequency ($\omega = 2\pi v$) and f(L/R) is a correction factor, which can be calculated rigorously from the solution of the Laplace-Young equation,[67] and is smaller than 1.004 for L/R greater than 8. Then, for L/R greater than 8, the following approximate equation is used.

$$\gamma \cong \frac{(\rho_1 - \rho_2)\omega^2 R^3}{4} \tag{2}$$

For L/R less than 8, one may also use the approximate Vonnegut equation.[54]

$$\gamma = \frac{(\rho_1 - \rho_2)\omega^2 R^3}{4}\left(1 + \frac{2R}{3L}\right) \tag{3}$$

The actual bubble or drop radius (R) is smaller than the radius obtained from the captured image due to light refraction in the cylindrical glass wall. It has been shown that at least for the maximum R at the center, [68]

$$R = R_{actual} \cong \frac{R_{observed}}{n_1} \tag{4}$$

where n_1 is the refractive index of the dense liquid, here being water or brine with n = 1.33.

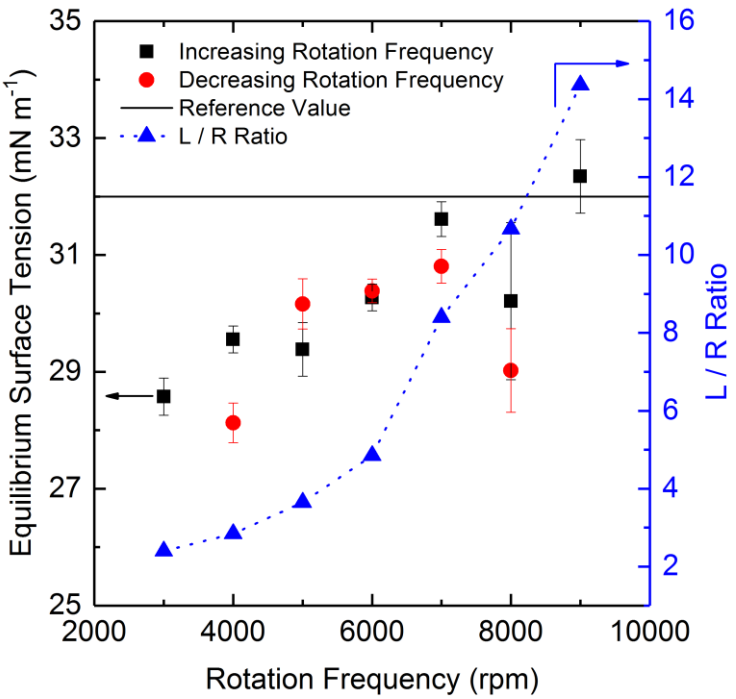

Figure 1. Dependence of the equilibrium surface tension of Triton™ X-100 aqueous solutions measured with the spinning bubble method. The reference value (—) was determined from the emerging bubble method.

Additionally, using the instrument software for L/R values less than 8 may introduce a significant systematic error. For instance, the EST values of Triton ^{TM} X-100 (TX100) aqueous solutions were measured for bubbles with various length-to-radius (L/R) ratios (Figure 1). When the L/R ratio was lower than 8, the available software was used to fit the LY equation to the bubble shape, after the refractive index correction for R. The correction factor for the radius at other locations on the bubble surface was assumed to be the same. To test the impact of this assumption on the determination of the tension values (γ) with the SBM or SDM for L/R less than 8, a standard solution of 3.4 mM TX100 with γ(EST) = 32 mN·m^{-1} was used. The EST was determined for a range of rotation frequencies (v), from 3,000 to 9,000 rpm, for either increasing or decreasing rotation frequencies. The measurements were repeated several times to test for their reproducibility, and the average and standard deviation values are given in Figure 1. The bubble volume was chosen to be large (~10 µL), to allow for large L/R ratios and large bubble deformations. The as-determined EST values were off by ~20% for L/R ≈ 2, and close to 32 mN·m^{-1} (by 5% off or better) for L/R greater than 8. Hence, it was decided, when possible, to avoid measurements of ST or IFT for the available instrument for L/R less than 8. To avoid this uncertainty and potential errors of as much as 20%, we have aimed at using large rotation frequencies such that the L/R ratios were larger than 8.

3.4 Area Perturbation Tests During Dynamic Tensiometry

Low and ultralow IFTs between a surfactant solution and a crude oil for EOR applications are generally measured with the spinning drop method (SDM). This is because the current emerging-drop-based or pendant-drop-based instruments are incapable of measuring IFTs below about 1 mN·m^{-1}. In order to establish whether a measured SST or SIFT is equal to the equilibrium value, one needs to test that the SST or the SIFT is stable and independent of area perturbations. As shown schematically in Figure 2, the stability of the first steady-state surface tension value (SST_1) is evaluated by monitoring the tension relaxation behavior upon abrupt changes of the surface area. The steady-state surface tension (SST) was defined as the plateau value beyond which the surface tension changes less than 1 mN·m^{-1} (or by less than 10%) in several (10 to 100) consecutive dynamic surface tension measurements. The equilibration timescales (t_{95}, t_1, or t_2) are defined as the time required for the DST value to change by 95% of the total change from the initial value to the steady-state value. When the t_{95} was large, larger time intervals between

measurements were used. If the subsequent steady-state tension values (SST_2 and SST_3) after each area perturbation are close to the original steady-state value (SST_1), the SST_1 is stable against area perturbations and the average of the three steady-state tension value is defined as the equilibrium surface tension (EST).

The source of area perturbations can be diverse and depends on the equipment setup and tensiometry techniques. In this work, two types of tensiometry were used, emerging bubble/drop method (EBM/EDM) and spinning bubble/drop method (SBM/SDM). For the emerging bubble method (EBM) and the emerging drop method (EDM), the interfacial area can be changed by abruptly varying the bubble or drop volume. Usually, the volume change by an automated syringe dispenser is a reliable way to apply abrupt and precise volume changes. For the spinning bubble method (SBM) or the spinning drop method (SDM), the area is changed, while maintaining the bubble or drop volume, by varying the rotation frequency (v) where the circular frequency (ω) is given by: $\omega = 2\pi v$. In this chapter, we present procedures for obtaining reliable SIFT and EIFT values from DIFT data for oil/aqueous solution systems with the EDM and, where possible, with the SDM.

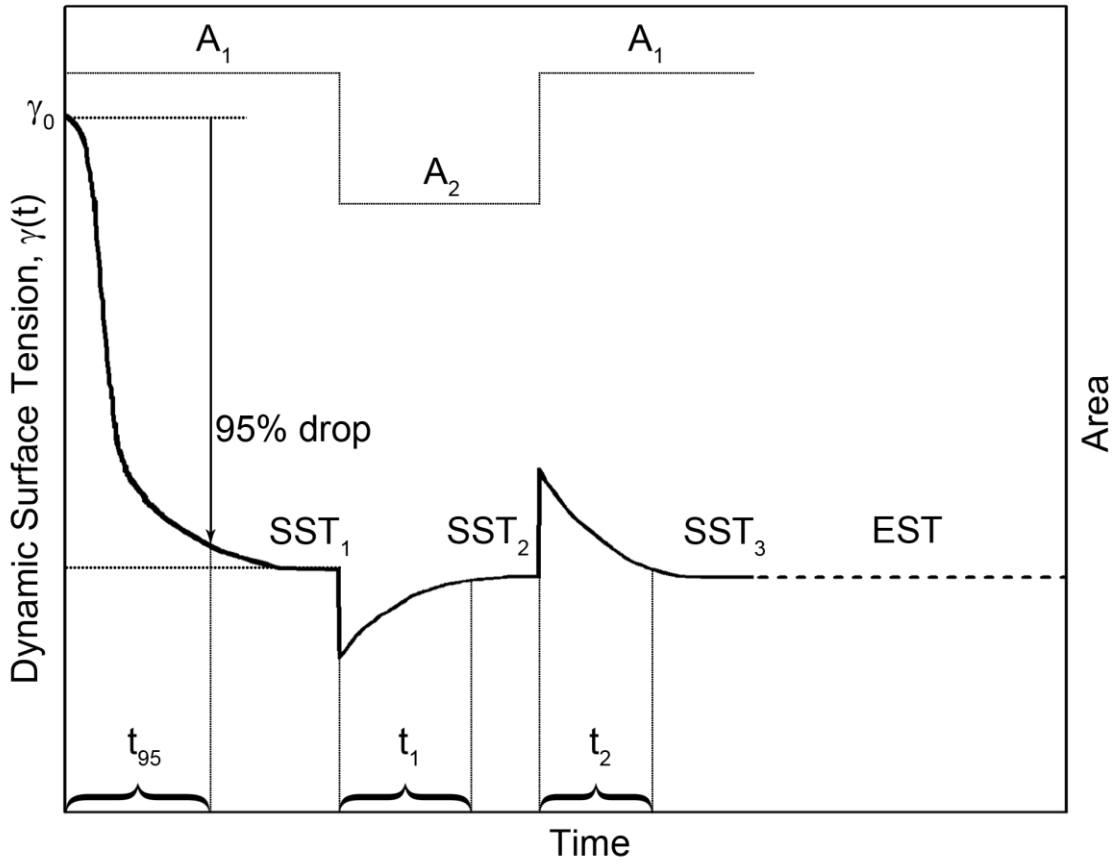

Figure 2. Schematic diagram of dynamic surface tension (DST), steady-state surface tensions (SST_1, SST_2, and SST_3), and equilibrium surface tension (EST). A_1 and A_2 are the surface areas of two differently-sized bubbles. The 95% timescale of equilibration from γ_0 is shown as t_{95}. The 95% timescales after each area perturbation are t_1 and t_2. The same patterns may be observed for the interfacial tensions with steady-state IFTs ($SIFT_1$, $SIFT_2$, $SIFT_3$) and the equilibrium IFT (EIFT). This is adapted from Chung, J., Boudouris, B. W., Franses, E. I. Accurate Determination of the Equilibrium Surface Tension Values with Area Perturbation Tests. *J. Vis. Exp.* (150), e59818, doi:10.3791/59818 (2019).

3.5 Results and Discussion

The equilibrium surface tension value of an aqueous commercial surfactant solution, Triton^{TM} X-100, was determined with the EBM and the SBM. The surfactant concentration was 5 mM, which was significantly higher than the CMC, 0.23 mM in water.[69] The SST_1, 31.5 ± 0.1 $mN \cdot m^{-1}$, was obtained approximately 20 s after the bubble was formed (Figure 3). After about 25 s, the surface area was compressed from A_1 = 11.4 mm^2 to A_2 = 9.0 mm^2 by reducing the bubble volume from V_1 = 3.8 μL to V_2 = 2.8 μL. The DST first dropped to 31 $mN \cdot m^{-1}$, and within 1 s, it increased to the SST_2 of 31.5 ± 0.1 $mN \cdot m^{-1}$. After about 50 s, the surface area was expanded

abruptly from A_2 = 9.0 mm^2 to A_3 = 11.4 mm^2 by increasing the bubble volume from 2.8 µL (V_2) to 3.8 µL (V_3). The DST value changed little and hence, the SST_3 was determined to be 31.5 ± 0.1 mN·m^{-1}. The three SST values were about the same. Therefore, the EST was determined to be 31.5 ± 0.1 mN·m^{-1}.

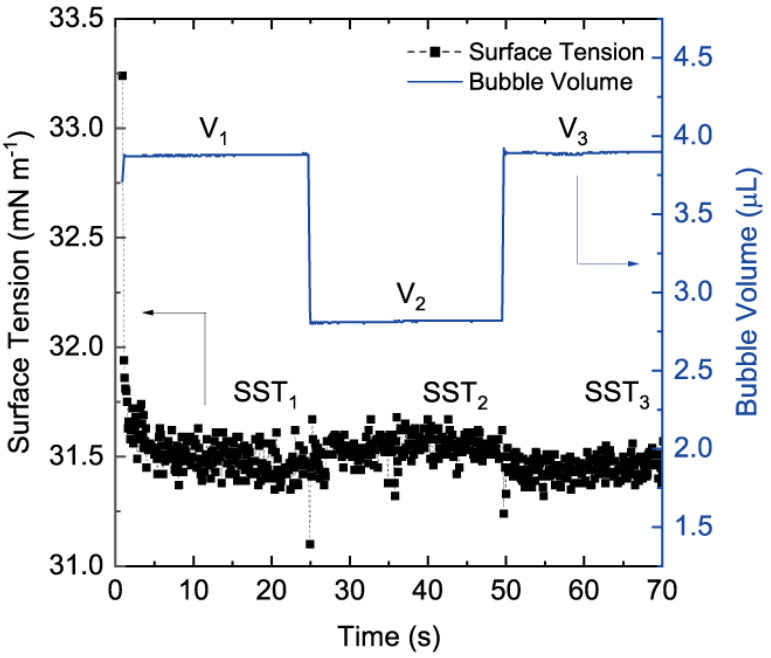

Figure 3. Dynamic Surface Tension (DST) of the model surfactant in DI water (5 mM) against air with the emerging bubble method (EBM). V1 is the initial bubble volume, and V2 and V3 are the bubble volumes after the first and the second volume, and area, perturbations, respectively. Prior to each perturbation, the dynamic surface tension (DST) values reached a plateau value, which is defined as the steady-state surface tension (SST). This is adapted from Chung, J., Boudouris, B. W., Franses, E. I. Accurate Determination of the Equilibrium Surface Tension Values with Area Perturbation Tests. *J. Vis. Exp.* (150), e59818, doi:10.3791/59818 (2019).

The EST of the same surfactant solution was determined with the SBM. At 9,000 rpm, the SST_1, 30.9 ± 0.1 mN·m^{-1}, of the same Triton^{TM} X-100 solution as that described above was reached about 500 s after the bubble was injected (Figure 4). Then the surface area was reduced by abruptly changing the rotation frequency from v_1 = 9,000 rpm to v_2 = 8,500 rpm. Then, the DST was decreased to 27.5 mN·m^{-1}, and then within 1 s rose to 30.6 mN·m^{-1}. Hence, the SST_2 was 30.6 ± 0.1 mN·m^{-1}. After ~630 s, the surface area was expanded by increasing the rotation frequency from v_2 = 8,500 rpm to v_3 = 9,000 rpm. The DST jumped to ~34 mN·m^{-1}, and then it decreased rapidly to a steady-state value of 30.8 ± 0.1 mN·m^{-1}, the SST_3. Hence, the EST was determined as 30.8 ±

0.2 mN·m^{-1}. The 2.2% difference in EST values from the two methods is probably due to certain systematic error.

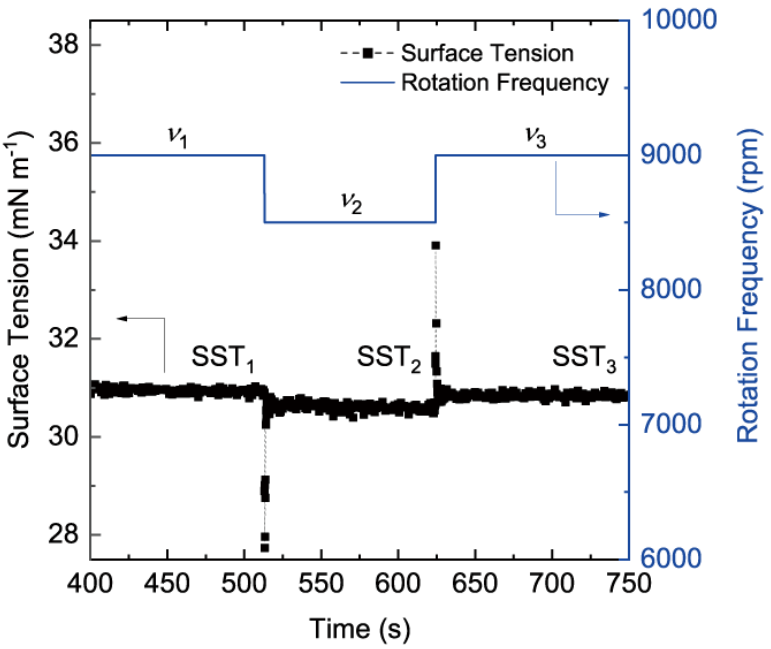

Figure 4. Dynamic Surface Tension (DST) of the model surfactant in DI water (5 mM) against air evaluated with the spinning bubble method (SBM). In this figure, ν1 is the rotation frequency prior to area perturbations, and ν2 and ν3 are the rotation frequencies after the first and the second frequency, and area, perturbations, respectively. Similar to the EBM method, prior to each perturbation, the dynamic surface tension (DST) values reached a plateau value, which is defined as the steady-state surface tension (SST). This is adapted from Chung, J., Boudouris, B. W., Franses, E. I. Accurate Determination of the Equilibrium Surface Tension Values with Area Perturbation Tests. *J. Vis. Exp.* (150), e59818, doi:10.3791/59818 (2019).

3.6 Conclusions

The emerging bubble method (EBM) and the spinning bubble method (SBM) are simple and robust methods for determining tension values for air/water or oil/water interfaces at atmospheric pressure. Prerequisite information for these methods is the density of each phase. No contact angle information is required for determining tension values.[64] A major limitation of these techniques is that the samples should have a low viscosity, and be single-phase or below the surfactant solubility. The two protocols, the EBM and the SBM, are used for measuring dynamic surface tension (DST) values and monitoring them as a function of time. When a steady-state surface tension (SST) value is reached, the stability of the SST value is tested by measuring the DST after applying area

perturbations. Then, unstable or metastable SST values can be screened out,[35] and reliable equilibrium surface tension (EST) values can be determined. The same tensiometer used for the EBM protocol can be also used for a pendant drop method configuration where the surfactant solution is suspended vertically at the end of the syringe tip. The pendant drop method has a disadvantage, relative to the EBM for the experiments requiring long times (over than about an hour), as the drop volume may decrease due to solvent evaporation. The pendant drop method may be preferred, however, when the available liquid sample volume is smaller than the minimum volume required for the EBM. The SBM method has certain advantages over the pendant drop method, the Du Noüy Ring method, or the Wilhelmy plate method because the sample is in a sealed tube throughout the measurements, thereby eliminating errors due to any solvent evaporation. In addition, interfacial tensions (IFTs) between two immiscible liquids, such as oil and water for enhanced oil recovery applications[2,35] or hydrocarbon and fluorocarbon for firefighting fluids,[70] can be determined with the same tensiometers and with the same protocols.

4. SURFACE TENSION BEHAVIOR OF AQUEOUS SOLUTIONS OF A PROPOXYLATED SURFACTANT AND INTERFACIAL TENSION BEHAVIOR AGAINST A CRUDE OIL

4.1 Overview

Equilibrium interfacial tensions (EIFTs) are important in determining the oil recovery efficiency in surfactant-based enhanced oil recovery (EOR) processes, in which ultralow IFT values (less than 10^{-2} mN·m^{-1}) are often needed. The dynamic interfacial tensions (DIFTs) for un-pre-equilibrated drops in contact with aqueous solutions and the adsorption mechanisms at the oil-water interface are important for the initial stages of EOR and for screening various surfactants for field applications. The IFT behavior of a commercial anionic surfactant, termed S13D, a single-chain propoxylated sodium sulfate salt has been studied. The synthetic brine used (9,700 ppm total dissolved solids) was similar to that in an actual reservoir of oil, from which purified crude oil samples were prepared.

The dynamic and equilibrium surface tensions (DSTs and ESTs) and the IFTs were measured at 24 °C, with the emerging bubble/drop method, or the spinning bubble/ drop method. The DSTs for surfactant concentrations from 0.1 to 10,000 ppm by weight have a simpler adsorption mechanism than the DIFTs, involving only diffusion from the aqueous phase and adsorption/desorption. Surface and interfacial tension relaxation tests after surface area perturbation were performed for establishing the validity of the ESTs and EIFTs. The critical micelle concentration (CMC) was 12 ppm in water and 1 ppm in brine. The lowest observed EIFT was 1 mN·m^{-1} with water and ultralow, 2×10^{-3} mN·m^{-1}, with brine. The equilibration timescales were shorter with brine than with water, for both DSTs and DIFTs, and slightly longer for DIFTs, because evidently the adsorbed surfactant desorbed and diffused away from the interface, for partitioning in the oil phase. The results suggest that the IFTs were associated with the typical adsorbed soluble monolayers at the oil-water interface, and that solubilization effects did not affect the measured DIFTs and EIFTs.

4.2 Introduction

Low (< 1 $mN \cdot m^{-1}$) and ultralow (< 10^{-2} $mN \cdot m^{-1}$) interfacial tensions (IFTs) between an oil phase and an aqueous phase containing surfactants, polymers, and salts are quite important in emulsion stability and particularly in two-phase flows occurring in certain enhanced oil recovery (EOR) processes.[1,8] Because of practical economic considerations in chemical EOR processes involving the use of surfactants, it is important to achieve low IFTs at surfactant concentrations; that is, at concentrations which are lower than 10 wt% or even lower than 1 wt%. Moreover, the surfactants or surfactant blends under consideration need to be tailored to the salt concentrations ("salinity"), temperature, oil type, and other reservoir-specific conditions.[5,15–18] Currently, selecting a surfactant in practice is mostly empirical, and is often primarily based on a combination of apparent phase behavior tests and IFT data or estimates of the IFT values.[7,11,17,18,23,28,30–32] No firm guidelines on the relationships between the surfactant molecular structures and the IFT values have been reported in the open literature, except for some systems where pure hydrocarbons were used as model oils.[33] Thus, a critical need exists for developing methods for screening surfactants properly by using reliable equilibrium IFT (EIFT) values, and also, dynamic (time-dependent) IFTs (DIFTs).

The EIFT is generally considered to be the most important parameter that affects the flow of aqueous and oil phases in underground oil reservoirs, based on its role in the capillary number.[11,18,23,28,31,32] Nonetheless, some reported IFTs may not have been established to uniquely define the EIFT values. Then, it is difficult to rigorously correlate the EIFT values to other properties, such as to the molecular structure, the surfactant solubility in water or oil, or the solubilization of oil in water and water in oil. Moreover, IFT values are often reported after a giving period of time for a specific experiment, without due consideration of the actual timescale of equilibration. Therefore, determining which of the many dynamic IFT values is *the* EIFT value may be somewhat arbitrary, because the IFT depends on time. To ensure that a steady-state IFT value (SIFT) is indeed the EIFT value, one needs to know the timescale of equilibration. Similar arguments can be made for the surface tension (ST), dynamic surface tension (DST), steady-state surface tension (SST), and equilibrium surface tension (EST).

The equilibration timescale (t_{95}, t_1, or t_2) is defined in this chapter as the time required for the DIFT or DST value to change by 95% of the total change from the initial value to the steady-state value. Such timescales can range from 1 s to more than 10^4 s, and depend on the surfactant

type, surfactant concentration, salinity, temperature, and the type of oil.[71,72] Even though DIFTs have been observed and reported, their time dependence and relationship to the EIFT have received little attention in the EOR literature.[55,73–78] The aim here is to develop systematic protocols and molecular insights for addressing these issues, in order to provide a methodology that will allow for appropriate screening of surfactants for a specific EOR or reservoirs. The results should lead to new insights on the fundamental physics associated with the interfacial tension in oil-water systems, and possibly afford researchers the ability to elucidate the mechanism or mechanisms involved in reaching ultralow IFTs.

We present ST and IFT results for a commercial propoxylated anionic surfactant, which has the capability of producing, against the crude oil studied here, low IFT values with water solutions and ultralow IFT values with the brine solutions used. We also report a limited ST study of a standard nonionic surfactant, for reference and calibration purposes. Moreover, the solubility of the surfactant and the critical micelle concentrations (CMC) of the surfactant in various aqueous solutions were determined, as no phase behavior information has been reported in the literature for this surfactant in water or a brine. The concentration dependence of the DST and of the EST for up to 10,000 ppm (1.0 wt% active, 1.2 wt% total) surfactant concentrations were determined. The t_{95} timescales and some t_1 or t_2 timescales of re-equilibration after area perturbation (see Figure 2) were also determined. Low and ultralow IFTs were observed only when salts were present in the aqueous solutions. These IFT values are inferred to be due to adsorbed monolayers, with little or no effect of dissolution or solubilization of oil in water or vice versa. The results could impact on the understanding of the ultralow tension mechanisms.

The IFT values studied here (both DIFT and EIFT) are for "un-pre-equilibrated" two phase systems of an oil drop vs. water solution or a brine solution. They are most relevant to the initial two-phase flow behavior when an aqueous solution of surfactant first contacts an oil phase. They correspond to the surfactant components being equilibrated among the aqueous and oil phases. As the oil phase components start equilibrating with the aqueous phase, and the aqueous phase components start equilibrating with the oil phase, the surfactant components may re-equilibrate further among the two phases, and the IFT value may change resulting to a second EIFT value. While the first EIFT value for an un-pre-equilibrated system may correspond to a "local equilibrium IFT", the second EIFT value may be a "global equilibrium IFT". Although the latter

IFT may be more relevant to the later stages of an EOR process, only the former IFT is the main focus of this chapter.

4.3 Results and Discussion

4.3.1 Dynamic Surface Tension and Equilibrium Surface Tension Results

In order to characterize the behavior of the surfactant molecules at the interface of the aqueous solution without crude oil interaction effects, the dynamic surface tensions (DST) of several S13D solutions against air were measured with the EBM at a fixed bubble area, as a first step towards establishing the EST values. The timescales (t_{95}) to reach a steady-state surface tension (SST) clearly decreased with increasing surfactant concentration. These values reached about 100 s at 100 ppm surfactant concentration in water, and decreased to less than 1 s at 1,000 ppm and 10,000 ppm surfactant concentration in water (Figure 5a). DSTs were also measured with the brine solution at surfactant concentrations ranging from 0.01 to 10,000 ppm (Figure 5b). The presence of the salts was observed to reduce the t_{95} values by a factor of about 5-10 compared to the results with water (Figure 6). A possible reason could be that the electrostatic repulsive forces between the charged surfactant molecules and the charged monolayer are lower in brine than in water. It was not possible to determine the DST behavior and t_{95} at higher surfactant concentrations, because t_{95} was smaller than the dead time of 1 s.

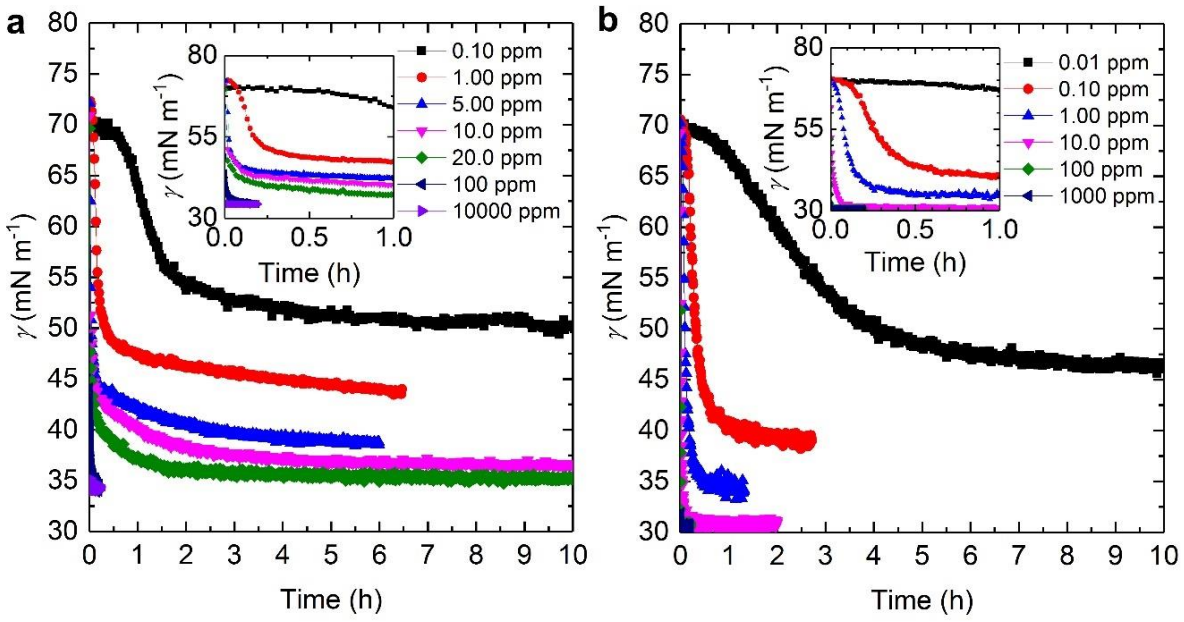

Figure 5. DST of S13D solutions in (a) water and (b) brine, as determined with the EBM without area perturbations. As the surfactant concentration increased, the dynamic surface tension decreased at more rapid timescales.

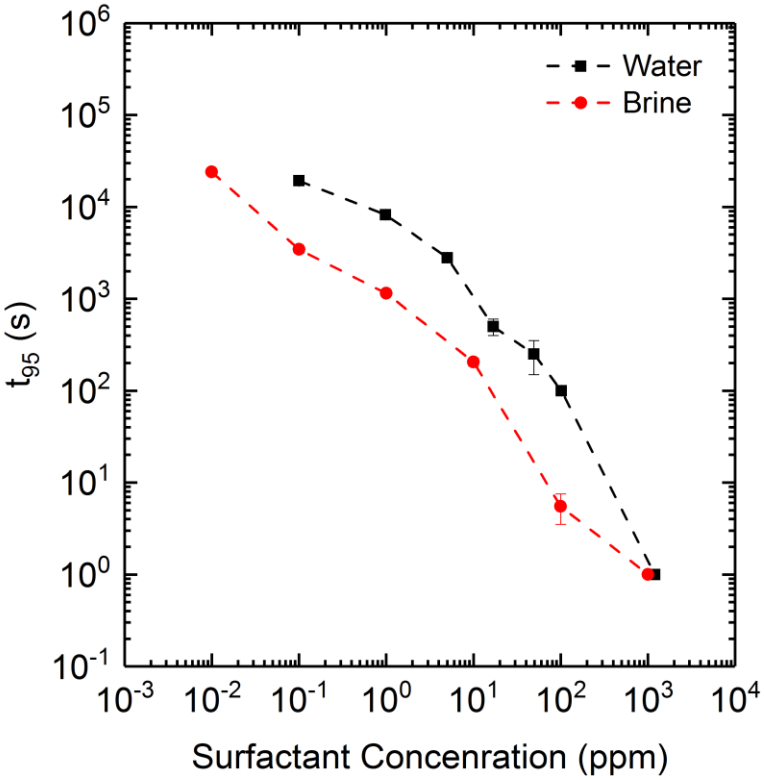

Figure 6. Timescales of surface tension equilibration (t_{95}) of S13D in water or brine. As the surfactant concentration increases, t_{95} decreases. For concentrations greater than about 1,000 ppm, the t_{95} is shorter than the dead time limit of 1 s.

The equilibrium surface tension (EST) values were assigned after applying several area perturbations, after which the relaxation of the dynamic surface tension (DST) was followed until the DST reached a steady state. An example of these measurements for a 100 ppm S13D in water is shown in Figure 7. In this example, the following values were found: $SST_1 = 35.1 \pm 0.3$ mN·m^{-1}, $SST_2 = 33.5 \pm 0.2$ mN·m^{-1}, and $SST_3 = 34.9 \pm 0.2$ mN·m^{-1}. Hence, the SSTs were stable to these area perturbations, and the EST was determined to be 34.2 ± 1.2 mN·m^{-1}. In addition, the determined equilibration times after area perturbations (t_1 and t_2) suggest that the surface tension relaxation dynamics are controlled by adsorption/desorption kinetics or, at least, mixed kinetics combined with diffusion rates (Figure 6).[79] The expected diffusion length for the surfactant molecules to reach the surface should be smaller after the area perturbations, because the desorbed molecules and micelles should be closer to the surface than at the beginning of the experiment. The similar equilibration times after the area perturbations (t_1 and t_2) compared to the initial t_{95} values indicate that the surface tension dynamics are not controlled primarily by the diffusion rate. The observed behavior of this surfactant is, therefore, quite similar to the DST behavior of typical soluble surfactants and soluble monolayers;[80] hence, it can be concluded that all surfactant components should be soluble in water or in the brine used.

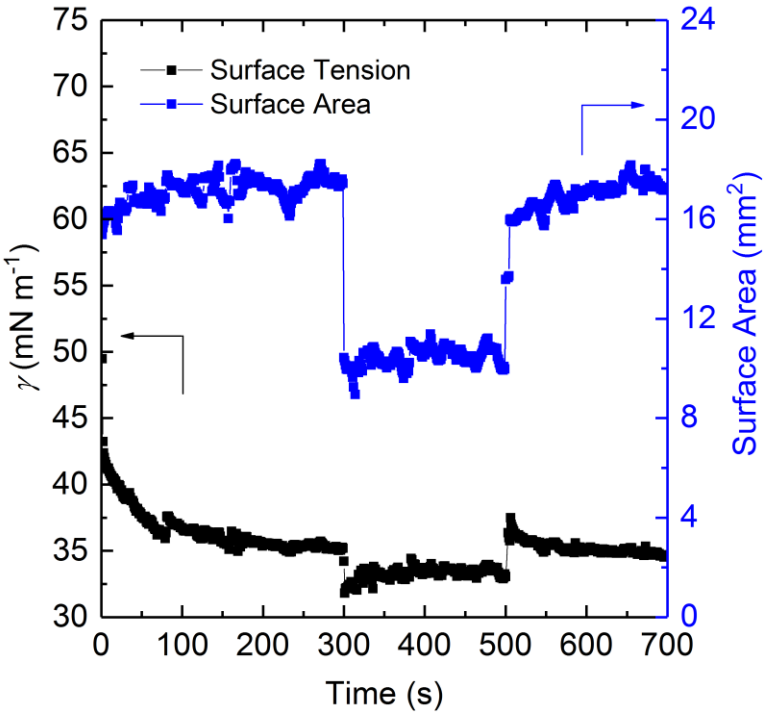

Figure 7. DST and SSTs of 100 ppm S13D in water, measured with the EBM at two bubble volumes, 5 µL or 3 µL, with respective surface areas, A_1 and A_2, as shown on the right vertical axis. The timescales of equilibration value were t_{95} = 100 s; t_1 = 100 s; t_2 = 100 s. The EST was 34.2 ± 1.2 mN·m^{-1}.

In order to establish the methods, the ESTs of a known surfactant, Triton^{TM} X-100, in water were also determined, with both the EBM and the SBM (Figure 8). The EST values were determined rigorously as a function of C_{surf} to compare the overall results from the emerging bubble method and the spinning bubble method, and compare the results to the literature. As seen in Figure 8 and Table 1, the two methods were in good agreement.

Table 1. CMC values and surface densities of Triton^{TM} X-100 in water

Property	From the EBM	From the SBM	Literature[69]
CMC (ppm)	131	127	143.8
Γ (10^{-10} mol cm^{-2})	3.1	3.0	2.91
$\bar{A}$ (nm^2·molecule^{-1})	0.54	0.55	0.57

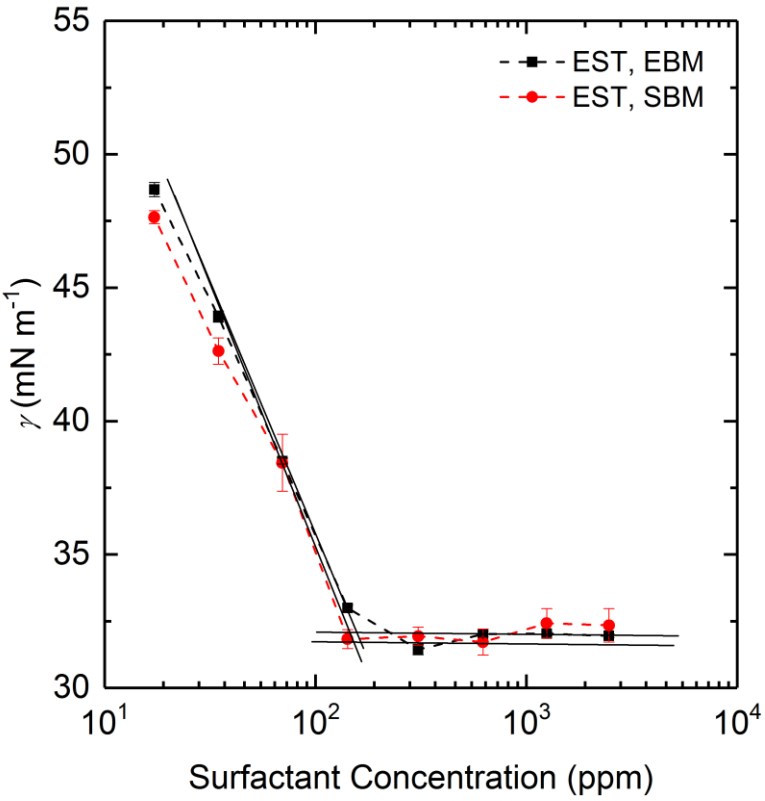

Figure 8. Equilibrium surface tension of TX100 solutions against air with the EBM and the SBM. The broken lines are shown for connecting the data, and the solid lines are used for determining the CMC and the surface density (Γ).

The resulting CMC values differed by less than 10% from the literature value.[69] This difference was not surprising because of the somewhat arbitrary ways of drawing the two intersecting straight lines in determining the CMC. The surface density (Γ) of the Triton™ X-100 below the CMC was found to be 3×10^{-10} mol·cm^{-2}, which is consistent with the literature value.[69] It was calculated from the slope of the γ vs. logC_{surf} plot and the Gibbs adsorption isotherm

$$d\gamma = -n\Gamma RT\, d\ln C_{surf} \quad (5)$$

where n = 1 for nonionic surfactants, and, for ionic surfactants, such as S13D, n = 2 in water solutions and n = 1 in brine solutions. From these data, the molecular area was determined to be 0.54 nm^2.

In order to compare the macroscopic behaviors of the adsorbed surfactant layer at the air-water interface and at the oil-water interface, the concentration dependence of the EST values of

S13D in water and brine was examined first. The EST values of S13D in water and in brine are plotted as a function of the surfactant concentrations in Figure 9. From these data, the CMC values were found to be 12 ppm and 1 ppm, respectively (Table 2). Another single-chain anionic sulfate surfactant has areas per molecule at the air/water interface at maximum surface saturation as follows: 0.35 nm^2 in water at 25 °C[81] and 0.32 nm^2 in 0.15 M aqueous NaCl solution at 23 °C.[82] The results indicate that the adsorbed monolayer density was higher in the brine used than in water, possibly because of the decreased repulsive interactions in the adsorbed monolayer head groups. These values will be compared to those at the oil-water or oil-brine interfaces.

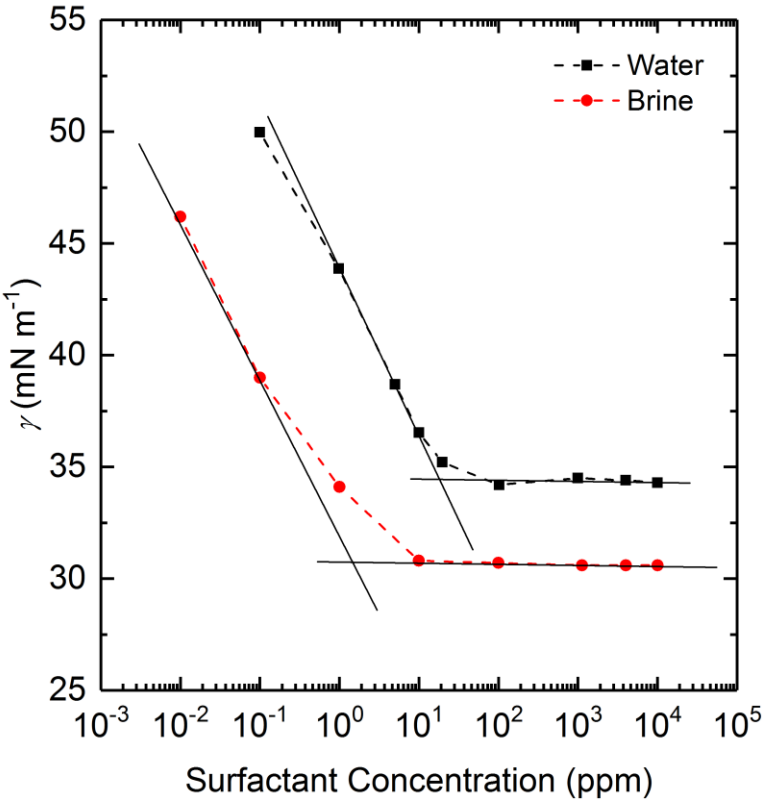

Figure 9. EST values as a function of S13D concentration in water and brine, measured with the EBM. The CMC is defined as the intersection of the two solid lines shown. From the slope of the line at surfactant concentration values below the CMC, the average surface density (Γ) was obtained.

Table 2. CMC values, surface densities, and molecular areas of S13D in water or brine

Solvent	CMC (ppm)	Γ ($\times 10^{-10}$ mol·cm^{-2})	$\overline{A}$ (nm^2)
Water	12	1.3	1.2
Brine	1	1.7	0.9

4.3.2 Dynamic Interfacial Tension and Equilibrium Interfacial Tension Results

The DIFT of water against oil with no added surfactant, started at about 21 mN·m^{-1} at t ≈ 1 s, and decreased to about 18 mN·m^{-1} at longer times (Figure 10, for 0.00 ppm). The IFT decrease was attributed primarily to possible adsorption of surface-active components, which are usually present in many crude oils. For 1 ppm of surfactant present, little change was observed relative to the 0 ppm solution. For surfactant concentrations of 10 ppm or greater, the DIFT decrease was significant compared to that at 1 ppm, indicating that these DIFT changes were due to S13D only, and were no longer affected significantly by any surface-active impurities in the oil. From these data, the SIFTs were determined, and the t_{95} timescales were calculated by using $\gamma_0 \approx 21$ mN·m^{-1} as the best estimate available of the oil/water interfacial tension with no surfactant.

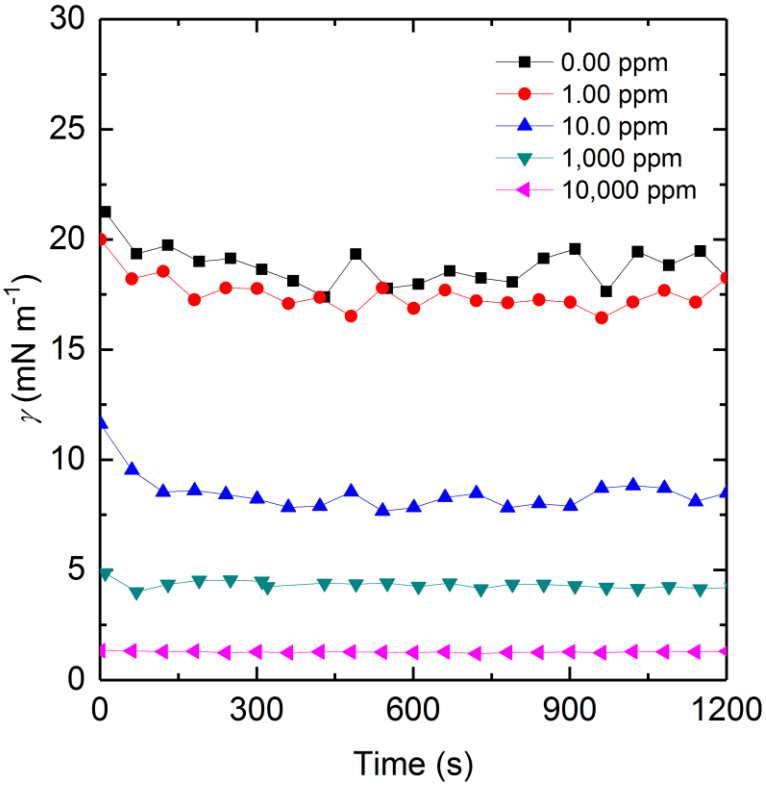

Figure 10. DIFT of S13D in water against oil, determined with the EDM without any area perturbations.

To determine whether the thus obtained SIFTs were the true equilibrium values, area perturbation tests were performed with both the EDM and the SDM, and the resulting DIFT relaxation behavior and SIFTs were observed. For one example, at a surfactant concentration of 10,000 ppm, the DIFTs are shown in Figure 11a. Although there were no abrupt changes of the DIFT values, and the recoveries of the SIFT values upon area perturbations were not clearly observed, the SIFTs before and after area perturbations were in good agreement; hence, the EIFT should be 1.3 ± 0.1 $mN \cdot m^{-1}$. As a second example, IFT values with the SDM for a concentration of 10 ppm S13D in water are shown in Figure 11b. The t_{95} value could not be determined because of the long dead time. The t_1 and t_2 values were found to be about 150 s. The second and third SIFTs were in good agreement with the first SIFT value, and the SIFT values obtained with the EDM (Figure 10). Hence, one can clearly conclude that the EIFT = 10 ± 1 $mN \cdot m^{-1}$. The plot of the EIFT as a function of $\log C_{surf}$ is presented later in this section.

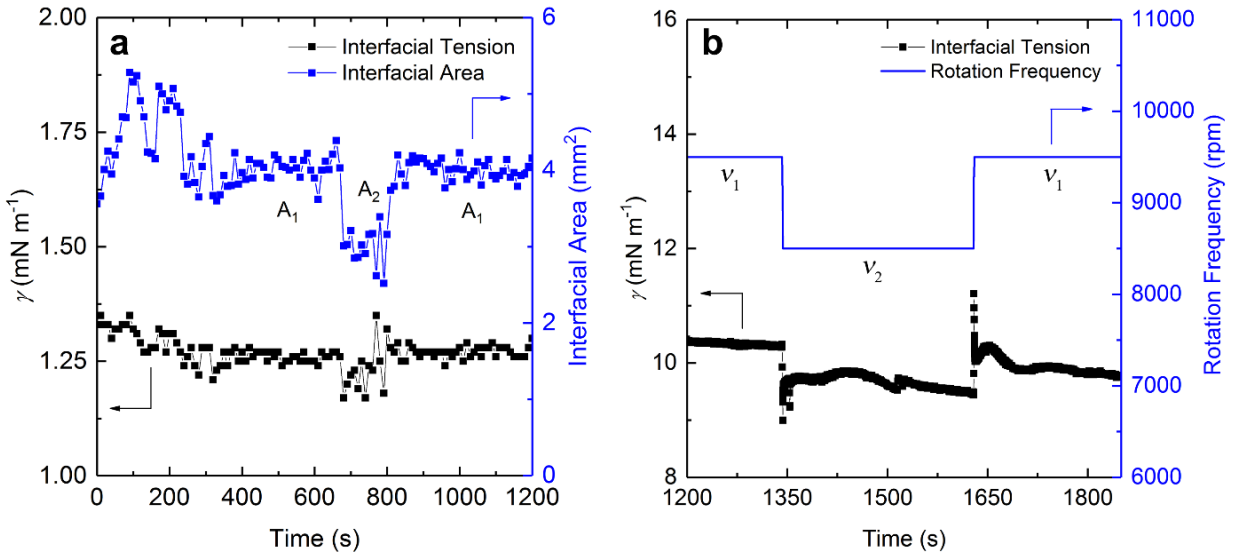

Figure 11. (a) DIFT and SIFTs of S13D in water at a concentration of 10,000 ppm surfactant measured with the EDM The areas, A_1 and A_2, correspond to V_1 = 1 µL and V_2 = 0.5 µL; t_{95} less than 1 s, and EIFT = 1.3 ± 0.2 mN·m^{-1}. The timescales, t_1 and t_2, after area perturbations were not determined because of the noise in the data. (b) DIFT and SIFTs of S13D in water at a concentration of 10 ppm surfactant measured with the SDM for ν_1 = 8,500 rpm and ν_2 = 9,500 rpm. The t_{95} value cannot be determined accurately because of the long dead time; $t_1 \approx t_2 \approx 150$ s; $SIFT_1$ = 10.3 ± 0.1 mN·m^{-1}; $SIFT_2$ = 9.6 ± 0.1 mN·m^{-1}; $SIFT_3$ = 9.9 ± 0.1 mN·m^{-1}; EIFT = 10 ± 0.5 mN·m^{-1}.

The DIFT values with brine solutions at various surfactant concentrations were examined in more detail, because of their potential practical importance. All measurements were performed above the CMC value, first at a surfactant concentration of 10 ppm, with both the EDM and the SDM, and then only with the SDM at higher concentrations. This is because the higher surfactant concentrations resulted in IFT values that were lower than the 1 mN·m^{-1}, which was the practical limit of the EDM with the available instruments. When the dynamic IFT (DIFT) values fell below about 1 mN·m^{-1}, for the smallest available syringe diameter of 0.178 mm, the injected oil drop deformed significantly, so no hydrostatic equilibrium was possible, and the drop broke (Figure 12) and resulting in a narrow jet interface profile. Thus, when an IFT value reaches this limit, one should use the spinning drop method (SDM), which can provide reliable IFT values and can allow area perturbations for studying IFT relaxation.

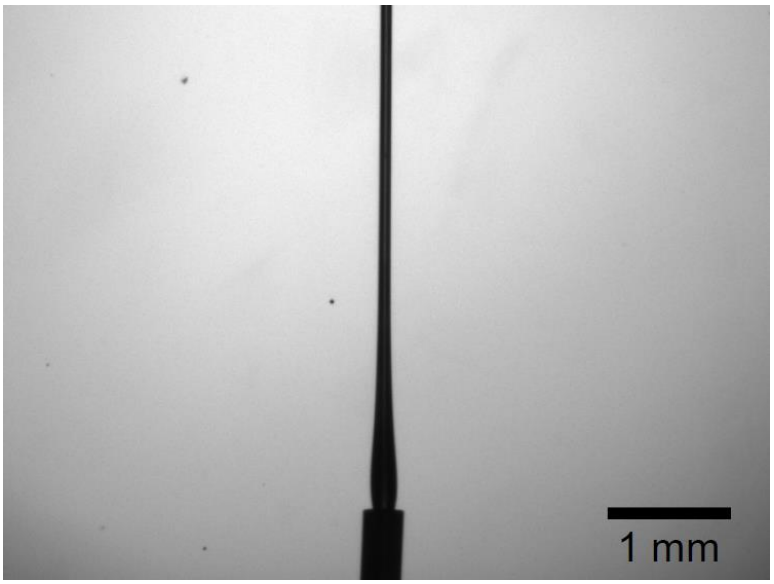

Figure 12. Photograph of a crude oil drop in contact with a solution of 10,000 ppm S13D in water. As soon as the crude oil drop was injected, it elongated, formed a jet, and did not form a drop at equilibrium.

At a surfactant concentration of 20 ppm, the first available DIFT measurement of 2 $mN \cdot m^{-1}$ was reached at ca. 500 s (Figure 13a). The DIFT dropped continuously to an apparent plateau of about 1.3 $mN \cdot m^{-1}$ at about 800 s. This *apparent* SIFT value was found to be unequal to the longer term SIFT, as shown from the IFT value responses to an area perturbation test. After the rotation frequency decreased, and the interfacial area decreased, the DIFT dropped precipitously to an SIFT of about 1.2×10^{-2} $mN \cdot m^{-1}$ (Figure 13b). From subsequent area perturbation tests, with consistent SIFT values indicated with a high degree of certainty that the EIFT was about $(1 \pm 0.4) \times 10^{-2}$ $mN \cdot m^{-1}$.

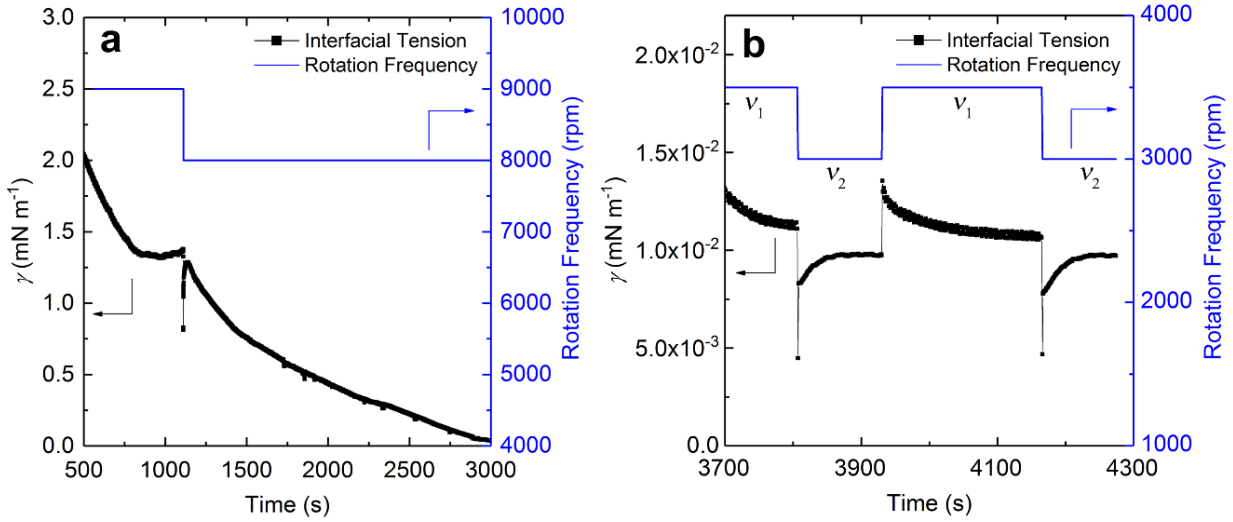

Figure 13. DIFT and a SIFT of a solution with a concentration of 20 ppm S13D in brine. (a) For t = 500 – 3,000 s, when the area was changed upon reaching an apparent SIFT = 1.3 mN·m^{-1}, the DIFT dropped to 0.8 mN·m^{-1}, and then it started to decrease again, indicating that the 1.3 mN·m^{-1} value was not a reliable SIFT. A more reliable SIFT was established at about 3,800 s. (b) From results for 3,700 – 4,300 s (the results for 3,000 – 3,700 s followed a continuous line, and are not shown here), four SIFTs were determined as (1.3 ± 0.8) × 10^{-2} mN·m^{-1}, (9.7 ± 0.5) × 10^{-3} mN·m^{-1}, (1.1 ± 0.1) × 10^{-2} mN·m^{-1}, and (9.6 ± 0.5) × 10^{-3} mN·m^{-1}, and the EIFT was estimated as (1 ± 0.4) × 10^{-2} mN·m^{-1}, which is significantly lower than the first apparent SIFT; $t_1 \gtrsim 40$ s, $t_2 \gtrsim 100$ s, and $t_3 \gtrsim 40$ s.

Similar data were obtained at surfactant concentrations of 50, 100, 1,000, 5,000, and 10,000 ppm. The data at 50 and 10,000 ppm are shown in Figure 14. The respective EIFTs were 5.5 × 10^{-3} mN·m^{-1} and 1.4 × 10^{-2} mN·m^{-1}, all in the ultralow and low IFT range. The data at surfactant concentrations of 100 ppm, 1,000 ppm and 5,000 ppm are not shown. The timescales t_1 and t_2 generally decreased with increasing C_{surf}.

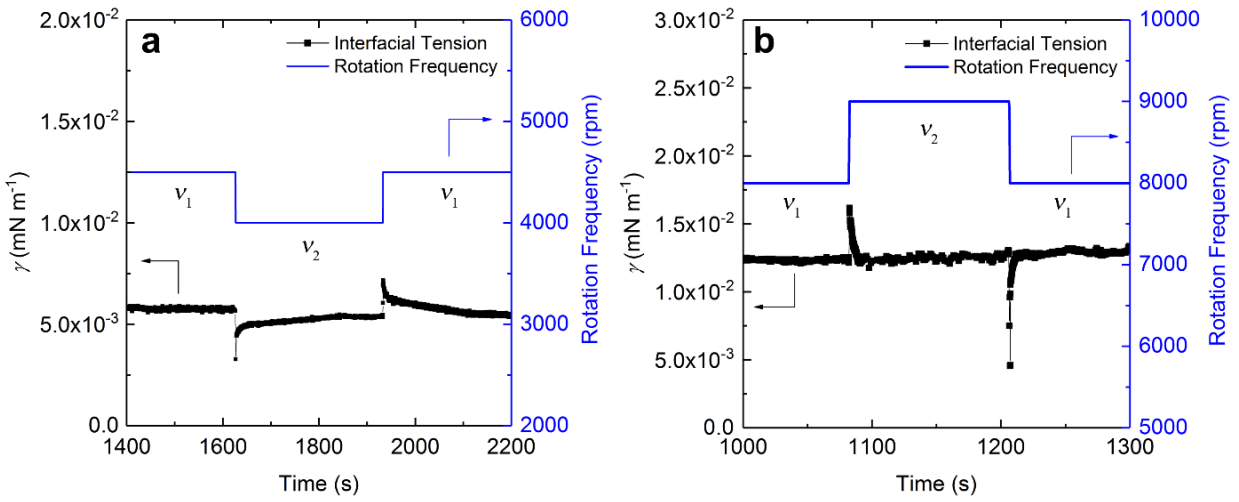

Figure 14. DIFT and SIFT of S13D in brine at (a) 50 ppm and (b) 10,000 ppm concentrations of surfactant obtained using the SDM. The timescales of equilibration and EIFT were (a) $t_1 \approx t_2 \approx 200$ s, EIFT = $(5.5 \pm 0.4) \times 10^{-3}$ mN·m^{-1} and (b) $t_1 \approx 7$ s, $t_2 \approx 5$ s; EIFT = $(1.4 \pm 0.1) \times 10^{-2}$ mN·m^{-1}.

In order to compare the behavior of the adsorbed surfactants at the oil-water and the oil-brine interfaces, the concentration dependence of the EIFT values were analyzed. In water, the EIFT decreased from 18 mN·m^{-1}, at 0.1 ppm surfactant concentration, to 7.5 mN·m^{-1} at 10 ppm, then to 1.2 mN·m^{-1} at 100 ppm, and then increased further to 4 mN·m^{-1} at 1,000 ppm (Figure 15a). A surface tension minimum was clearly detected. This behavior seems to be consistent with the CMC of 12 ppm, obtained from the EST data. The results with brine cannot be seen clearly in a γ–logC_{surf} plot, because the interfacial tension values are quite low; hence, the results are also plotted as logγ–logC_{surf} in Figure 15b. At a surfactant concentration of 10 ppm, the two EIFT values from the two methods are quite similar, 2.2 and 2.0 mN·m^{-1}, giving confidence to their accuracy. The tension minimum at a surfactant concentration of 100 ppm in water and 1,000 ppm in brine can be explained by the fact that the S13D surfactant is a mixture of many surface-active components. While a more surface-active component adsorbs at a low concentration and reduces the IFT significantly, it is solubilized into mixed micelles and is less available to adsorb at higher concentrations. Then the less surface-active components adsorb more to the interface and the IFT values became higher. By using the data obtained at surfactant concentrations of 10 and 100 ppm for water solutions and those of 10 and 20 ppm for brine solutions, rough estimates of the γ–logC_{surf} were obtained, and the surface density values were estimated from these data (Table 2). The maximum surface area of another single-chain anionic sulfate surfactant at the hexadecane/water

interface at 23 °C as a reference are 0.38 nm^2 in 0.01 M or 0.15 M NaCl solutions.[82] The results indicate that the surface density values and the molecular areas of S13D adsorbed from either water or brine are typical of monolayers. Moreover, as also observed for the EST values (Table 3), the surface density values (Γ) were larger in brine than in water, indicating a more extended conformation of the hydrophobic group at the interface, and possibly weaker electrostatic repulsive forces among the adsorbed surfactant molecules at the oil/brine interface, allowing a closer packing at the interface.

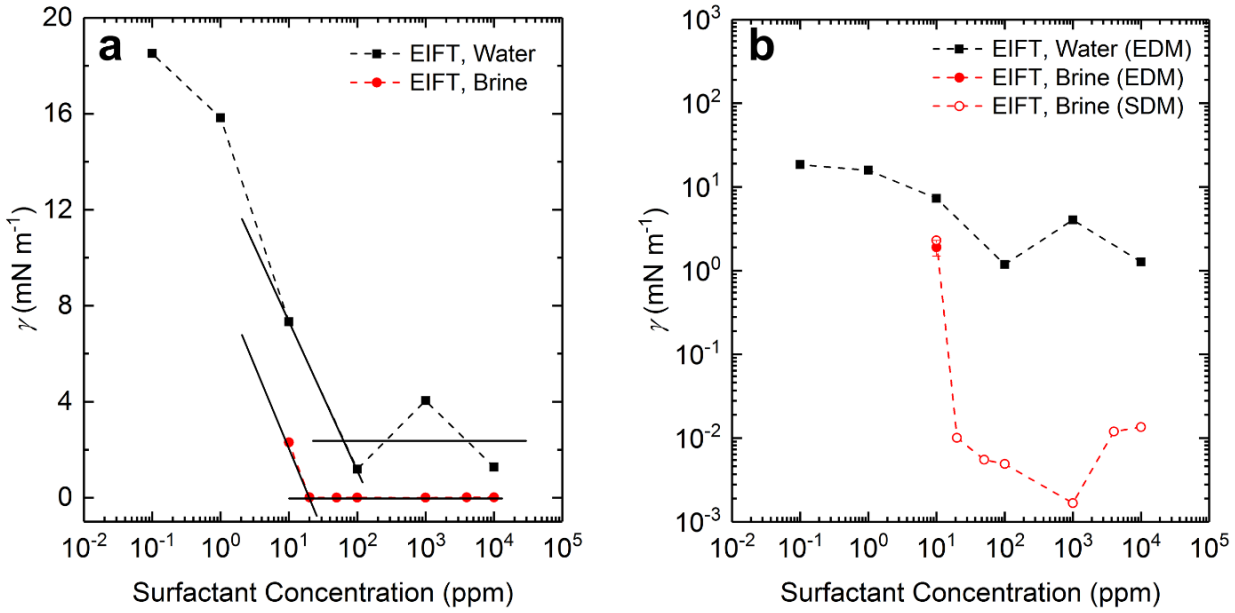

Figure 15. EIFT values of S13D solutions in water or brine as a function of the surfactant concentration in (a) semi-log plot, and (b) logarithmic plot. EIFT values were measured with the EDM for the solutions in water and for the surfactant concentration of 10 ppm in brine and with the SDM for the solutions in brine.

Table 3. Surface densities and molecular areas of S13D at oil-water interfaces

Solution	Γ ($\times 10^{-10}$ mol·cm^{-2})	$\overline{A}$ (nm^2)
Water	1.7	0.97
Brine	3.1	0.54

The EIFT values of 1 wt% S13D surfactant in water or brine against this crude oil were compared, in a limited study, with the EIFT values of n-dodecane with water or a NaCl brine at the same ionic strength as the brine used here (0.15 M and 8,700 ppm). The results (see Table 4) show that the EIFT value with water is lower with n-dodecane than with the crude oil (A vs. B). The EIFT value with brine is higher for n-dodecane than with the crude oil (C vs. D). Replacing the synthetic brine with the NaCl brine increases the IFT slightly from 0.014 to 0.025 $mN \cdot m^{-1}$ (C vs. E) for the crude oil, and from 0.041 to 0.070 $mN \cdot m^{-1}$ for n-dodecane. Overall, this surfactant can produce low IFT values also with n-dodecane or the NaCl brine. The results here are not limited, therefore, to this crude oil or the brine used. More research is needed to understand the reasons for the observed differences.

Table 4. Comparison of the EIFT values of S13D in water, brine, or NaCl brine against crude oil or n-dodecane

	Oil Phase	Aqueous Phase	EIFT ($mN\ m^{-1}$)
A	Crude Oil	DI Water	1.28
B	n-dodecane	DI Water	0.21
C	Crude Oil	Brine	0.014
D	n-dodecane	Brine	0.041
E	Crude Oil	NaCl Brine	0.025
F	n-dodecane	NaCl Brine	0.070

The time-dependent behavior of the DST values without area perturbations, and their relaxation after area perturbations, were quite similar to those of typical soluble surfactant monolayers at air-water interface. The surfactant can be plausibly assumed to diffuse from the aqueous phase and adsorb at, or desorb from, the interface. In addition, the timescales of the DIFT values were lower in brine than in water (Figure 16), as also observed for the timescales of the DST values (shown again for comparison). For both water and brine, the t_{95} values for DIFTs were longer than those for DSTs, reflecting the more complex mechanism of the IFT equilibration

process, which may have involved desorption of the surfactant and partitioning or dissolution into the oil phase.

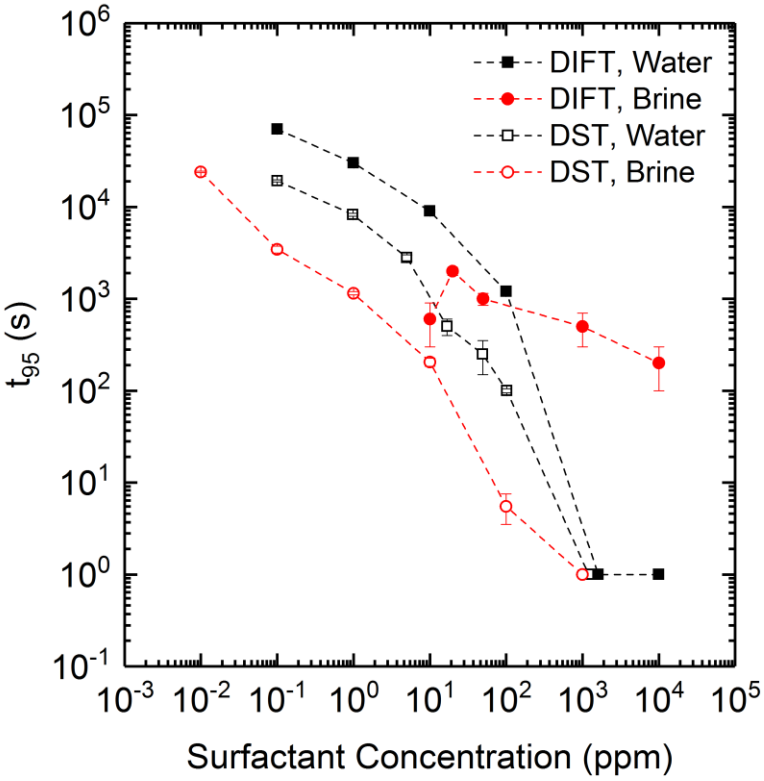

Figure 16. Timescales of equilibration (t_{95}) of DST measured with the EBM and of the DIFT measured with the EDM or the SDM.

The mechanisms suggested by the results are shown schematically in Figure 17 along with some more complex mechanisms involving solubilization. Steps 1 and 2 represent the surface tension equilibration mechanism involving surfactant (monomers, micelles, or both) diffusion to the interface and adsorption/desorption equilibration between the aqueous phase and the interface. Steps 1 - 4 represent the interfacial tension equilibration mechanism before any solubilization effects start influencing the process, and describe only the surfactant mass transfer to and from the interface. With oil, some of the initially adsorbed surfactant is transferred to the oil phase, and the IFT equilibration becomes slower than the DST equilibrations. The results here are for the so-called un-pre-equilibrated EIFTs (see Section 1.1), in which the surfactant was probably at equilibrium in the two phases and the interface, but no oil had been transferred to the water phase, and/or no water had been transferred to the oil phase, to any significant extent. In both the EDM

and SDM data, the volumes of the oil drops were much smaller (0.1%) than the volume of the aqueous phase, and remained essentially constant in the timescales of the IFT measurements. Hence, it is quite likely that little, if any, dissolution of oil in the aqueous phase occurred in the timescales of the IFT measurements, and thus there was no significant solubilization. Therefore, the mechanism of the IFT equilibration in the experiments reported may not have involved steps 5 - 8 to any significant extent. If and when oil and water reach equilibrium in the two phases at longer times (without stirring, or at shorter times if considerable stirring is used for enhancing the equilibration rates), the mechanisms of the IFT equilibration may change, slightly or substantially. Then, there could be a different EIFT, the so-called "pre-equilibrated" EIFT. Such a study should be combined with equilibrium phase behavior studies, and is the focus of the later chapter.

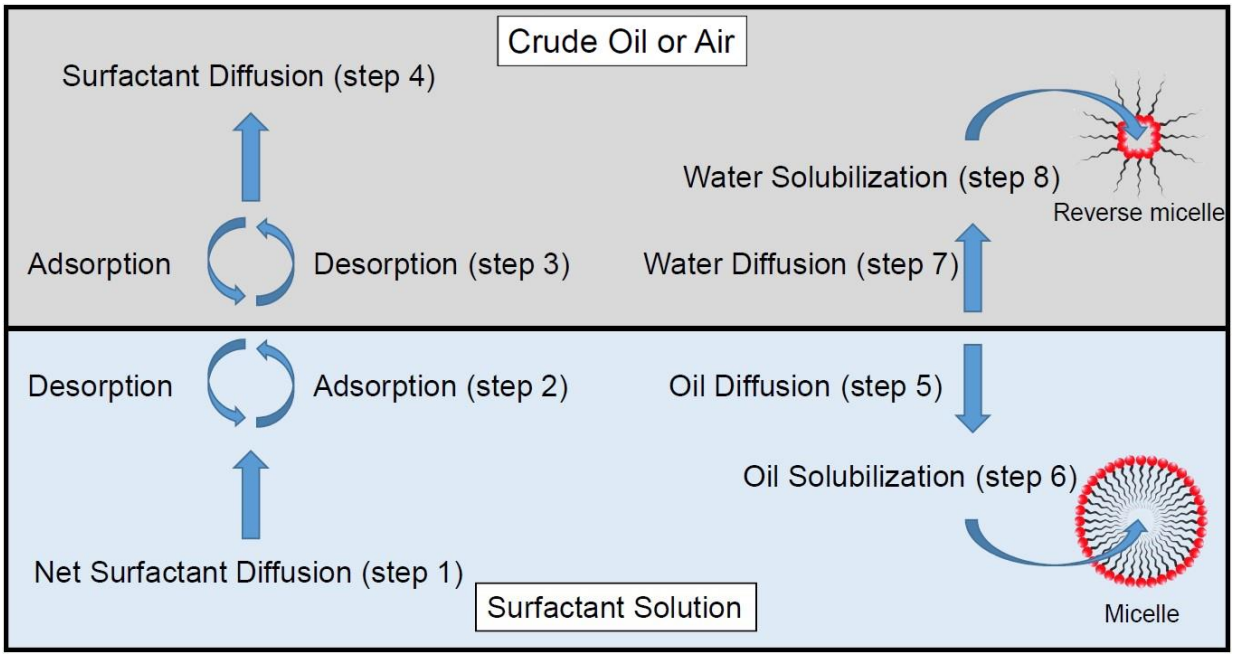

Figure 17. Possible mechanisms of surface tension (ST) and/or interfacial tension (IFT) equilibration for a molecular solution or a micellar solution of a surfactant against air or oil. Only steps 1 and 2 apply to ST equilibration. Steps 1 - 4 are for the IFT equilibration of an un-pre-equilibrated biphasic system. Steps 1 - 4 with swollen micelles may apply to IFT equilibration of a pre-equilibrated biphasic system. Steps 5 - 8 are for the further IFT equilibration for a pre-equilibrated biphasic system.

4.3.3 Further Discussion and Potential Impact

The DIFT and EIFT values of an aqueous solution against oil are critical parameters for evaluating surfactant formulations for EOR processes. In addition, maintaining low EIFT values,

as the surfactant concentration is decreased due to adsorption losses, is critical for the overall performance of surfactant formulations throughout an entire EOR process. The responses of the SIFTs to area perturbations are important for establishing valid EIFT values for un-pre-equilibrated systems. Moreover, they are important for probing the effects of continuous changes of the interfacial area between the aqueous phase and oil phase during multiphase flow processes in porous solids. Also, even though the brine and surfactant used in this study are multicomponent mixtures, and the crude oil is a highly complex and multicomponent mixture, the observed DIFT and EIFT behavior seems to be rather simple, and the observed low and ultralow IFTs seem to be produced from adsorbed monolayers, with no evidence of a third phase present.

4.4 Conclusions

The commercial propoxylated anionic surfactant S13D at 24 °C has a high solubility both in water and in the synthetic brine of eight salts with a total concentration of about 9,700 ppm or about 0.15 N. The solubility exceeds 25 wt% in water and 20 wt% in brine. Above these concentrations the surfactant forms gel-like phases. The CMC values of this surfactant determined from the equilibrium surface tensions are only about 12 ppm and 1 ppm in water and in brine, respectively. Hence, in the data presented here most of the surfactant is in micellar form. The surface densities of the equilibrium adsorbed monolayers are 1.3×10^{-10} mol·cm^{-2} in water and 1.7×10^{-10} mol·cm^{-2} in brine, and the molecular areas are 1.2 nm^2 and 0.9 nm^2 in water and brine, respectively.

The dynamic surface tension values were measured with the emerging bubble method until steady-state values were obtained. The dynamic bubble profiles fit well with the Laplace-Young (LY) equation for all surface tension measurements. The timescales of equilibration, t_{95}, decreased with surfactant concentration from 24,000 s to less than 1 s, for surfactant concentrations ranging from 0.1 to 10,000 ppm, and were lower with the solutions in brine. It was concluded that the steady-state surface tension values were indeed the equilibrium surface tension because they were stable to area perturbations.

Similar procedures were used for the dynamic, the steady-state, and the equilibrium interfacial tension values of water solutions or the same synthetic brine solutions against un-pre-equilibrated crude oil drops, in the same surfactant concentration range. When the emerging drop method was used, and the LY equation also fitted the drop profiles well. The spinning drop method

was also used for many examples of water solutions, and exclusively when the interfacial tension (IFT) values were lower than 1 $mN \cdot m^{-1}$. The equilibrium IFT values with water solutions ranged from about 18 $mN \cdot m^{-1}$ at 0.1 ppm to as low as 1.2 $mN \cdot m^{-1}$ from 100 to 10,000 ppm. The equilibrium IFT values with brine solutions reached much lower values of about $10^{-2} - 2 \times 10^{-3}$ $mN \cdot m^{-1}$ from 20 ppm to 10,000 ppm. Such low and ultralow IFT values are particularly essential for increasing the oil recovery percentages in enhanced oil recovery processes. It is also significant that such low values are obtainable for the surfactants for a wide concentration range.

The surface density (ST) values of the equilibrium surfactant layers at the oil-water or oil-brine interfaces were higher than at the air-water-solution or air-brine-solution interfaces. This suggests that the adsorbed surfactant interacts more strongly with the oil than with air. These values also suggest that the surface layers at the oil-water or oil-brine interfaces are monolayers. The same conclusion can be drawn from the dynamic IFT data and the IFT relaxation results after area perturbations. Generally, the timescales of equilibration were longer for the IFTs than for the STs, evidently because of partitioning or transfer of the surfactant from the surface monolayer to the oil phase. The timescales of IFT equilibration were shorter with brine solutions than with water solutions at low concentrations, and longer at higher concentrations (1,000 ppm and 10,000 ppm).

These results are useful in understanding the mechanisms and timescales of equilibration of low and ultralow IFT values associated with un-pre-equilibrated drops for enhanced oil recovery. Even for such oil drops, the IFT values can reach stable equilibrium values, which have been established more rigorously than in previous studies. The results suggest that dynamic and equilibrium IFT data can be used for screening surfactants for their potential effectiveness in EOR applications.

4.5 Experimental

Tap water was first purified by reverse osmosis, and then introduced into a Barnstead™ MicroPure™ Water Purification System with a mixed ion exchange resin. Salts were used as received from Fisher Chemical in certified ACS grade except for $CaCl_2 \cdot 2H_2O$, which was reagent grade and purchased from Fisher Science Education. The brine contained eight salts, with a total equivalent normal concentration of 0.150 N (see Table 5). The synthetic brine, similar in composition to an actual reservoir brine, was prepared in a 1 L volumetric flask containing a Teflon-coated magnetic stirring bar. First, pure water, which was degassed in vacuum for 30

minutes in order to remove dissolved CO_2 and O_2, was added to 6532.1 mg of sodium chloride (NaCl). After the salt was dissolved completely, 12.4 mg of potassium chloride (KCl) were added. Then the following salts were added in the following amounts and order: 4.41 mg of manganese (II) chloride tetrahydrate ($MnCl_2 \cdot 4H_2O$); 322.0 mg of magnesium (II) chloride hexahydrate ($MgCl_2 \cdot 6H_2O$); 221.4 mg of barium chloride dihydrate ($BaCl_2 \cdot 2H_2O$); 10.6 mg of sodium sulfate decahydrate ($Na_2SO_4 \cdot 10H_2O$); 2292.3 mg of sodium bicarbonate ($NaHCO_3$); and 385.0 mg of calcium chloride dihydrate ($CaCl_2 \cdot 2H_2O$). The solution density was 1.004 $g \cdot cm^{-3}$. The resulting normal concentration of each salt and each ion are shown in Table S1. The total dissolved salts (TDS) concentration was about 9,700 ppm by weight.

Table 5. Normal concentrations of salts and ions in the brine in decreasing order

Salt or Ion	Normality (N)
NaCl	1.11×10^{-1}
$NaHCO_3$	2.73×10^{-2}
$CaCl_2$	5.24×10^{-3}
$MgCl_2$	3.17×10^{-3}
$BaCl_2$	1.82×10^{-3}
KCl	1.69×10^{-4}
Na_2SO_4	6.64×10^{-5}
$MnCl_2$	5.25×10^{-5}
Total	1.50×10^{-1}
Na^+	1.39×10^{-1}
Ca^{2+}	5.24×10^{-3}
Mg^{2+}	3.17×10^{-3}
Ba^{2+}	1.82×10^{-3}
K^+	1.69×10^{-4}
Mn^{2+}	5.25×10^{-5}
Cl^-	1.22×10^{-1}
HCO_3^-	2.73×10^{-2}
SO_4^{2-}	6.64×10^{-5}

In order to prepare the crude oil for the experiments, crude oil samples (provided by the Pioneer Oil Company) were first centrifuged at 1,700 rpm and average acceleration of 600 g, for 60 minutes in order to separate any solid particles and water droplets. Then the crude oil was filtered through a 0.5 µm metal filter. The filtrates appeared homogeneous, dark brown, translucent, and had a low viscosity (~10 cP at 25 ℃). The ultraviolet-visible (UV-Vis) absorption spectra in n-dodecane for concentrations ranging from 0.1 to 100 ppm were obtained using a Cary 60 spectrophotometer with a path length of 1 cm (Figure 18). The absorbance from 1,100 nm to 500 nm were much smaller than those of at 500 to 250 nm, did not show any peaks, and are not shown here. Only one major peak was observed at $\lambda \approx 260$ nm, arising primarily from aromatic components of the crude oil. The absorbance at the peak and the other wavelengths were proportional to the concentration of the oil. As a model oil phase, n-dodecane (anhydrous, ≥ 99%) was purchase from Sigma-Aldrich and used as received.

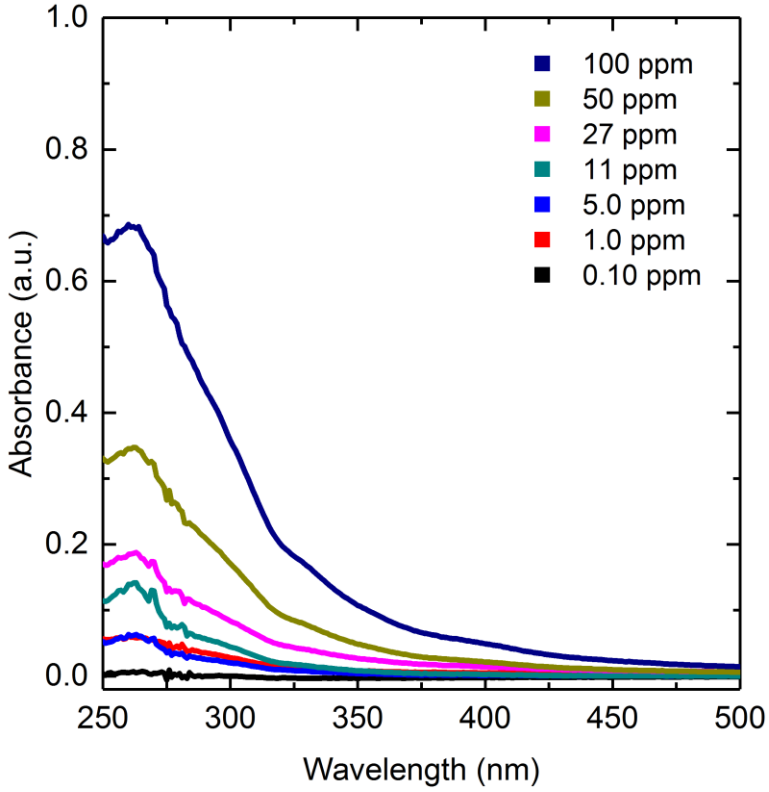

Figure 18. UV-Vis absorbance spectra of a crude oil at various concentrations in n-dodecane.

The commercial surfactant is PETROSTEP® S-13D HA (or "S13D" briefly) from the Stepan Company (Northfield, IL), is a clear viscous liquid. It contains about 81% (by weight)

anionic surfactant components ("81% active"). The composition of the remaining mass is proprietary information. The concentration values reported refer to the concentration of active surfactant, unless stated otherwise. The S13D surfactant contains single chain propoxylated sodium sulfate surfactant components, and its average molecular weight is 1,032 $g \cdot mol^{-1}$. Although the precise molecular structure of the surfactant used here is not available to us, we are aware of the structure of a similar surfactant, called "Petrostep S13D, 85% active", reported recently.[83] The reported structure was "tridecyl alcohol 13 propoxy sulfate". Also, the structures of another similar surfactant is reported as $C_{13}(PO)_{13}$-Sulfate of which hydrophobic part is a 13 carbon, isotridecyl product.[84]. Another widely-studied nonionic surfactant, Triton ™ X-100 (TX100), was used for testing our procedures. It was obtained from Sigma-Aldrich. TX100 is a mixture of ethoxylated non-ionic compounds with a branched hydrocarbon chain and with 3 to 18 ethoxyl groups.[85] At 25 °C, it is a clear, colorless, and low-viscosity liquid. Both surfactants were used as received. During the dissolution of the S13D in water or brine, the liquid sample was mixed by hand, in order to minimize foam formation. Heating was avoided to prevent formation of metastable supersaturated solutions. Since the surfactant phase and IFT behavior depend on the temperature, the results here could primarily apply to EOR for oil reservoirs which are at temperatures close to 25 °C. Nonetheless, the methods to evaluate surfactant phase and IFT behavior could be similar to those used here. Each borosilicate or quartz container was first soaked in pure water for 24 h to leach any ionic impurities. Then each container used for tension measurements was washed once with the sample solution before sample loading for tension measurements. The liquid densities were measured by using an Anton Paar DMA 5000 density meter, in which the density was obtained from the vibrational frequency of a given amount of liquid. The instrument was calibrated using water. All density values were measured at 24 °C. Each reported value is the average of five consecutive measurements.

5. PHASE AND RHEOLOGICAL BEHAVIOR OF AQUEOUS MIXTURES OF AN ISOPROPOXYLATED SURFACTANT

This chapter is reproduced with permission from **Chung, J.**; Yang, Y.-J.; Tang, H.; Santagata, M.; Franses, E.I.; Boudouris, B.W., Phase and rheological behavior of aqueous mixtures of an isopropoxylated surfactant. *Colloids and Surfaces A: Physicochemical and Engineering Aspects* **2018**, *554*, 60-73. Copyright 2018 Elsevier B.V. Chung, J.; Franses, E.I.; and Boudouris, B.W. were in charge of outlining and writing the paper and putting all the techniques together. Chung, J. was in charge of obtaining density and conductivity data and the data analyses and contributed to small-angle X-ray scattering spectroscopy and the data analyses. Yang, Y.-J. was in charge of visual and polarizing microscopy, dynamic light scattering, and cryogenic transmission electron microscopy. Yang, Y.-J, also contributed to small-angle X-ray scattering spectroscopy and the data analyses. Tang, H. and Santagata, M. conducted rheology measurements and the data analyses.

5.1 Overview

Establishing the phase and rheological behavior of a surfactant is a critical step for assessing its potential efficacy for a range of applications, such as detergency and enhanced oil recovery (EOR). Most efforts have applied the full suite of fundamental characterization techniques to simple model surfactant systems that are often too costly to be utilized in commodity applications. Conversely, we evaluated here the behavior of aqueous mixtures of a commercial, isopropoxylated anionic surfactant, and we analyzed the supramolecular structures of the surfactant aqueous mixtures using a combination of microscopy, light scattering, and x-ray scattering techniques. A phase map was obtained at 25 °C across the full range of surfactant in water concentrations, in water and in one salt concentration (9,700 ppm). Specifically, the phases identified were a hexagonal liquid crystalline phase (H_1) and a lamella liquid crystalline phase (L_α). The structure of the micellar solution (L_1) was determined by dynamic light scattering (DLS), cryogenic transmission electron microscopy (cryo-TEM), conductimetry, densitometry, and x-ray scattering. The data acquired from these techniques provided information about the micellar sizes and their aggregation numbers. As surfactant concentration increased, the H_1 and L_α phases were observed, and the rheological behavior of these solutions was characterized. In addition, the effect of increased ionic strength on the phase behavior was quantified for both micellar solutions and liquid crystalline phases. As the ionic concentration increased from 0 to 9,700 ppm (ionic strength of 150 mM), the trend of observed phases remained the same, but the structural parameters and

domain sizes were changed slightly. Importantly, despite the multicomponent nature of the surfactant, the phase behavior of the aqueous surfactant mixtures and their rheological behavior followed the same trends as those observed for common single-component, single-chain, anionic surfactants. Thus, this effort points towards a potential universality of the trends of phase behavior of surfactant-water systems, even for complex commercial surfactant mixtures. Therefore, this could be of significant utility when surfactant formulations are considered for EOR and other applications.

5.2 Introduction

The phase and the rheological behavior of aqueous mixtures of surfactants with water are important for many applications, including detergency, consumer products, synthesis of nanomaterials, drug delivery, and enhanced oil recovery (EOR).[58,86–90] Such mixtures may form a variety of mesophases or lyotropic liquid crystals (LCs), such as hexagonal, lamellar, or cubic LCs. The nano- and microstructures of such liquid crystalline phases depend on the molecular structure of the various surfactant components, their concentrations, and the presence of other additives, such as salts and alcohols.[91–93] Moreover, surfactants at concentrations below the solubility limit and above the critical micelle concentration (CMC) form reversible physical aggregates called micelles.[59,93,94] The sizes and the microstructures of the micelles depend on the surfactants molecular structures, or the "surfactant packing parameters," which may vary with system conditions (e.g., salt concentration and solvent composition).[59] Those parameters have been applied only to surfactants with hydrocarbon chains in their hydrophobic groups. Thus, establishing the phase behavior and quantifying the rheological properties of key surfactants of interest are critical for the end-use applications of many surfactant-water systems.

A variety of "extended" surfactants have been recently developed. They have either their hydrocarbon chain extended with a poly(propylene oxide) moiety, or their hydrophilic head group extended by a poly(ethylene oxide) moiety, or both. Several isopropoxylated anionic surfactants recently have been synthesized for potential utilization in chemical enhanced oil recovery.[95,96] In such applications, it is important for the surfactant, relative to conventional hydrocarbon chain anionic surfactants,[2,95–99] to have: (i) a long hydrophobic portion within the molecular structure of the surfactant, (ii) a low CMC, (iii) a high surface activity of the surfactant, such that it has the ability to decrease the interfacial tension (IFT) between the water and the oil phases at low

surfactant concentrations, and (iv) a high "salinity" tolerance or a small effect of the aqueous phase salinity on the solubility for the surfactant in water. There are several reports on the effects of the types of these surfactants and other additives on the ability to produce ultralow (less than 0.01 mN m^{-1}) IFTs and the oil recovery efficiency for model surfactant systems.[95,96,100,101] However, little information is available regarding commercial extended surfactants and their phase and rheological behavior of water-based mixtures. It has not been established what types of liquid crystals may form as the surfactant concentration increases. Thus, there is a crucial need to examine critically such surfactants and elucidate these underlying properties. Only two reports have been found on the phase behavior of one "extended" surfactant, which is both isopropoxylated and ethoxylated,[102,103] and no rheological behavior of any such surfactant has previously been reported. The effects of the added isopropoxyl moieties are not clear and may be different from the cases where the hydrophobic chain is extended by adding hydrocarbon groups.

Here, we evaluated a commercial alkyl isopropoxylated sulfate surfactant, Petrostep S-13D HA (or S13D). Such surfactants can be used for EOR and for environmental remediation applications because of the capability of their aqueous solutions to have low or ultralow IFT values against certain hydrocarbons or crude oils, and their solubilization capacity for organic solutes.[96,100,101,104] The S13D surfactant has a low CMC, of about 15 ppm (total concentration) in water at 24 °C, and about 1.2 ppm in some salt solutions.[35] Moreover, all water-surfactant mixtures, examined with surfactant concentrations ranging from 0 to 100 wt%, looked clear and transparent, although at certain concentration ranges some gels or gel-like materials are observed.[35]

A conventional surfactant with a hydrocarbon chain having the same carbon atoms as S13D, would be expected to have nearly zero water solubility. Its chain melting transition temperature, or Kraft point, would probably be quite high, making it impossible to form micelles or lyotropic liquid crystals with water at 25 °C, or to be soluble in hydrocarbons. By contrast, S13D has a large solubility in water and the brine tested, and a high solubility in n-dodecane and some crude oils (results are not shown), and quite low IFT values against these hydrocarbons.[35] Hence, the presence of a highly disordered isopropoxylated hydrophobic moiety acting as a chain-extender maintains a high hydrophobicity, while moderating the effects of a much longer hydrocarbon chain on the phase behavior.

We provide results for a general survey of the phase behavior of S13D with water or salt solutions with increasing concentration, and the corresponding relation to the rheological

properties. A similar progression of the types of phases is observed as for conventional single-hydrocarbon chain anionic surfactants. These are: a micellar solution, a hexagonal liquid crystalline (HLC or H_1) phase, and a lamellar liquid crystalline (LLC or L_α) phase.[56,105] The formation of such LCs is important in the processing of surfactants during their production or use, and possibly for other applications. The liquid crystalline properties and their microstructures are characterized with polarized light microscopy and small angle x-ray scattering (SAXS). The formation of LCs may be important for the application to chemical EOR, if they form at low concentrations or when oil is present.[2,58] For these reasons, the solution physicochemical behavior is studied in detail with: dynamic light scattering (DLS), for measuring micellar sizes; cryogenic transmission electron microscopy (Cryo-TEM), for visualizing the micelles directly; densitometry, for evaluating the effects of micellar formation and possibly their dissociation; and conductimetry, for determining the micellar charges and dissociation. These results also provide some indirect, yet useful, information on how the monomers pack in the micelles in water or salt solutions. The packing of the monomers at the oil-aqueous interface also affects the interfacial tension, which is a key parameter of controlling EOR efficiency.[35] Moreover, the complex rheological behavior, namely, the shear viscosities of micellar solutions and the storage and loss moduli of the various liquid crystalline phases and some dispersions, are reported. The specific rheological patterns for each one of the LC phases[92] are determined and discussed. In combination with the SAXS results, certain disorder-to-order phase transitions and order-to-order phase transitions can be identified from the rheological behavior. This effort demonstrates that commercially useful surfactant mixtures show similarities with simpler pure anionic surfactants in their phase behavior, self-assembly, and rheological properties. These data highlight key fundamental results, while also providing ideas for the potential translation to critical surfactant-water industrial applications.

5.3 Results and Discussion

5.3.1 Visual and Polarizing Microscopy Observations

Visual and polarized optical microscopy (POM) observations (Table 6 and Figure 19) provided a preliminary assessment for the phase behavior of the surfactant-water and surfactant-brine mixtures. At surfactant concentrations below 25 wt%, the surfactant-water mixtures were solutions that were clear, low-viscosity, and non-birefringent solutions. They most probably are

micellar solutions. At 30 to 35 wt%, the mixtures remained transparent and became more viscous. The samples showed some birefringence with polygonal POM textures (Figure 19a), suggesting the presence of liquid crystalline particles suspended in the solution. At 37.5 and 40 wt%, the mixtures were clear gels, birefringent, with large polygonal-shaped POM textures (Figure 19b). Immediately after sample preparation, the 50 wt% mixture was a cloudy, birefringent, and viscous liquid. After about one week the mixture separated into two distinct clear and birefringent layers, suggesting the presence of two coexisting phases. At concentrations between 60 to 80 wt%, the mixtures were also clear gels. Some paper-sheet POM textures for typical lamellar liquid crystals[40] (Figure 19c) were observed at 60 to 70 wt%. Some liposome-like structures with Maltese cross patterns (Figure 19d) were observed at 80 wt%. At 90 wt%, the mixture was a yellowish, transparent, and non-birefringent solution, which looked similar to the 100 wt% surfactant liquid.

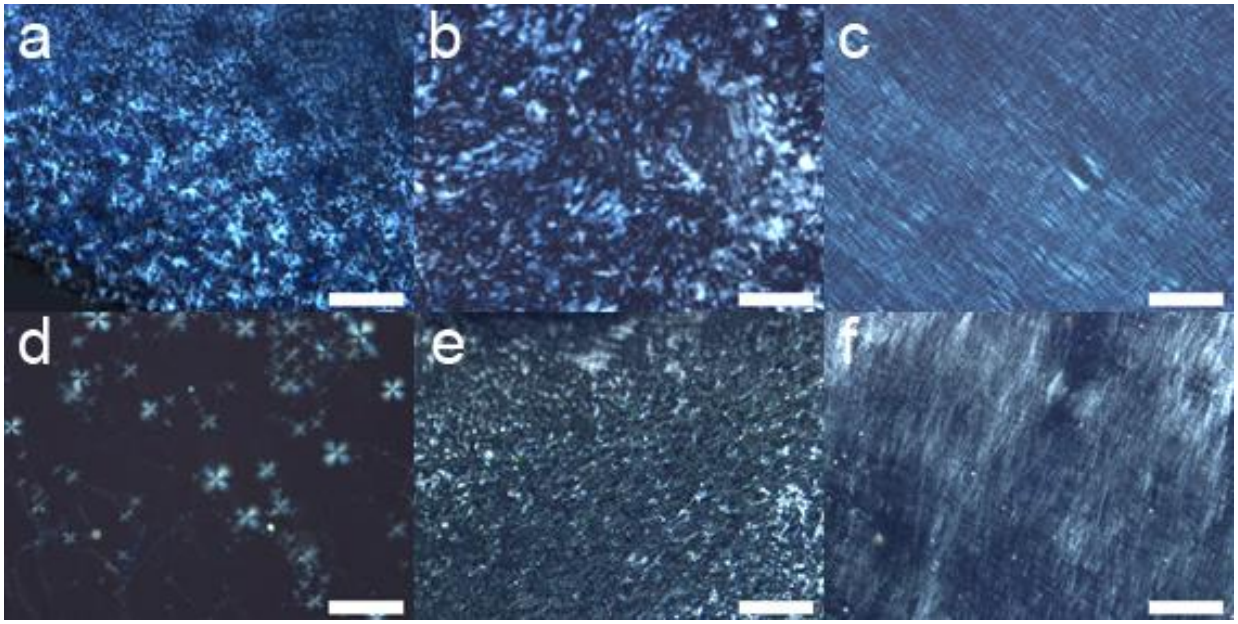

Figure 19. Polarized optical microscopy images of liquid crystalline textures with water (a-d) or brine (e,f) at various surfactant concentration: (a) 30 wt%, (b) 37.5 wt%, (c) 65 wt% , (d) 80 wt%, (e) 40 wt%, and (f) 60 wt%. Typical lamellar liquid crystal textures are observed in c, d, and f; typical hexagonal liquid crystal textures are observed in a, b, and e. The scale bar shown in the figures is for 200 μm.

Hence, as the surfactant absorbs water, it changes from a liquid isotropic phase (100 wt%) to a series of liquid crystals, probably one with a lamellar and one with a non-lamellar nanostructure. At low concentrations, below 25 wt%, an isotropic micellar solution forms, as

inferred also from the equilibrium surface tension data.[35] This pattern of phase formation with increasing concentration, of a micellar solution to various liquid crystalline phases is quite similar to these of conventional single-chain non-isopropoxylated anionic surfactants, such as sodium dodecyl sulfate (SDS) at higher temperatures. One important difference is that, whereas SDS is a crystalline solid at 24 ℃, S13D is a liquid apparently because of the disordering influence of the isopropoxylated moiety.[56,105]

Table 6. Summary of visual and polarizing microscopic observations of surfactant-water and surfactant-brine mixtures

c_s, wt%	surfactant-water mixtures	surfactant-brine mixtures
≤ 25	clear, non-birefringent, low viscosity liquid	
30 - 35	transparent, birefringent, viscous liquid	cloudy, birefringent, viscous liquid
37.5, 40	transparent, gel, birefringent	
50	cloudy, birefringent, viscous liquid, separated into two layers	cloudy, birefringent, viscous liquid, separated into three layers
60-80	transparent, birefringent, gel	
90	transparent, yellowish, non-birefringent, viscous liquid	
100	transparent, yellowish, non-birefringent, viscous liquid	

For the surfactant-brine mixtures, although there were some differences compared to the surfactant-water mixtures, indicating a substantial salt effect. A similar phase behavior pattern of micellar solutions and the same types of liquid crystalline phases were observed. At concentrations below 25 wt%, the mixtures were also clear and non-birefringent. The viscosity increased with increasing surfactant concentration. The 30 to 40 wt% mixtures were cloudy and had low viscosities. The dispersed particles were birefringent, with polygonal-shaped POM textures (Figure 19e). Hence, these mixtures were biphasic dispersions. After about one week, the 50 wt% mixture, which was initially cloudy and birefringent, separated into three distinct layers, suggesting the presence of three phases. At concentrations above 60 wt%, the surfactant-brine

mixtures looked similar to the surfactant-water mixtures at the same concentrations. The 60 to 80 wt% mixtures were clear and birefringent gels, with paper-sheet-like POM textures; see Figure 19f. At 90 wt%, the mixture was a yellowish, transparent, isotropic liquid solution.

5.3.2 Solution Behavior of Aqueous Micellar Solutions

This section focuses on the characterization of micelles in solution phases and other parameters of S13D, such as molar volumes and partial densities. The micellar sizes were estimated from dynamic light scattering and electron microscopy results in Section 5.2.2.1. Electrical conductimetry data were used in Section 5.2.2.2 to obtain information on micellar charges. In Section 5.2.2.3, densitometry was used to obtain partial molar volumes and partial densities of the surfactant.

Although the exact composition of the S13D is not available, several parameters can be estimated from the average molecular structure of the active components. The fully extended chain length of the S13D was estimated by considering general C-C and C-O length for isopropyl oxide (PO) group and Tanford equation[106] for the hydrocarbon part. The PO group in S13D is an isopropoxy group, and its length, l_{PO}, can be estimated as follows.

$$l_{PO} = 1 \times (\mathrm{C-C}) + 2 \times (\mathrm{C-O}) = 1 \times 1.54\ \text{Å} + 2 \times 1.43\ \text{Å} = 4.40\ \text{Å} \quad (6)$$

The estimated average molecular formula of S13D is CH_3-$(CH_2)_5$-(CH_3)CH-$(CH_2)_5$-O-$[CH_2(CH_3)CH\text{-}O]_{13}$-$SO_3^-Na^+$, and the maximum possible length of the extended hydrophobic chain (l_c) can be estimated as

$$\begin{aligned} l_c &= 1 \times (\mathrm{C-H}) + 11 \times (\mathrm{C-C}) + 1 \times (\mathrm{C-O}) + 12 \times (\mathrm{PO}) + 2 \times (\mathrm{S-O}) \\ &= 1 \times 1.54\ \text{Å} + 11 \times 1.265\ \text{Å} + 1 \times 1.43\ \text{Å} + 12 \times 4.40\ \text{Å} + 2 \times 1.49\ \text{Å} \\ &= 72.378\ \text{Å} \approx 7.2\ \text{nm} \end{aligned} \quad (7)$$

If two S13D surfactants overlapped, the minimum length, l_m, of these two overlapping extended chains is

$$l_m = 1 \times (\mathrm{C-H}) + 11 \times (\mathrm{C-C}) + 1 \times (\mathrm{C-O}) + 12 \times (\mathrm{PO}) + 3 \times (\mathrm{S-O}) \approx 7.4\ \text{nm} \quad (8)$$

Therefore, the diameter of a spherical micelle ranges from 14.4 nm for fully extended and not-interdigitated chains; to 7.4 nm for fully extended and interdigitated chains. If the chains are not fully extended, the diameter can be as low as 2 nm for highly disordered chains.

5.3.2.1 Dynamic Light Scattering and Cryogenic Electron Microscopy Results

In EOR or other industrial applications, the micelle dimensions are important as they impact the solution viscosity, solubilization capacity, and interfacial tension dynamics against oil. In water for 5 wt% to 15 wt% surfactant concentrations, the effective, and "apparent," hydrodynamic diameter, d_h, (as calculated from the Stokes-Einstein equation, which is valid for large spheres in a solvent continuum with the no-slip boundary condition) of the micelles was found to be about 3.2 ± 0.2 nm (Table 7).

Table 7. Average hydrodynamic diameters (from DLS) of the micelles in water or in brine at various surfactant concentrations and micellar properties

c_s, wt%	d_h, nm		Aggregation Number, N_{agg}		Headgroup Surface Area, a, nm^2	
	water	brine	water	brine	water	brine
5	3.2 ± 0.2	6.7 ± 0.7	11	93	3.2	1.5
10	3.0 ± 0.3	6.1 ± 0.8	9	71	3.4	1.7
15	3.4 ± 0.2	6.5 ± 0.6	13	86	3.0	1.6
20	4.8 ± 0.4	*	35	*	2.1	*

*Not available; the concentration is probably above the solubility of the surfactant in the brine solution.

At 20 wt%, the d_h-value was 4.8 ± 0.4 nm. The larger value at the higher concentration may be due to a higher micelle aggregation number, N_{agg}, due to a possible change of the micellar shape, or to an effect on d_h of the higher viscosity and inter-micellar interactions. Both values were much smaller than twice the length of the surfactant fully extended chain, $2l_c$, which was 14.4 nm.[40] They were even smaller than the minimum length of two interdigitating fully extended chains (i.e., 7.4 nm).[106] This implies that, in the micelles, the hydrocarbon chains are quite disordered or fluid-like, and that the PO (isopropyl oxide) chains are also disordered, or

"mushroom-like." On the assumption that the micelles are spherical, and ignoring any effects of solubilization of the impurities in the micelles, the micelle aggregation number N_{agg} is $\pi d_h^3/6V_t$, where V_t is the volume of a surfactant monomer, which is obtained from the surfactant density and the molecular weight. The thus-found aggregation number is about 11 at 5 wt%-15 wt%, and 35 at 20 wt% (see Table 7). The resulting areas, *a*, per head group of the surfactant monomer in the micelles are quite high, varying from 3.4 nm^2 to 2.1 nm^2. The resulting surfactant packing parameters $P=v_0/al$,[10] where v_0 is the hydrophobic chain volume, and *l* is the length of the extended fluid chain in the micelle, were found to be about 0.1 for micelles in water and 0.15 for the micelles in brine. These values, well below 1/3, are fully consistent with the formation of micelles. The average distance between the sulfate anions on the micelle surface is large, about 1.7 nm, and the Debye length (κ^{-1}) is about 80 nm, as found from the following equation for an ionic strength of 0.015 mM.[59]

$$\kappa^{-1} = \sqrt{\frac{\varepsilon_r \varepsilon_0 k_B T}{2 N_A e^2 I}} \tag{9}$$

Here, ε_r is the dielectric constant, ε_0 is the vacuum permittivity, k_B is the Boltzmann constant, T is the absolute temperature, N_A is Avogadro's number, *e* is the elementary charge, and *I* is the ionic strength.

Hence, no significant screening of the electrostatic repulsive forces is expected, and there should be little counterion binding. The Cryo-TEM image (Figure 20) for the 10 wt% mixture shows circular objects, probably micelles, with a similar micellar diameter of ca. 3 nm.

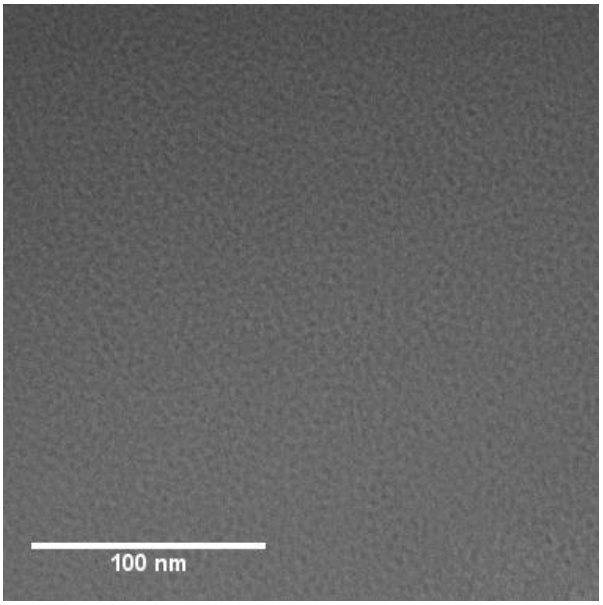

Figure 20. Cryo-TEM images of surfactant-water mixture at loading of 10 wt%. The dark circles are probably the spherical micelles which were inferred from the DLS results.

In brine, at 5 wt% to 15 wt% surfactant concentrations, the effective hydrodynamic diameters of the micelles were found to be about 6.4 nm, with a resulting aggregation number N_{agg} = 91, and a surface area per head group of about 1.4 nm^2 per molecule. The distance between the head groups was found to be ~1.4 nm. Evidently, the high ionic strength of 150 mM, with a resulting Debye length of only 0.8 nm, significantly decreased the repulsive electrostatic interactions among the sulfate groups in the micellar surface and allowed the formation of larger micelles.[107,108] Hence, the hydrophobic group was more extended in brine than in water, but the micelle sizes were still much smaller than $2l_c$. A Cryo-TEM image for the 10 wt% mixture had poor resolution, probably due to the high ionic strength, and is not shown.

5.3.2.2 Electrical Conductimetry Results

The difference between the conductivity of the surfactant-water mixtures and that of the aqueous medium, $\kappa - \kappa_0$ increased strongly with the surfactant concentration, where κ_0 was 5.5 × 10^{-2} μS·cm^{-1}. From 1.0×10^{-4} wt% to 7.5 wt%, or from 7.8×10^{-4} mM to 63 mM, it increased from 5.8 μS·cm^{-1} to ca. 4,000 μS·cm^{-1} (Figure 21a). This increase indicates that the surfactant micelles substantially dissociated into counterions and charged micelles. The molar conductivities, Λ, (Figure 21b) ranged from a huge value of about 1,500 S·cm^2·mol^{-1} at 6.0×10^{-3} mM, below the

CMC which is 15 ppm[35] or 0.015 mM, to a more modest asymptotic value of ca. 65 $S \cdot cm^2 \cdot mol^{-1}$ at concentrations from 16 mM to 63 mM. These values can be interpreted as follows. Generally, for molecularly dispersed (non-micellar, non-aggregating) 1:1 strong electrolytes Na^+X^-, such as Na^+Cl^-, the molar conductivity, $\Lambda_{\pm}^{\infty}$, at infinite dilution can be expressed as follows.

$$\Lambda_{\pm}^{\infty} = \Lambda_{+}^{\infty} + \Lambda_{-}^{\infty} \tag{10}$$

Here, Λ_{+}^{∞} and Λ_{-}^{∞} are the individual ion molar conductivities at infinite dilution. For example, for NaCl at 25 °C, $\Lambda_{Na^+}^{\infty}$ = 50 $S \cdot cm^2 \cdot mol^{-1}$, $\Lambda_{Cl^-}^{\infty}$ = 70 $S \cdot cm^2 \cdot mol^{-1}$, and Λ_{NaCl}^{∞} = 120 $S \cdot cm^2 \cdot mol^{-1}$. For SDS, or Na^+DS^-, for which Λ_{SDS}^{∞} = 70 $S \cdot cm^2 \cdot mol^{-1}$ $\Lambda_{DS^-}^{\infty}$ = 20 $S \cdot cm^2 \cdot mol^{-1}$.[109] The molar conductivities decrease modestly with increasing ionic strength because of interionic Debye-Hückel-Onsager (DHO) interactions.[110] For example, Λ_{SDS} decreases to about 65 $\mu S \cdot cm^2 \cdot mol^{-1}$ at the CMC of 8 mM. Above the CMC, the SDS micellar molar conductivity ranges from 40 to 30 $S \cdot cm^2 \cdot mol^{-1}$, and it is due to contributions from both Na^+ and the charged micelles.[109]
These effects can be captured by the following equation.[109]

$$\Lambda = \Lambda_{+}^{\infty} f(1-\beta) + \Lambda_{-}^{\infty} f\left(N_{agg}\right)^{\frac{2}{3}}(1-\beta)^2 \tag{11}$$

Here, β is the counterion binding fraction, and f is a factor used to account empirically for the DHO interactions; usually $f < 1$, or $f = 1$, if there are no DHO interactions. Equation (11) implies that if β were zero, or the micelles were fully dissociated, then the aggregation would cause an *increase* in Λ. If β were large (e.g. $\beta = 0.8$ or more), as in SDS, then Λ would decrease, as observed for the SDS and other examples.

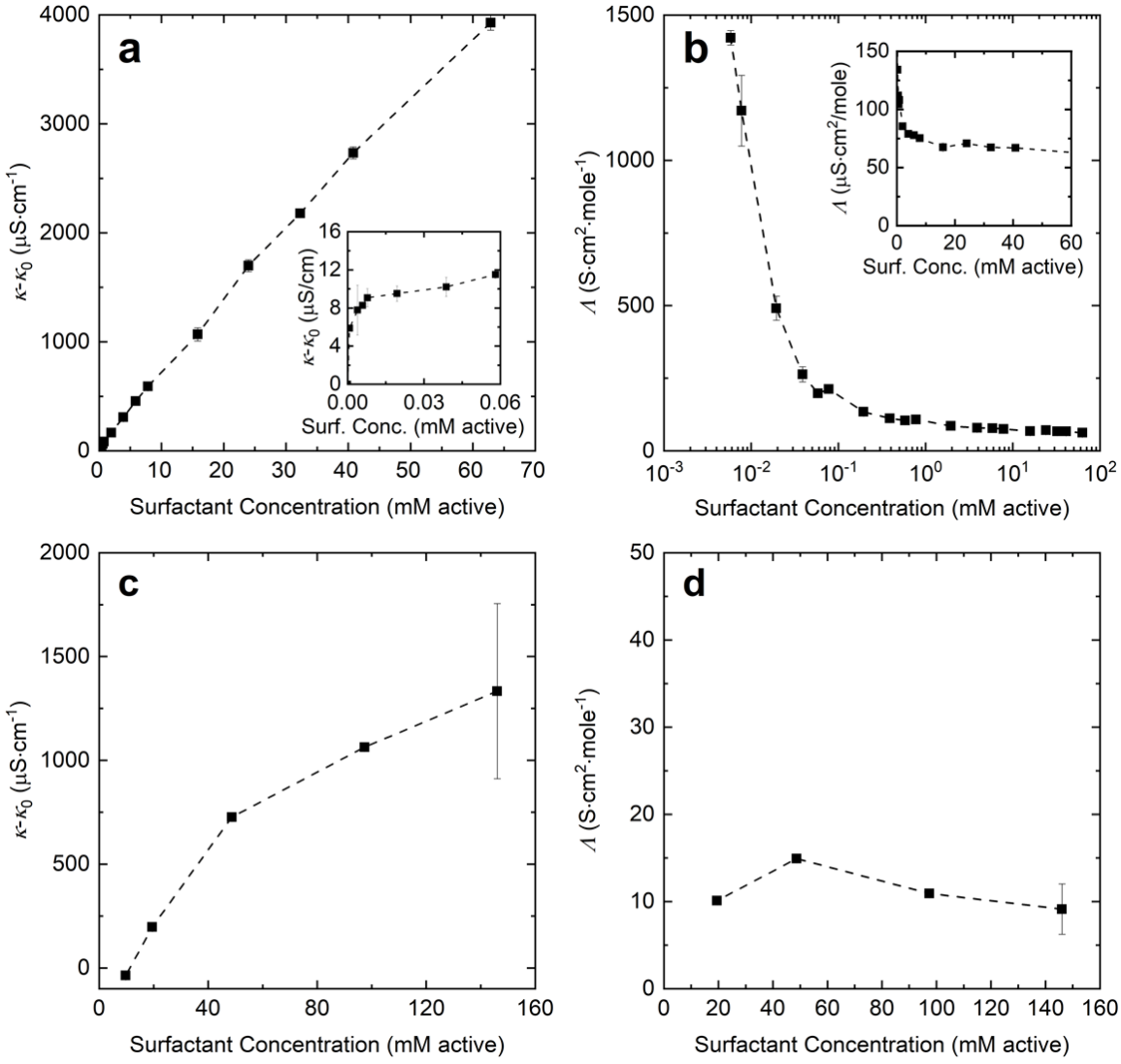

Figure 21. Conductivity (a, c) and molar conductivity (b, d) of surfactant-water solutions (a, b) and surfactant-brine solutions (c, d). The drop in the molar conductivity in b indicates significant changes in mechanism of the conductivity with surfactant concentration increase. The smaller molar conductivities of brine solutions compared to those of water solutions (d vs. b) indicates the higher counterion binding.

The large values of Λ, 1,500 S·cm^2·mol^{-1}, for S13D in water at the lower concentrations can be explained by the presence of highly charged (with $\beta << 1$ or $\beta \approx 0$) of micellar or pre-micellar aggregates at about the CMC, or below; the values of 1,500 S·cm^2·mol^{-1} to 500 S·cm^2·mol^{-1} cannot be explained by any plausible presence of ionic impurities of the S13D surfactant. The drop in Λ to 65 S·cm^2·mol^{-1} beyond the CMC can be accounted for, in part, by β values which become higher, as the concentration increases, and, in part, by increasing effects of

DHO interactions, which are known to increase drastically with increasing ionic strength.[109] Because the value of Λ = 65 S·cm^2·mol^{-1} at the higher concentrations was larger than the value Λ of sodium at infinite dilution, 50 S·cm^2·mol^{-1}, and of course higher than 40 S·cm^2·mol^{-1} for sodium with DHO inter-ionic interactions, the micelles should have a significant contribution to the molar conductivity. From Eq. (11) with Λ_+^∞ = 50 S·cm^2·mol^{-1}, Λ_-^∞ = 15 S·cm^2·mol^{-1}, and N_{agg} = 10, the value of β is estimated to be $\beta \sim 0.33$ for f =1 and $\beta \sim 0.28$ for f = 0.9, indicating that there is some counterion binding at the higher surfactant concentration.

For surfactant-brine mixtures, the conductivity difference $\kappa - \kappa_0$ (Figure 21c), where κ_0 = 15,600 μS·cm^{-1}, increased from 200 μS·cm^{-1} to 1,330 μS·cm^{-1} at concentrations ranging from 14.5 mM to 180 mM (2.47 wt% to 18.5 wt%). The molar conductivities ranged from 9 S·cm^2·mol^{-1} to15 S·cm^2·mol^{-1}, much lower than that of Na^+ ions alone (50 S·cm^2·mol^{-1}); see Figure 3d. For the larger micelles (N_{agg} = 91) and the higher ionic strength (150 mM), these small values imply that β must be quite large. The micelles should contribute to the conductivity, but they may not contribute significantly to the ionic strength, because their radius of 3 nm is larger than the Debye length (~0.8 nm), implying that the micelles behave like large particles rather than small ions. The approximate value of β is estimated as follows. The molar conductivity of the brine is 15,600/150 = 104 S·cm^2·mol^{-1}, or about 20% lower than Λ_{NaCl}^∞. Here, f is taken to be equal to 0.8, because the effect of the DHO interactions causes a decrease of about 20% in Λ. Then, from Eq. (11), we obtain $\beta \approx 0.87$. The results of more counterion binding (lower fractional dissociation) at the high ionic strength are consistent with the inferences from densitometry (see Section 5.2.2.3). The surfactant liquid as received has a low conductivity of only around 8.2 μS·cm^{-1}, and a molar conductivity of 10.4 S·cm^2·mol^{-1}. Even though the origin of these small values is unclear, they suggest that the ionic surfactant is mostly non-dissociated.

5.3.2.3 Densitometry Results

For probing the effects of micellar formation and their dissociation, the densities of the mixtures were measured, and the partial densities of the surfactant in water or in brine were calculated. With increasing surfactant concentration from 0 to 20 wt%, the specific volume of the solution decreased from 1.002 to 0.987 cm^3·g^{-1} for the surfactant-water mixtures, and from 0.996 to 0.982 cm^3·g^{-1} for the surfactant-brine mixtures (see Figure 22). The curves of $1/\rho$ vs. w_1 deviated significantly from the ideal solution curves. Hence, the dissolved surfactant introduces a

significant solution nonideality. Moreover, the value of ΔV_{mix} was negative, implying that the solutions became denser after mixing.

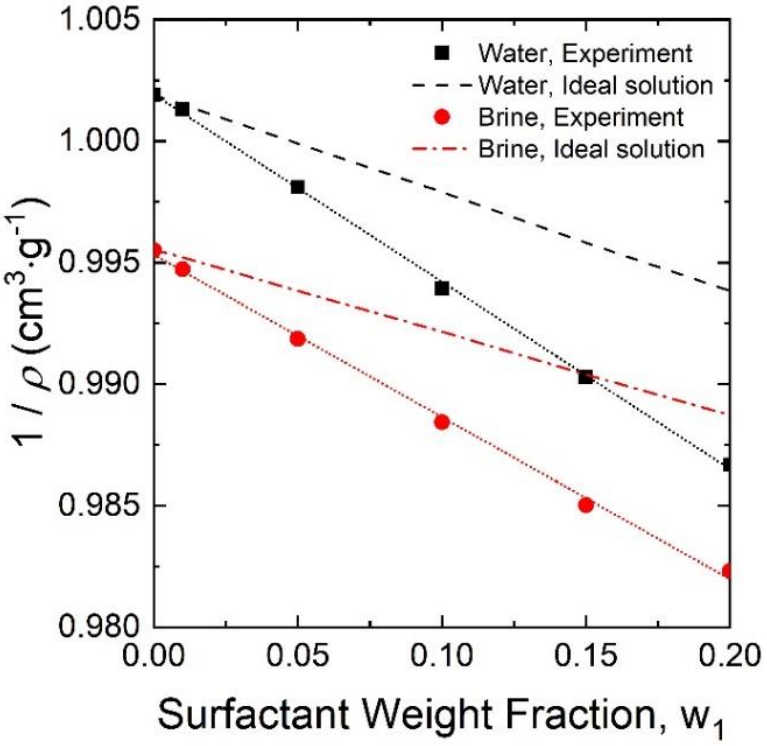

Figure 22. Specific volumes of aqueous surfactant solutions with water (■) or with brine (●); the predictions of the specific volumes for ideal solutions (with ρ_1^0 = 1.05 g·cm^{-3}, ρ_2^0 = 1.002 g·cm^{-3} or 0.996 g·cm^{-3} for water or brine, and $\Delta V_{mix} = 0$) are shown as a black dashed line for water or as a red dashed-dot line for brine. The average partial densities of the surfactant for nonideal solutions are found from the slopes of the fitted lines and Eq. (3), as described in the text.

On the assumption that the specific volume of the water or brine does not change upon mixing, the average partial density of the surfactant in the micelles was independent of the micellar concentration, and equal to 1.085 g·cm^{-3} in water and 1.074 g·cm^{-3} in brine. These values are large relative to the density of the surfactant (1.05 g·cm^{-3}), suggesting that the surfactant molecules become denser upon dissolution, micellization, and some ionic dissociation, as inferred from the conductivity data. Typically, as an electrolyte dissolves in water, it dissociates and hydrates; its density increases because of strong attractive electrostatic attractive interactions between the ions and the water of hydration.[111] In one example, whereas the density of NaBr crystals is 3.2 g·cm^{-3},[112] the sum of the partial densities of hydrated Na^+ and Br^- ions at infinite dilution is 4.04 g·cm^{-3} or a 26% increase.[111] For the surfactant in water, the density increase is only 3.3%. This density

increase is probably not due to any changes in the partial density of the isopropoxylated hydrocarbon chains, because the hydrocarbon chains should be liquid-like in the surfactant liquid and should remain liquid-like in the micelles. The effect of any change in the density of the isopropoxylate moieties at the two states is unclear. The change should be due to the partial ionic dissociation and hydration of the sodium and sulfate ions. In brine, the density increase is smaller, only about 2.3%, probably because the percentage of the dissociation is smaller, as also inferred from the conductivity results.

5.3.3 SAXS Results for Solutions, Liquid Crystalline Phases, and Multiphasic Dispersions

To corroborate the initial data described above, SAXS analyses were performed. Using this technique, the domain spacing values for the different self-assembled nanostructures were quantified, and the phases associated with the various water-surfactant and brine-surfactant mixtures were identified. For the isotropic liquid surfactant-water mixture, at 10 wt%, only a broad peak was observed at $q^* \approx 1.10$ nm^{-1}, indicating a lack of long-range order, as expected (Figure 23a). We presume that the peak arises primarily from the shell-like structures of the sulfate head groups around the micelle core and the condensed or dissociated counter-ions around the micelles.[108,113–115] The resulting average spacing, $2\pi/q^* \approx 5.71$ nm, represents the distance from the center of one head group on a micelle to the center of another head group across the micelle.[116,117] This value is larger than the micelle diameter, 3 nm, obtained from the DLS data. The difference is not surprising, because the dimension obtained from the SAXS analysis is an average distance between two electron-dense areas of the head groups and the counterions, including the Stern layer and the Gouy-Chapman layer; a micelle schematic is shown in Figure 24.

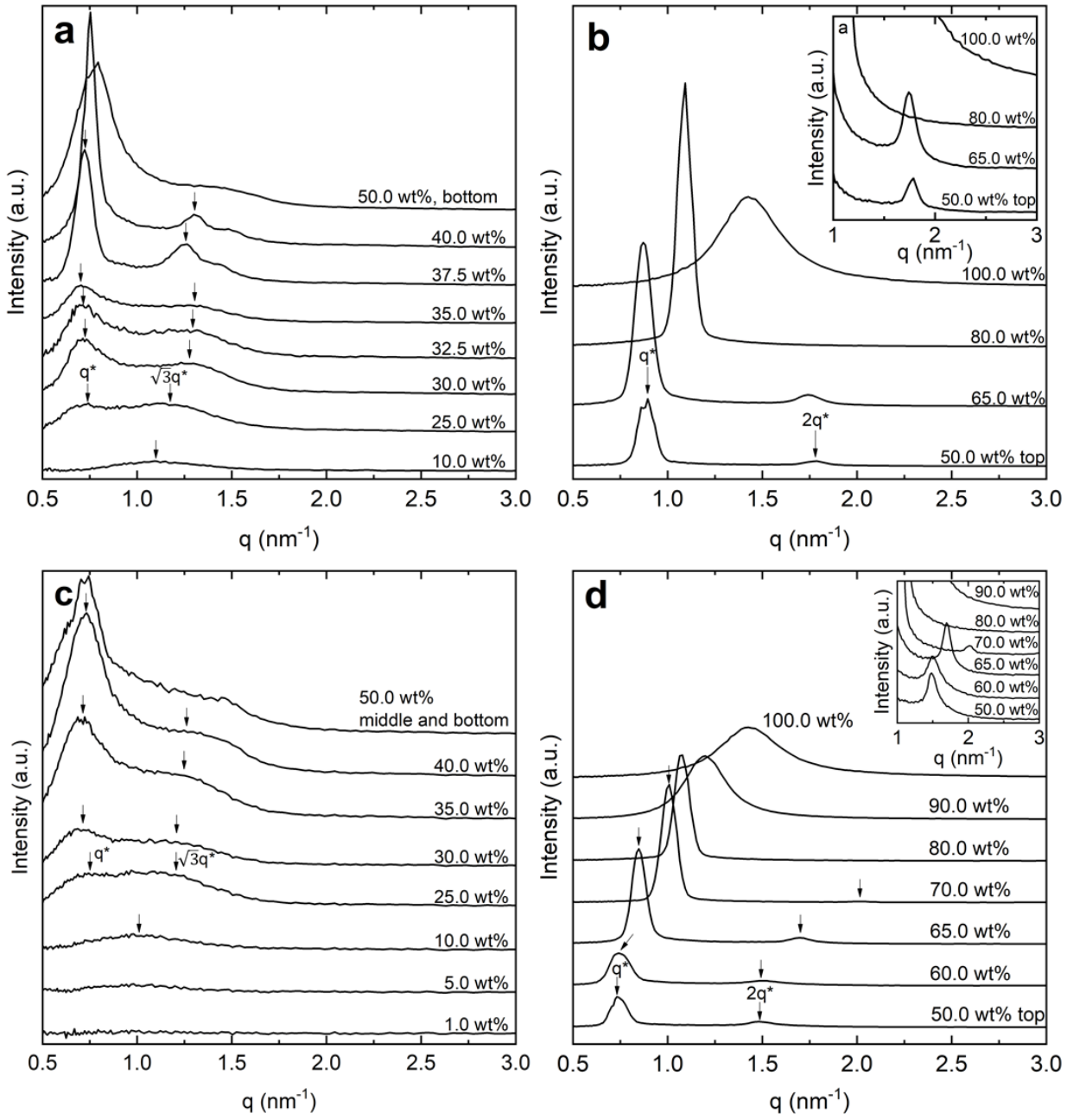

Figure 23. SAXS spectra for the surfactant-water mixtures (a) below 50 wt% and (b) above 50 wt% and for the surfactant-brine mixtures (c) below 50 wt% and (d) above 50 wt%.

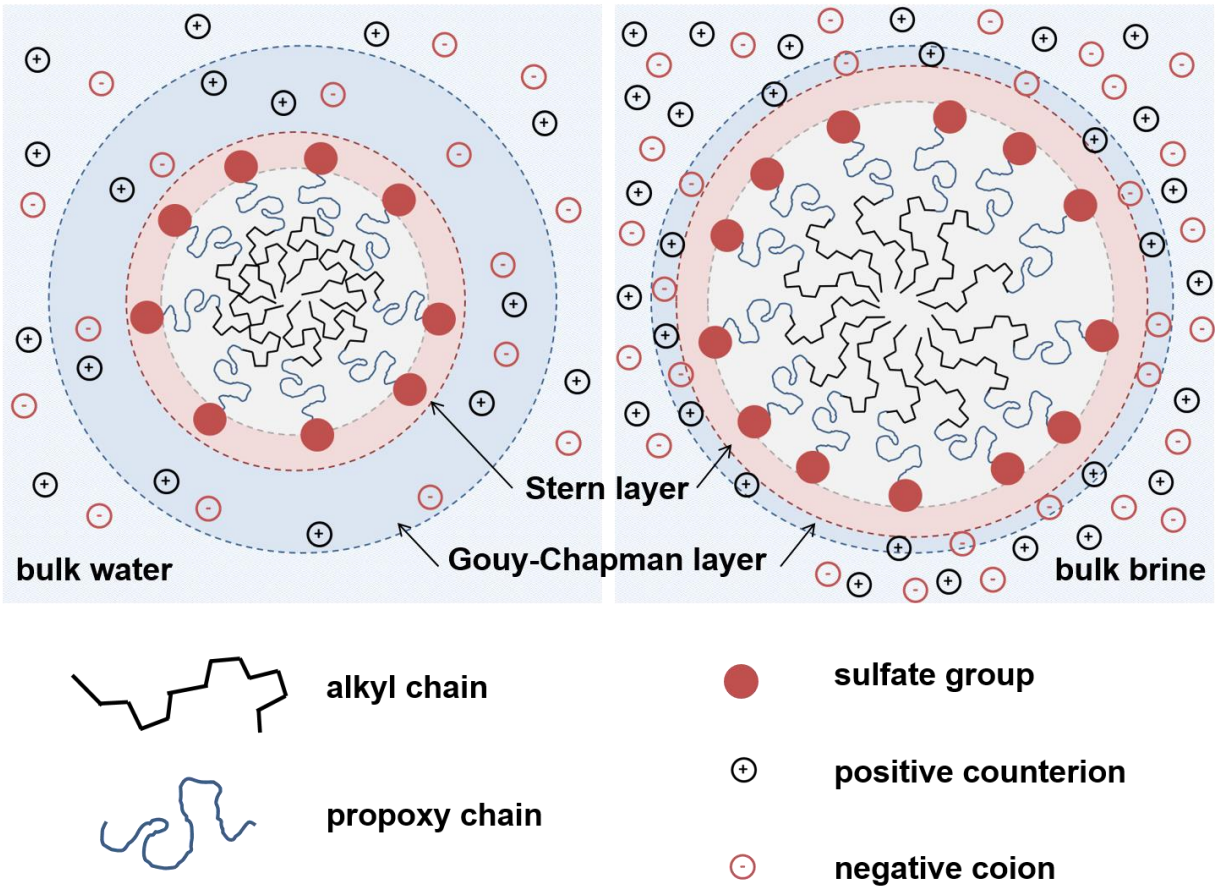

Figure 24. Schematic diagrams of a surfactant micelle in water and in brine. As ionic strength of the solvent increased from 0 (water, left) to 150 mM (brine, right), Debye length got smaller, and the thickness of the polar group and the counterion became thinner. The sketches of the alkyl and isopropoxy chains are not aimed to represent physical conformations but to differentiate the two chain types.

At 25 wt%, two broad peaks were observed at $q^* \approx 0.705$ nm^{-1} and 1.20 nm^{-1}. These peaks probably overlapped also with an underlying peak of the micellar solution, at $q^* = 1.10$ nm^{-1}. Because the ratio equaled $1.70 \approx \sqrt{3}$, we interpret these data to indicate the formation of a hexagonal liquid crystalline phase H_1, for which, the relative values, q_1:q_2:q_3 …, usually follow the relationship 1:$\sqrt{3}$:2 ….[91,92,118] The distance, a, between the centers of adjacent cylindrical elements or aggregates was obtained from the q^*-value to be 10.1 nm in Equation (12) and plotted later in Figure 25.

$$q* = \frac{4\pi}{\sqrt{3}a} \qquad (12)$$

Hence, at surfactant concentrations above its solubility in water, a hexagonal liquid crystal phase, H_1, formed. It evidently consisted of rod-shaped micelle-like units, which were ordered in two dimensions. At this concentration, this H_1 phase was dispersed in a saturated micellar solution.

At 30 to 35 wt%, a major peak was observed at $q^* \approx 0.716$ nm^{-1}, with a "shoulder" at $q^* \approx 1.28$ nm^{-1}. The a-value was again 10.1 nm (Figure 25a), implying the presence of the same hexagonal liquid crystalline phase, coexisting with the micellar solution.[119] Hence, the mixtures with 25, 30, 32.5 and 35 wt% were biphasic dispersions. At 37.5 and 40 wt%, the major peak shifted slightly to 0.716 and 0.762 nm^{-1}, and this indicates that the a-value decreased to 10.1 and 9.52 nm. This spacing decrease was attributed to the shrinking of the water channels between the adjacent cylinders as the amount of the water decreases. Evidently, at these concentrations, as suggested by the X-ray scattering patterns, only the H_1 phase was present.

At 50 wt%, where the sample separated into two layers (as reported in section 5.2.1), and probably two phases. The bottom layer had the same SAXS pattern of an H_1 phase, with $q^* \approx 0.795$ nm^{-1} and $a \approx 9.12$ nm. The top layer had $q^* \approx 0.879$ nm^{-1} and 1.77 nm^{-1} and the ratio equaled 2.01 (Figure 23b), indicating an LLC structure, or a phase L_α, for which, the positions of the reflection usually follow the relationship, q^*, $2q^*$, and $3q^*$. The lamellar periodicity, d, or the distance between two adjacent lamellae was determined to be $d = 2\pi/q^* = 7.15$ nm. Thus, the 50 wt% sample was a biphasic H_1+L_α dispersion.

At 65 wt%, an LLC structure was also detected with $q^* \approx 0.867$ nm^{-1} and the ratio equaled to 2.01, and $d = 7.23$ nm. The thickness of the water layer l_w in the lamellae is equal to $d(1\text{-}\varphi) = 2.6$ nm, where φ is the volume fraction of the surfactant and can be obtained from the weight fraction and the partial densities of the surfactant and water. At 80 wt%, only one sharp peak was detected, with a similar shape as the main peak at 65 wt%. For this reason, and because of the observed birefringence, this sample was presumed to be an L_α phase. The reason for the absence of the second peak is unclear; however, it may be due to some destructive interference.[120] Within the L_α phase region, as the water weight fraction decreased, the water layer thickness and the distance between the lamellae layers decreased, as expected; see Figure 7b.[92,119] For the surfactant alone (100 wt%), only one broad peak at $q^* \approx 1.43$ nm^{-1} was observed, confirming an isotropic liquid phase structure, with some local microdomains. The length scale from the peak is $2\pi/q^* \approx 4.39$ nm.

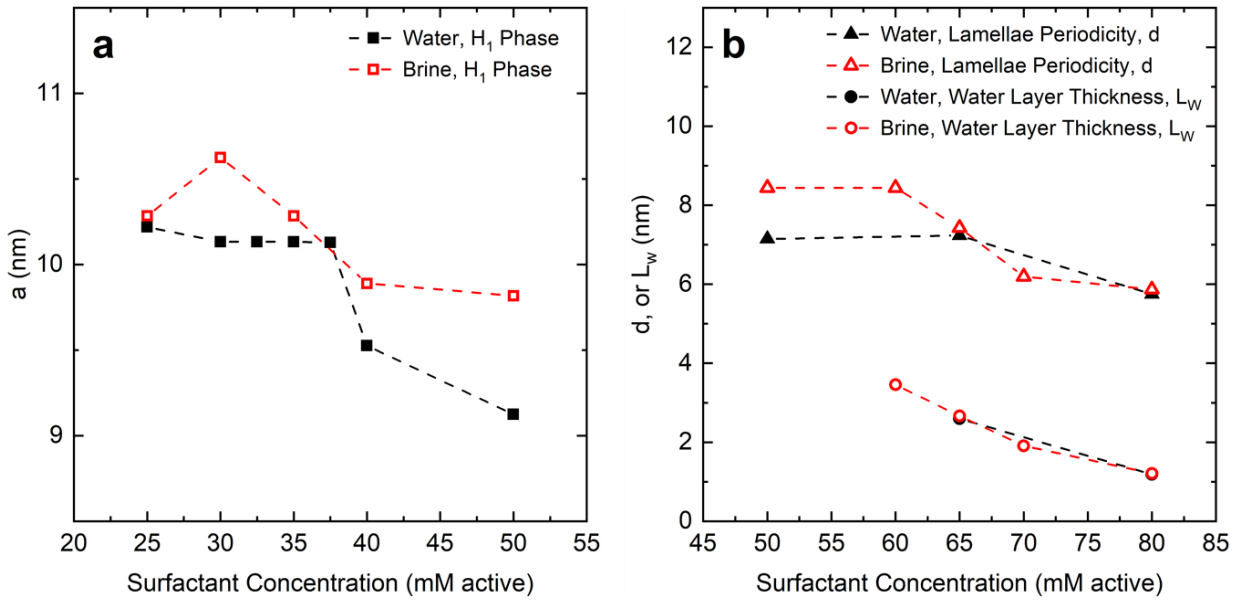

Figure 25.(a) Distance, a, between the centers of adjacent cylinders of the hexagonal structures as a function of surfactant concentration for the surfactant-water mixtures (■) and the surfactant-brine mixtures (□). (b) Lamellae periodicity, d, of the lamellar structures (▲ or △), and the thickness L_w of the water layer in the lamellar structures (● or ○) as a function of surfactant concentration. The closed and the open symbols represent the surfactant-water mixtures and the surfactant-brine mixtures, respectively. The broken lines are used to guide the eye.

For the surfactant-brine mixtures, similar trends were observed in Figures 23c and 23d. For 1 to 10 wt%, only one peak was observed for all concentrations at $q^* \approx 1.00$ nm^{-1}; it was attributed again to the core-shell structure of the ionic micelles.[108,113–115] The peak intensity increased as the micelle concentration increased, as expected, suggesting no effects of intermicellar interactions.[116,121] The average distance between two electron-dense regions across the micelle is around 6.2 nm, which was consistent with the micelle diameter measured with the DLS. Evidently, the high ionic strength (~150 mM) of the brine leads to a small Debye length (~0.8nm), yielding a thinner layer of polar groups and counterions (Figure 24).

At 25 wt%, a broad double peak was observed, with $q^* \approx 0.706$ nm^{-1} and 1.21 nm^{-1}, and the ratio equaled to 1.71, suggesting again the presence of an H_2 phase, which is dispersed in a micellar solution, hence an L_1+H_1 biphasic dispersion. At 30, 35, and 40 wt%, the major peak was found at $q^* \approx 0.714$ nm^{-1}, with a shoulder at $q^* \approx 1.31$ nm^{-1}. Because the ratio of the major peaks was about 1.84, slightly larger than $\sqrt{3}$, and the shoulder was not sharp as observed in the water system, we infer that the mixtures had probably an HLC phase dispersed in a saturated micellar

solution. A broad peak of the micellar solution was apparently superposed on the second peak of phase H_1, shifting its position to a slightly higher q^* value. The corresponding a-values were about 10.3 nm (Figure 25a).

At 50 wt%, the sample separated into three distinct layers suggesting three phases. The SAXS curves for the sample consisting of the middle and the bottom layers were similar to the one for 40 wt%, indicating a similar structure, an HLC coexisting with a micellar solution. By contrast, the top layer was inferred to be an L_α phase with the major peak ratio of 2.01. The first prominent peak was observed at ~0.744 nm^{-1}, corresponding to d = 8.44 nm. At 60 and 70 wt%, the data suggest also an LLC structure of an L_α phase. At 80 wt%, the sharp major peak and the observed birefringence suggest also an L_α phase. With increasing concentration within the one-phase L_α region, the q^* value increased. The d-value decreased from 8.44 nm at 60 wt% to 5.87 nm at 80 wt%, probably due to the confined water layer becoming thinner with decreasing water concentration (Figure 25b). The water layer decreased from 3.46 nm at 60 wt% to 1.21 nm at 80 wt% while the lipid chain length remained constant, around 2.34 nm. At 90 wt%, a broad peak suggests an L_2 liquid isotropic phase similar to the one of the 100 wt% surfactant liquid. The added water was probably absorbed by the possible micro-domains in the liquid surfactant and increased the dimension $2\pi/q^*$ from 4.39 nm to 5.26 nm. The SAXS results, on their own, identified the phases present in each mixture, as well as their nanostructures, or the domain spacing of the structure observed. However, the use of SAXS for determining the boundaries between the phases with large accuracy would have required a large number of tests; the support from the visual and microscopic observations was, therefore, necessary to construct an overall phase map below. An additional phase, a bicontinuous cubic phase (V_2), is often observed with conventional surfactants,[122] and it was also reported for the extended surfactant.[103] It appears unlikely that such V_2 phase exists with S13D, because then no H_1 + L_α biphasic region would be observed, and no biphasic regions H_1 + V_2 and V_2 + L_α were observed. Their absence could be due to the multicomponent nature of the surfactant.

5.3.4 Phase Maps of the Surfactant-Water or Surfactant-Brine Mixtures

An apparent phase map has been constructed for these systems at 22 °C (Figure 26). From the data available, for the surfactant-water mixtures, four single-phase regions and two biphasic regions were determined. The progression of phases with increasing surfactant concentration is as

follows: (1) a micellar solution phase, L_1; (2) a hexagonal liquid crystalline phase, H_1; (3) a lamellar liquid crystalline phase, L_α, and (4) an isotropic liquid phase, L_2. In these systems, (a) a biphasic L_1+H_1 region was clearly observed, (b) a biphasic H_1+L_α region was inferred, and (c) a possible L_α+L_2 biphasic region was not detected at the concentrations examined. No other liquid crystalline phases were detected.

For the surfactant-brine mixtures, the same four phases, L_1, H_1, L_α and L_2, were detected. The progression of the phases actually observed is L_1, L_1+H_1, L_1+H_1+L_α, L_α, and L_2. The presence of the three phases was discussed in section 2.7. Therefore, the presence of the salts for this brine introduces some minor quantitative shifts of the phase boundaries of S13D with water, but the qualitative phase map remains the same.

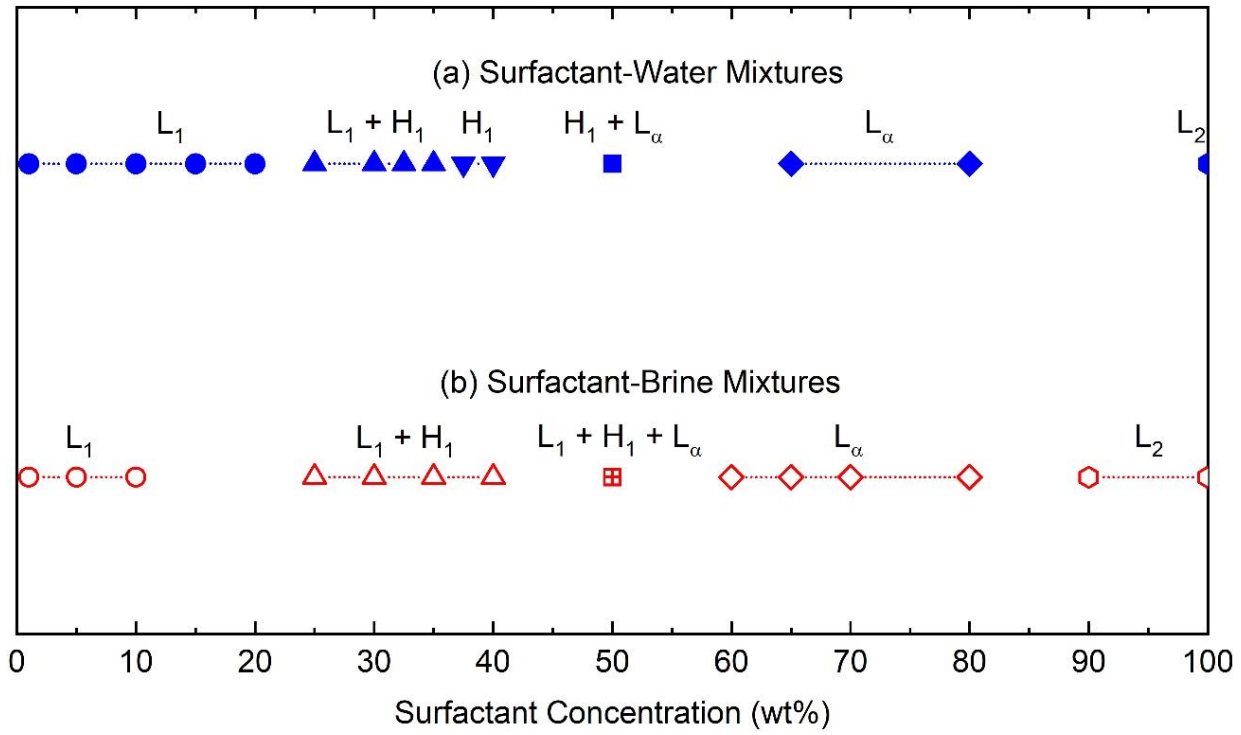

Figure 26. Phase maps at 22 ℃ of (a) the surfactant-water mixtures and (b) the surfactant-brine mixtures, as determined using visual observations, polarizing microscopy, and SAXS. Different symbols represent different phases or dispersions. The broken lines are used to guide the eye.

No detailed tests of the stability of the phases were done to establish phase equilibrium more rigorously, or to probe for any possible metastability effects. Nonetheless, we expect that there is a small probability that the detected phases were non-equilibrium, because (i) the liquid

surfactant formed the ordered phases H1 and Lα spontaneously when it was mixed with water or brine; (ii) the mixing was done isothermally; and (iii) the phases were stable. Further studies of the stability of the phases or dispersions to heating or cooling could provide more definitive tests. However, these robust initial data indicate that multicomponent surfactants can have similar phase behavior as that seen for single-component, single-chain, non-extended anionic surfactants. This similarity indicates the potential impact of the presented results and has significant implications for the uses to application-relevant surfactant-water mixtures.

5.3.5 Rheological Behavior of the Isotropic L_1 and L_2 Phases

The L_1 phases, for 1 wt% to 20 wt%, and the L_2 phases from 90 wt% to 100 wt% behaved essentially as Newtonian fluids. For shear rates, $\dot{\gamma}$, between 1 and 100 s^{-1}, the shear viscosities were the same, to within 20% or less. With increasing surfactant concentrations from 1 to 20 wt%, the viscosity at $\dot{\gamma} = 100$ s^{-1}, increased from 1.0 to 5.27 cP (Figure 27a). For the L_2 phase, the viscosities were high, 1,600 cP at 100 wt%, and approximately 1,000 cP at 90 wt%.

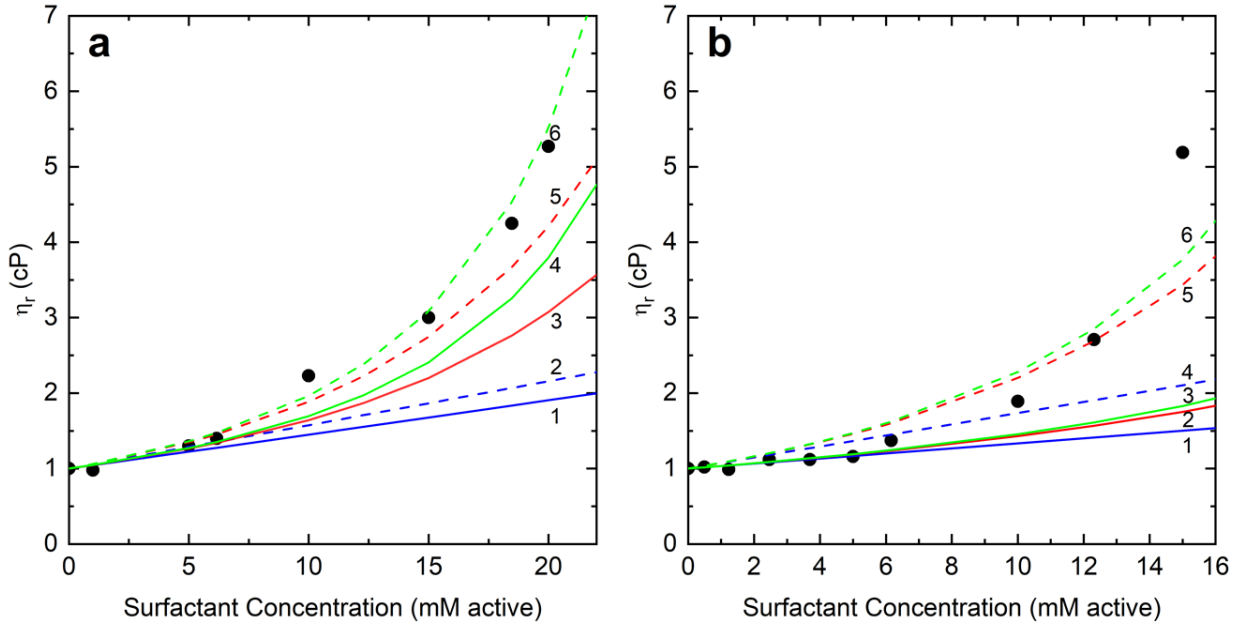

Figure 27. Relative viscosities (●) of isotropic solutions of surfactant-water mixtures (a) and surfactant-brine mixtures (b) as a function of the surfactant concentration, and predictions from various literature equations for spheres, with an intrinsic viscosity $[\eta] = 2.5$ or for oblate spheroids with $[\eta] = 3.2$ or 5.5; see text for details. Line 1: Einstein's equation for spheres; Line 2: Einstein's equation for spheroids; Line 3: Eq. (16) for spheres; Line 4: Eq. (16) for spheroids; Line 5: Krieger-Dougherty Equation, Eq. (17), for spheres; Line 6: Krieger-Dougherty Equation, Eq. (17), for spheroids.

The relative viscosities, $\eta_r = \eta/\eta_s$, of the micellar solutions, where η is the solution viscosity and η_s is the viscosity of the solvent, were compared to the predictions of various model equations, in which the micelles were treated as "dispersed particles." The effective volume fraction, $\varphi_{m,\ hydrated} \equiv \varphi_m$, of the hydrated micelles was estimated from the non-hydrated micelles volume fraction $\varphi_{m,\ non\text{-}hydrated}$, the micelle diameter d_h of around 3 nm in water, and the hydrated radius of the sulfate group, $\sigma_{sulfate}$, ca. 0.37 nm.[123–125]

$$\phi_m = \phi_{m,non-hydrated}\left(1 + \frac{2\sigma_{sulfate}}{d_h}\right)^3 \tag{13}$$

The non-hydrated micelles volume fraction was calculated from the density ρ of the solutions, and the partial density $\overline{\rho_1}$ of the surfactant.

$$\phi_{m,non-hydrated} = \frac{\rho}{\overline{\rho_1}} w_1 \tag{14}$$

The generalized Einstein relation, Eq. (15), is used first,

$$\eta_r = 1 + [\eta]\phi_m \tag{15}$$

where $[\eta]$ is the intrinsic viscosity, generally, a parameter based on the particle shape; for a spherical particle $[\eta]$ = 2.5, and for an oblate spheroid with an axial ratio of 2.0, $[\eta]$ = 3.2, as calculated from the Simha theory.[59] Equation (10) is valid for non-interacting particles with relatively low volume fractions, well below 0.1, at which there are no significant interparticle hydrodynamic interactions.[59,126] For higher volume fractions, the effect of particle "crowding" should be considered. Then, a general empirical equation for the relative viscosity vs. φ_m was used as follows.[59]

$$\eta_r = (1 - \phi_m)^{-[\eta]} \tag{16}$$

Equation (16) reduces to the Eq. (15) for $\varphi_m \ll 1$. To account for the maximum allowed value of ϕ_{m}, or ϕ_{max}, due to excluded volume and packing effects, Eq. (16) as modified by Krieger and Dougherty was used[59,126]

$$\eta_{\mathrm{r}} = \left(1 - \frac{\phi_{\mathrm{m}}}{\phi_{\mathrm{max}}}\right)^{-[\eta]\phi_{\mathrm{max}}} \tag{17}$$

where ϕ_{max} is taken to be 0.64 for a randomly close-packed spheres.[59]

The predictions from Eqs. (15)-(17), for $[\eta]$ = 2.5 or 3.2, are shown in Figure 27a (Line 1–5). The predictions from Eq. (15) fit the data only for the concentrations up to 5 wt% for either shape, and underestimate the data significantly at the higher concentrations, at which the data follow more closely the predictions from Eqs. (16) and (17). Equation (17) with $[\eta]$ = 3.2 fits the data the best. The small discrepancies may be attributed to interactions among the micelles, or to the effects of increasing micelle sizes at the highest concentration. Even though one may infer that the micelles have an oblate spheroidal shape with an axial ratio of 2.0, there is no direct evidence for it. Hence, an assumption of a spherical shape was used for calculation of the aggregation numbers in Section 5.2.2.1.

For surfactant-brine mixtures, the micellar solutions, for 0.5-20 wt%, behaved also as Newtonian fluids (Figure 28). For 0.5 wt% to 15 wt%, the viscosity at $\dot{\gamma}$ = 100 s^{-1} increased from 1.0 cP to 5.2 cP (see Figure 27b Line 1). The relative viscosities were compared to the predictions of Eqs. (15)-(17) with $[\eta]$ = 2.5 for spherical particles or 5.5 for oblate spheroids with an axial ratio of 6.0.[59] Equation (17) with $[\eta]$ = 5.5 best fits the data up to 12 wt%. The discrepancy at the higher concentrations of 15 wt% may be due to significant micellar interactions or to the formation of larger micelles or non-spherical micelles.

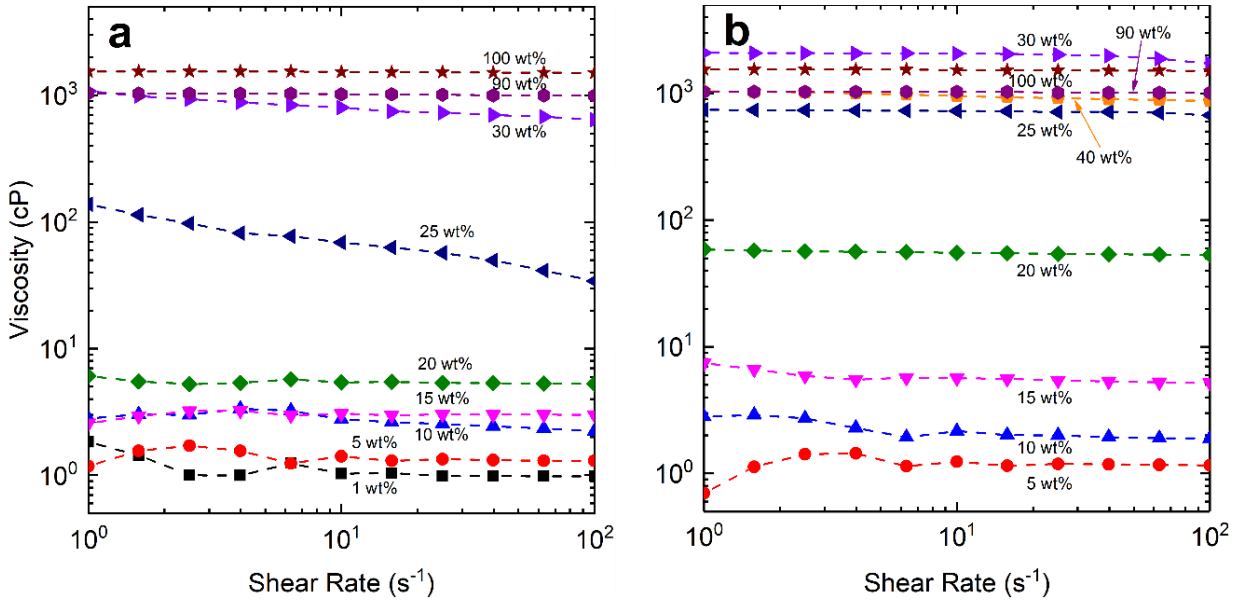

Figure 28. Shear viscosities of (a) surfactant-water mixtures and (b) surfactant-brine mixtures. For 1 and 5 wt% surfactant-water mixtures and for the 5 wt% surfactant-brine mixture, the accuracy of the viscosity data at shear rates below 10 s^{-1} is limited by the instrument response.

5.3.6 Rheological Behavior of Lyotropic Liquid Crystals and Biphasic Dispersions

5.3.6.1 Surfactant-Water Mixtures

Unlike the samples in the L_1 phase, the L_1+H_1 biphasic dispersions (25 wt% and 30 wt%) showed a shear thinning behavior (Figure 28a). No measurements of $\eta(\dot{\gamma})$ were obtained for the samples in the H_1 phase (37.5 wt% and 40 wt%) or the L_α phase (60 wt% and 70 wt%), because they showed a gel-like behavior with an apparent yield stress. Instead, the storage and the loss moduli, G′ and G″, were measured with oscillatory tests (Figures 29 and 30) as a function of the shear strain and the frequency. The corresponding phase angles $\delta = \tan^{-1}$ (G″/G′) were then calculated.

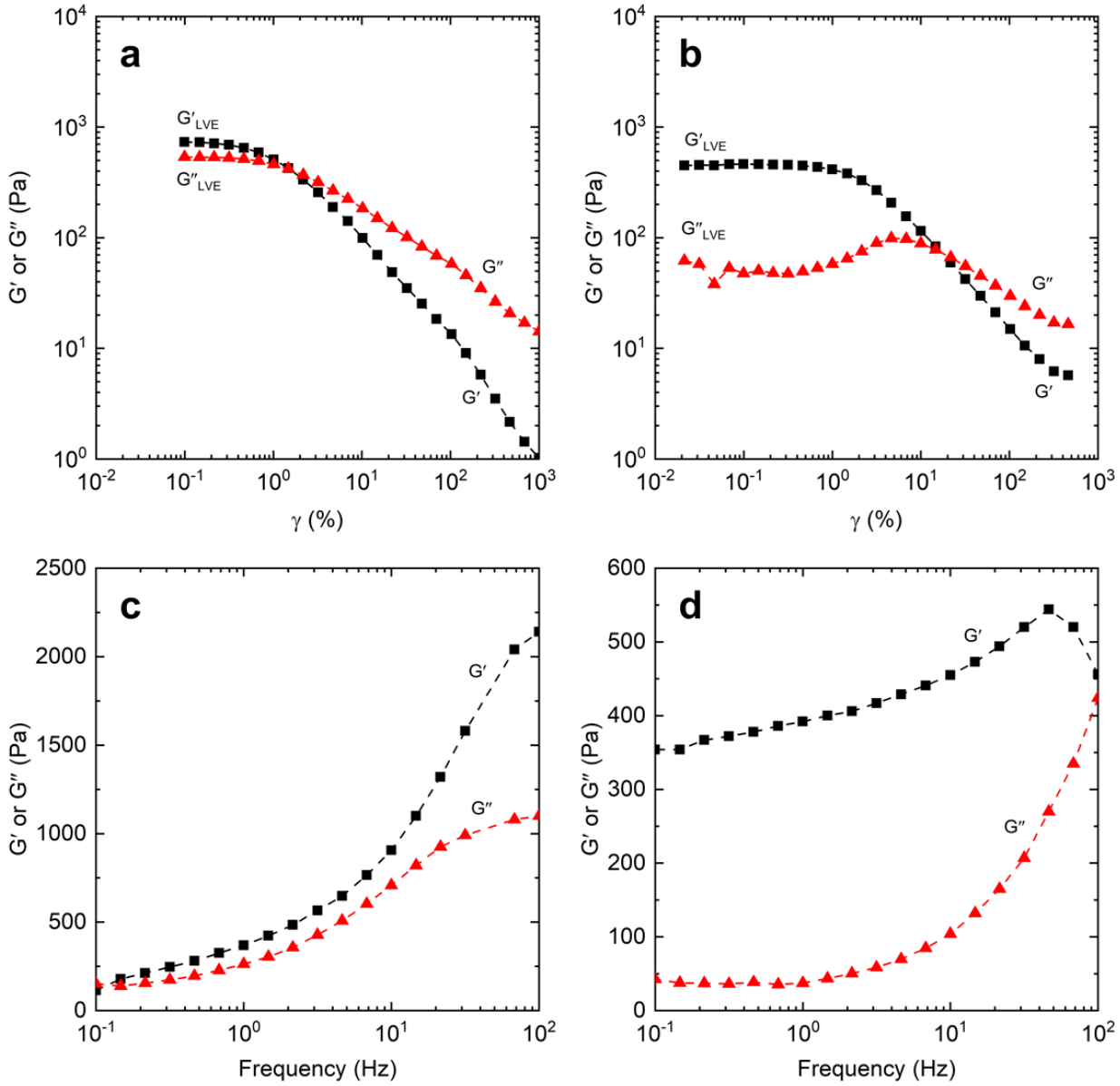

Figure 29. Amplitude sweeps at 1Hz (a, b) and frequency sweeps at 0.1% strain (c, d) for surfactant-water mixtures at 40 wt% (a, c), and 65 wt% (b, d). See Table 3. The data close to the limit of the instrument, i.e., at frequencies close to 100 Hz, are not considered reliable, because of possible inertial and other instrument artefacts.

In the amplitude sweep tests, at 1 Hz for all gel-like samples, G′ was higher than G″ at the lower range of strains, indicating a viscoelastic solid behavior. With increasing strain, both moduli decreased. Beyond a critical strain, γ_{crit}, at which G′ = G″, G′ fell below G″, indicating a transition to a viscoelastic fluid behavior. The materials with a higher γ_{crit}, could sustain a larger deformation before flowing. The shear stress corresponding to γ_{crit} can be used as an estimate of the yield stress,

τ_y, of the material. For the samples in the H_1 phase (37.5 wt% and 40 wt%) and in the linear viscoelastic (LVE) region, the plateau values of G'_{VLE} and G''_{VLE} decreased from 1,600 Pa to 729 Pa and from 680 Pa to 533 Pa, respectively (Figure 29a and Table 8). The phase angle in the LVE region increased from 23° to 36°, indicating that the hexagonal liquid crystal was softer and less elastic at the higher concentrations. As the concentration increased, γ_{crit} and τ_y also decreased. In the frequency sweep tests and for 40 wt% (Figure 29c), or in the H_1 phase region, G′ was larger than G″ over most of the frequencies, and hence the rheological behavior was mostly elastic. As the frequency increased, G′ increased more rapidly than G″, and δ decreased from 53° to 28°; hence, the material exhibited an even more elastic response. A crossover of G′ and G″ was observed at the low end of the frequency range examined (Figure 29c). The inverse of this crossover frequency is the longest relaxation time τ_{max}, which is the characteristic time after a structured material relaxes back to its unperturbed state. At 37.5 wt% the crossover was estimated by extrapolation at lower frequencies, in which measurements are not available. At 40 wt% and 37.5 wt%, τ_{max} = 9 s and 20 s. The results indicated that the hexagonal liquid crystal structure relaxes fast to its initial state after the removal of the stress.[92]

Table 8. Rheological data from amplitude sweeps at 1 Hz of surfactant-water mixtures at various concentrations

c_s, wt%	G'_{LVE}[a], Pa	G''_{LVE}[a], Pa	δ	γ_{crit}, %	τ_y, Pa
37.5	1,600	680	23	7.0	32.4
40	729	533	36	1.5	8.9
60	231	24	6	21.7	12.0
65	460	48	6	14.0	19.3
70	390	70	10	7.5	8.0

[a] G′ and G″ in the constant linear viscoelastic range; see Figure 29.

For the samples in the L_α phase (60 wt% to 70 wt%), a different complex rheological behavior was observed. In the linear viscoelastic region of the amplitude sweep tests, G'_{VLE}, G''_{VLE}

and δ were much smaller than the ones in the H_1 phase (Figure 29b and Table 8). These results indicate that the lamellar liquid crystalline phase was softer, but exhibited a more elastic behavior, than the hexagonal liquid crystal. The slight increase in δ from 6° to 10° at 70 wt%, may be due to the smaller thickness of the water layer in the lamellar structure. Relative to the H_1 phase, the lamellar liquid crystal also has a greater critical strain γ_{crit}. Moreover, the behavior is markedly frequency-dependent (Figure 29c and 29d). In the frequency sweep tests, and at 65 wt% (L_α phase) even though G′ was larger than G″ over a large frequency range (Figure 29d), G″ increased faster than G′, indicating some mechanical dissipation. Because no low-frequency crossover was observed, τ_{max} was probably quite large, suggesting that the lamellar liquid crystal showed some plastic behavior, consistent with published reports for similar systems.[92,127] One plausible physical mechanism for this plasticity is having successive lamellae sliding past each other, so that there is no driving force for the structure to relax back to its original state. By extrapolating G′ and G″ to their crossover frequency, a short relaxation time was inferred at a high frequency (Table 9), τ_{min} = 0.009 s, which probably corresponds to relaxation of the confined water layer. This relaxation time was of the same order as reported values for water layers confined in ultrathin lamellae in other types of systems.[128] At 60 wt% and 70 wt%, the relaxation times were about 0.008 s and 0.015 s. As the water content decreased, the water layer thickness decreased, and hence, the relaxation times of the confined water layers were longer. Generally, the results for the micellar solutions were quite reproducible, qualitatively and quantitatively.

Table 9. Relaxation time of confined water obtained from the data of frequency sweeps

c_s, wt%		60	65	70
τ_{min}, s	Water	0.008	0.009	0.015
	Brine	0.011	*	*

*No data are available at these conditions.

5.3.6.2 Surfactant-Brine Mixtures

At 25–40 wt% surfactant with brine, the dispersions had shear-thinning behavior, similar to the surfactant-water mixtures (Figures 28 and 30). The amplitude data at 40 wt% and at 1 Hz (and also at 10 Hz; data are not shown) showed that G″ was much higher than G′ at all strains, indicating a very small elasticity with phase angles ranging from 80° to 89°. These data support the previous inferences that the mixtures were "fluid biphasic dispersions." A similar behavior to that reported for the surfactant-water mixtures was also observed at 60 wt% in brine for the amplitude and the frequency sweeps in the L_α region (Figures 30b and 30c). The phase angles were so small, ~8° that no low-frequency relaxation was observed, and a high-frequency relaxation was observed with a τ_{min} = 0.011 s (Table 9)." At 65 wt% and 70 wt% in brine, no data are available.

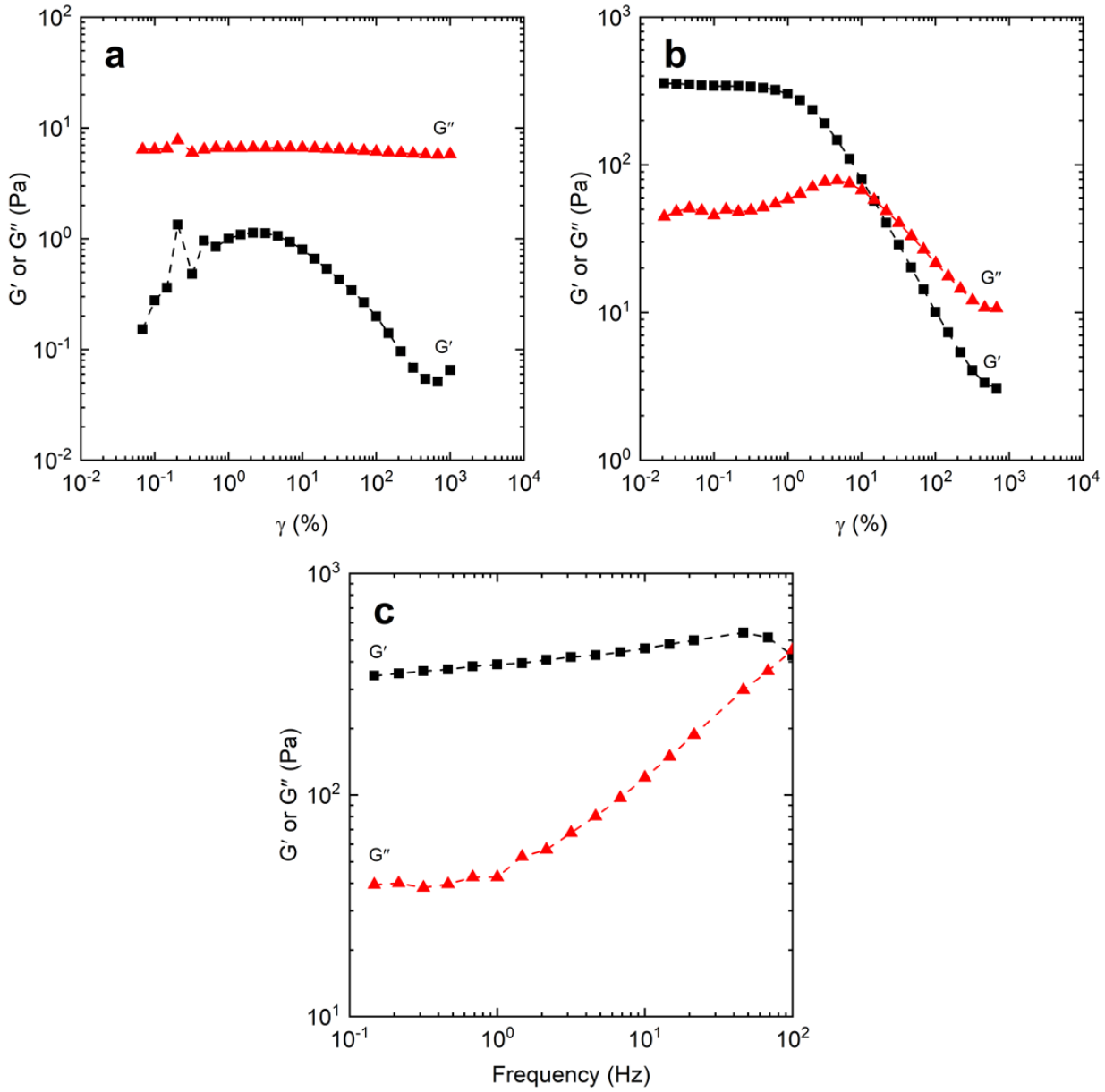

Figure 30. Amplitude sweeps at 1 Hz for (a) 40 wt% and (b) 60 wt% surfactant-brine solutions; (c) frequency sweep at 0.1% strain for 60 wt% surfactant-brine solution. The 40 wt% surfactant-brine solution had so small elasticity, with phase angles are between 80° and 89°, indicating that the solution behavior was primarily viscous.

5.4 Conclusions

The phase behavior and rheological properties of S13D, a commercial isopropoxylated, EOR-relevant, anionic surfactant, were established for the first time. Certain water solutions and brine solutions where the salt loading mimicked the conditions of an actual reservoir were fully characterized. The surfactant has a high solubility in both water and brine at 25°C. The high solubility and its salt dependence are due to the formation of micelles above a very low CMC, 15 ppm in water and 1.2 ppm in brine.[35] The micelles are highly charged at the low ionic strength of pure water. In brine, the micelles have a much larger counterion condensation fraction, and are significantly larger, 6 nm, compared to 3 nm in water, indicating weaker electrostatic repulsive forces among the polar head groups. Then, in brine, the hydrophobic chains become more extended in the micelles, consistently with their behavior at the aqueous/oil interfacial region.[35]

Above the solubility, the S13D surfactant in both water and the brine used forms a hexagonal liquid crystalline phase, H_1. At higher concentrations it forms a lamellar liquid crystalline, L_α phase, which is gel-like and less stiff than the H_1 phase. Importantly, the micellar and liquid crystalline phases observed followed a similar trend in their phase and rheological behavior as those for common single-component, single-chain, non-extended anionic surfactants. This nanostructural behavior, as observed using many direct and indirect structural characterization techniques, was consistent with the observed rheological behavior, similarly, as observed for non-extended surfactants. The gel phases were characterized, and the associated yield stresses were quantified. The rheological data of the micellar solutions could be of significant practical use when considering formulations for mixing, pumping, and delivery of the surfactant-water mixtures. The rheological data of the lyotropic liquid crystalline phases, on the other hand, are important in the processing of the surfactants in their production or uses. These results provide valuable engineering and fundamental insights, which indicate some universality of the phase behavior of PO-extended and non-extended surfactants.

5.5 Experimental

5.5.1 Materials

Petrostep S-13D HA® (or S13D briefly) was obtained from the Stepan Company, and it was received as a clear, yellowish viscous liquid. It is an alkyl isopropoxylated sulfate with a single C_{13} hydrocarbon chain and with an average number of 13 (n = 13) isopropoxy groups. The molecular structure of a similar compound produced by the Stepan Company and reported in the literature has a slightly branched hydrocarbon chain, and the reported formula $CH_3(CH_2)_5(CH_3)CH(CH_2)_5O[CH_2(CH_3)CHO]_{13}SO_3Na$ corresponds to an average molecular weight of 1,032 g·mol^{-1}.[35,40,83,84] S13D is 81% sulfated (i.e., "active"), by weight, according to the manufacturer. The weight concentrations reported in this article are for the total amount of surfactant used. The molar concentrations were calculated for the active anionic components of the active surfactant. Its density at 25 °C was found to be 1.05 g·cm^{-3}. Ultrapure water was obtained from a Milli-Q water system (from Millipore), which uses distilled water as an input. For the brine (salt solution) used, sodium chloride (NaCl), potassium chloride (KCl), manganese (II) chloride tetrahydrate ($MnCl_2·4H_2O$), magnesium (II) chloride hexahydrate ($MgCl_2·6H_2O$), barium chloride dihydrate ($BaCl_2·2H_2O$), sodium sulfate decahydrate ($Na_2SO_4·10H_2O$), and sodium bicarbonate ($NaHCO_3$) were purchased from the Fisher Chemical. Calcium chloride dihydrate ($CaCl_2·2H_2O$) was purchased from Fisher Science Education. The salts were in solid form, and they were used as received.

5.5.2 Sample Preparation

A brine solution was prepared, containing the above salts to mimic the brine composition in an actual oil reservoir. The concentration of each salt is 1.12×10^{-1} (NaCl), 1.66×10^{-4} (KCl), 2.23×10^{-5} ($MnCl_2·4H_2O$), 1.58×10^{-3} ($MgCl_2·6H_2O$), 9.06×10^{-4} ($BaCl_2·2H_2O$), 3.29×10^{-5} ($Na_2SO_4·10H_2O$), 2.73×10^{-2} ($NaHCO_3$), and 2.62×10^{-3} mM ($CaCl_2·2H_2O$), respectively. The total dissolved solids concentration is about 9,700 ppm, and the total ionic strength is about 150 mM. The detailed procedure used for the brine solution preparation follows a previous report.[35] The surfactant samples were prepared by mixing the surfactant with either the water or the salt solution with magnetic stirring overnight at 23 ± 1 °C. Certain mixtures, which formed gels and containing air bubbles after mixing, were centrifuged at about 12,000 rpm (~20,000 G) to remove the bubbles.

5.5.3 Polarized Optical Microscopy (POM)

A Leitz Ortholux optical microscope with cross polarizers was used at a temperature of 23 ± 1 ℃. Each sample was placed on a microscope slide and covered by a cover glass to avoid water evaporation. Photomicrographs were taken at ×20 magnification.

5.5.4 Dynamic Light Scattering (DLS)

The intensity-averaged hydrodynamic diameters, d_h, of the surfactant micelles in water or in brine were measured with a Brookhaven Zeta PALS dynamic light scattering instrument at 22 ℃, at a wavelength, λ_0, of 659 nm and a scattering angle, θ, of 90°. The samples with surfactant concentrations of 5, 10, 15, and 20 wt% in water and of 5, 10, 15 wt% in brine were measured without dilution. The sample with 20 wt% in brine was also examined, but no reliable data were obtained, probably due to the surfactant concentration being above the solubility limit. Each data set was composed of 10 measurements of one minute each. Each date set at a given concentration was repeated three times, to ensure reproducibility of the measurements.

5.5.5 Conductimetry

The electrical conductivities of surfactant-water mixtures, with concentrations up to 7.5 wt% (68 mM), and of surfactant-brine mixtures, with concentrations up to 18.5 wt% (180 mM), were measured at 22 ℃ with a Fisher Scientific Accumet Conductivity Probe. The cell constant of the probe was 1.0 cm^{-1}. The cell was calibrated with a standard 0.01 M KCl aqueous solution. The conductivity difference of the mixture and its aqueous medium, $\kappa - \kappa_0$, was calculated and reported. The molar conductivity was also calculated using the following equation, $\Lambda = (\kappa - \kappa_0)/c_s$, where c_s is the molar concentration.

5.5.6 Densitometry

The densities, ρ, of the surfactant-water mixtures and the surfactant-brine mixtures with the concentration below 20 wt% were measured, to five significant figures, with an Anton Paar DMA 5000 density meter at 22 ℃. Each data set was the average of five consecutive measurements. Each concentration was tested at least three times, and the averages and the standard deviations were reported.

The specific volumes, $1/\rho$, were calculated from the data, and these values were used to obtain the partial densities of the surfactant in water or in brine as follows. Each mixture, for simplicity, is assumed to behave as a binary solution, which is to contain one surfactant pseudo-component, component 1, and water or brine as component 2. The specific volume varies with the weight fraction, w_i, of each component as follows.

$$\frac{1}{\rho} = \frac{w_1}{\rho_1^0} + \frac{w_2}{\rho_2^0} + \Delta V_{\text{mix}} \tag{18}$$

Here, ρ_1^0 and ρ_2^0 are the pure component densities, and ΔV_{mix} is the change of the specific volume upon mixing, which should be zero for an ideal solution. The specific volume can also be shown to be the weighted sum of the effective or partial densities, $\overline{\rho_1}$ and $\overline{\rho_2}$, which can be different from ρ_1^0 and ρ_2^0, for obtaining implicitly a measure of the non-ideal solution effects.

$$\frac{1}{\rho} = \frac{w_1}{\overline{\rho_1}} + \frac{w_2}{\overline{\rho_2}} \tag{19}$$

The effective partial densities may depend generally on the weight fractions of the components. Because the mass fractions of the water are high, one may assume that its partial density remains constant upon mixing; that is, $\overline{\rho_2} = \rho_2^0$.Then Equation (19) can be rewritten as follows.

$$\frac{1}{\rho} = \frac{1}{\rho_2^0} + w_1\left(\frac{1}{\overline{\rho_1}} - \frac{1}{\rho_2^0}\right) \tag{20}$$

The partial density of the surfactant can be obtained from Eq. (20) at each value of w_1. If the data show a linear dependence on w_1, then the average partial density of the surfactant can be obtained from the average slope of the plot of $1/\rho$ vs. w_1.

5.5.7 Small Angle X-ray Scattering (SAXS)

Each of the measurements of the scattering intensity as a function of the scattering vector ($q = \frac{4\pi}{\lambda}\sin(\frac{\theta}{2})$) was done for four hours under vacuum at 22 °C with a Rigaku small angle X-ray

scattering system with a copper Kα (λ = 1.54 Å). X-ray source and a multi-wire xenon-filled detector. The scattering distance was 0.66 m, as determined from a silver behenate calibration. In each run, approximately 0.1 mL of the sample was loaded into a borosilicate glass capillary tube with a diameter of 1.0 mm (Charles-Supper Company). The open end of each tube was then melted and sealed using a butane torch. The sealed end was coated with Duco Cement epoxy (Hampton Research), and the epoxy was cured overnight to ensure a vacuum-resistant seal. The sample tubes were mounted on a sample stage within the vacuum-maintained X-ray scattering chamber.

SAXS data were obtained for surfactant-water mixtures with surfactant concentrations of 10, 25, 30, 32.5 35, 37.5, 40, 50, 65, and 80 wt%, and surfactant-brine mixtures with surfactant concentrations of 1, 5, 10, 25, 30, 35, 40, 50, 60, 65, 70, 80, and 90 wt%. The surfactant was also examined as received (100 wt%). The 50 wt% surfactant-water mixture separated into two distinct layers, which were separated and characterized individually. The 50 wt% surfactant-brine mixture separated into three layers, the presence of which is not inconsistent with the phase rule, because the surfactant and the brine are not single component.[93] The top layer was separated easily and characterized. Because the middle and bottom layers could not be sampled properly, they were homogenized and characterized together.

5.5.8 Cryogenic Transmission Electron Microscopy (Cryo-TEM)

Cryo-TEM images were taken at the Electron Microscopy Center at Indiana University in Bloomington, IN. The samples were placed on a Quantifoil holey-carbon grid at 4 °C under 100% humidity using FEI Vitrobot, and were blotted gently and immediately frozen in a liquid ethane bath. The micrographs were taken under magnification of 22,500X with a JEOL 3200FS electron microscope; the acceleration voltage was 300 kV. Several images were taken to ensure absence of artifacts, and at various degrees of stage tilting, to gauge the micelle shape.

5.5.9 Rheological Measurements

The rheological tests were conducted at 24 °C, with a Physica MCS 301 rotational rheometer with a double-gap-coaxial-cylinders (DG) geometry for samples with viscosities below 10 cP, and with a cone-and-plate (CP) geometry for all other samples. Shear-rate ramps with a range of shear rates from 1 to 100 s^{-1} were done for fluid samples to examine their possible

Newtonian or non-Newtonian behavior. For gel samples, only oscillatory tests were done. The amplitude sweeps at 1 Hz and 10 Hz were performed first, for determining the linear viscoelastic region, in which the frequency sweeps were subsequently performed. Generally, the results for the micellar solutions were quite reproducible, qualitatively and quantitatively. The results for concentrations at which liquid crystals or dispersions formed were only qualitatively reproducible. The values of G′ and G″ could vary by a factor of up to three for the same concentration but different sample. They seemed to depend on the details of sample preparation, mixing, or sample stressing history.

6. EFFECTS OF THE WATER-OIL VOLUME RATIO AND PREMIXING OR PRE-EQUILIBRATION ON THE INTERFACIAL TENSION AND PHASE BEHAVIOR OF BIPHASIC MIXTURES

6.1 Overview

The interfacial tension (IFT) between an aqueous surfactant solution and displaced crude oil in a tertiary oil recovery process is the most important parameter affecting the oil mobilization. The key question, which has not been addressed previously in a systematic way, is which IFT is the most relevant to the oil recovery: the un-pre-equilibrated IFT, or the IFT obtained after the aqueous solution has equilibrated, totally or partially, with the oil. The un-pre-equilibrated IFT values may be close to the IFT values of oil/water during the initial stages of the oil recovery process before phase equilibration. Conversely, the pre-equilibrated IFT values may be close to the IFTs during the later oil recovery stages, because then the phases are closer to equilibrium. Here, we compare the IFT behavior in the laboratory at 24 °C and at 1 atm of un-pre-equilibrated and pre-equilibrated systems of a crude oil, a brine containing eight salts, and a commercial surfactant. The synthetic brine used is similar to the one present in an actual oil reservoir. The surfactant used here is a commercial anionic surfactant, PETROSTEP® S-13D HA, which is the sodium salt of a single-extended-isopropoxylated-chain sulfate. The pre-equilibrated equilibrium IFT (EIFT) values are quite different from the un-pre-equilibrated EIFT values. In addition, the effects of three mixing methods and the water-to-oil volume ratio (WOR) on the pre-equilibrated IFT were evaluated. Of the three methods examined here, (A) mild mixing, (B) magnetic stirring, and (C) shaking vigorously by hand, method C combined with centrifugation is the best method to evaluate the phase behavior and EIFT of premixed systems and produces mixtures that are the closest to the equilibrium state. For method C, the surfactant concentration in the aqueous layer after equilibration was the lowest due to surfactant partitioning into the oil phase. Moreover, the WOR affects the pre-equilibrated EIFT in brine systems significantly because of the different proportions of surfactant components that partition into the oil phase. For the surfactant at an initial concentration of 0.8 g·mL-1 in the aqueous phase, as the WOR decreases from 2.33 to 0.43, or as the oil volume fraction in the mixture, φ, increases from 0.3 to 0.7, the surfactant concentration in the aqueous layer drops to the range from 5.9 $g \cdot mL^{-1}$ to 2.2 $g \cdot mL^{-1}$, and the EIFT increases by a factor of ~70. In addition, the pre-equilibrated EIFTs are different from the un-pre-equilibrated

EIFTs at the same surfactant concentration in the aqueous layer evidently because of preferential partitioning of the various surfactant components. This phenomenon can be accounted for with a simple two-phase extraction model, if the more surface-active component partitions preferentially in the oil. Therefore, the effects of the mixing method and centrifugation, the WOR, and the preferential partitioning of surfactant components into the oil phase should be evaluated for general surfactant screenings for uses in EOR applications.

6.2 Introduction

One means by which to facilitate the mobilization of trapped oil in porous reservoirs is by injecting a surfactant-containing solution in enhanced oil recovery (EOR) processes.[2,28] In such applications, it is critical to have low (< 1 $mN \cdot m^{-1}$) or ultralow (< 10^{-2} $mN \cdot m^{-1}$) interfacial tension (IFT) values between the surfactant aqueous solution and the crude oil.[1,3–5,7,8] This is because the oil mobilization generally depends on the reservoir wettability and the capillary number [96,98,129] $N_c \equiv \mu U/\gamma$, where μ and U are the viscosity and the characteristic velocity of the displacing aqueous brine solution, respectively, and γ is the interfacial tension between the oil and aqueous phases. N_c is the ratio of the viscous forces applied by the displacing liquid on the oil to the strong capillary forces that resist the oil displacement in pores of variable diameter and oil droplets of nonuniform curvature.[5,9–11,13] Thus, it is desired to have large values of N_c, to effectively mobilize the trapped oil. Moreover, there is no single value of IFT characterizing a mixture of oil and a surfactant solution in brine. In fact, there is the initial dynamic IFT, which reaches an initial equilibrium state, the "un-pre-equilibrated" equilibrium IFT, and the IFT at longer term equilibrium or "pre-equilibrated" IFT. Ideally, an optimal formulation should have low or ultralow IFT at short and long time. However, as the equilibration proceeds, the IFT may vary substantially. Thus, it is important to compare both equilibrium IFT (EIFT) values.

In order to design a chemical formulation for a given crude oil, temperature, pressure, and the salinity of the aqueous solution or "brine" relevant to the oil reservoir, a robust protocol for evaluating surfactants is necessary. The protocol usually involves observations of the apparent phase behavior of brine surfactant solutions and crude oil mixtures usually at a water-to-oil volume ratio (WOR) of 1.0.[130,131] In addition, IFTs are sometimes measured or estimated from these tests.[17,19–25,132] Generally, IFT values correspond to two cases: (a) two phases, an oil phase and an aqueous phase, or (b) three phases, a middle-phase microemulsion, which contains most of the

surfactant and has high volume fractions of oil and water, a residual aqueous brine phase, and a residual oil phase. Such phase behavior observations are more useful if the observed phases are at equilibrium. Premixed or "pre-equilibrated" IFT values for three-phase cases are usually measured and reported, one between the residual aqueous phase and the middle-phase microemulsion, and one between the middle-phase microemulsion and the residual oil phase. At the "optimal salinity", these IFT values are often ultralow and equal to each other.[18,28,29,132] The solubilization ratios, in grams of oil per gram of surfactant and grams of water per gram of surfactant, are high, equal to each other, and correlate with very low EIFTs.[30] For two-phase systems at equilibrium, the EIFT between the oil and the aqueous phases is usually measured.

In practice, when an aqueous solution first contacts some oil drops trapped in an oil reservoir, the two-phase water/oil flow is impacted by the "un-pre-equilibrated" IFT value, which results after only the surfactant is distributed between the two phases and the interface.[35] As the aqueous solution keeps flowing, however, in an oil-containing porous solid, the water solution and the oil start to equilibrate by diffusion or dispersion of the surfactant, oil, and aqueous phase components, and either two phases remain or a third phase may appear. For the two-phase case, the "premixed" IFT becomes more relevant than the un-pre-equilibrated EIFT. The premixed IFT is expected to depend on time until equilibration is complete. Moreover, as more oil is transported into the aqueous solution, the effective WOR that affects the IFT decreases. Hence, to design effective aqueous surfactant formulations for practical EOR applications, it is critical to have data of premixed, or pre-equilibrated, IFT values for a range of WORs.

Additionally, a relevant question is whether each oil/aqueous mixture separates into two or three phases after premixing and pre-equilibration. One should determine whether any observed layer is a single phase or a two-phase emulsion. In all cases examined here for 8,000 ppm surfactant solution mixtures, either with crude oil or with *n*-dodecane, only two equilibrium phases were established, and no middle-phase microemulsion was detected. Hence, the mechanism of low EIFTs involves primarily adsorption of surfactants at the oil/aqueous interfaces.[35] A systematic comparison was made between the un-pre-equilibrated and the premixed or pre-equilibrated EIFTs. For the first time, we established that these IFTs can be quite different, with the latter ones depending strongly on the WOR, for both crude oil and *n*-dodecane. Moreover, the preferential partitioning of surfactant components from the aqueous phase to the oil phase was inferred from the dependence of the EIFT on the WOR. As the most surface-active components partition

preferentially into the oil phase from the aqueous phase, those components are less available to adsorb at the interface and eventually increase the EIFT to substantially higher values compared to the un-pre-equilibrated EIFT. This hypothesis is described with a conceptual model for two components in Section 6.2, and is consistent with the data presented here. Importantly, the preferentially partitioning among the surfactant components should be fully evaluated for each surfactant formulation in surfactant screening studies and in evaluating results of EOR processes. In total, this work aims to provide a structured methodology for evaluating, and potentially selecting, surfactants in the laboratory in order to provide a first principles-based approach to improving oil recovery in an emerging energy recovery sector.

6.3 Model of Surfactant Extraction from Aqueous Solutions into the Oil Phase

Even though most commercial surfactants, such as S13D, may consist of many components, a straightforward conceptual model is considered here for a simpler binary surfactant, which is partially extracted from an aqueous solution into the oil phase (Figure 31). The oil and the aqueous phases are assumed to be completely immiscible.[133] Any aggregation and solution nonideality effects in the water or in the oil, and ionic and solubilization effects are ignored. When a volume V_o^0 of oil is equilibrated with a volume V_w^0 of an aqueous solution containing two surfactants, surfactant 1 and 2, with initial concentrations of $C_{1,w}^0$ and $C_{2,w}^0$, and a total concentration of $C_{T,w}^0$ where $C_{T,w}^0 = C_{1,w}^0 + C_{2,w}^0$, the surfactant concentrations in water at equilibrium decrease to $C_{1,w}$ and $C_{2,w}$ because of the transport of surfactants into the oil phase. The surfactant concentrations in the oil phase, $C_{1,o}$ and $C_{2,o}$, are related to $C_{1,w}$ and $C_{2,w}$ via the individual dimensionless Nernst partition coefficients.[133]

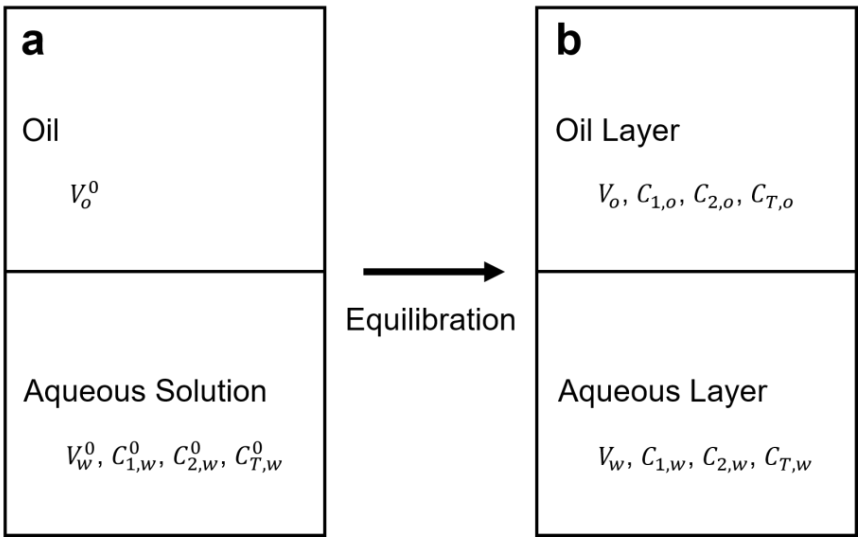

Figure 31. Schematic diagram of a simple extraction model for two surfactant components between an oil and an aqueous solution. In (a) the un-pre-equilibrated EIFT can be obtained, and in (b) the premixed or pre-equilibrated EIFT can be obtained.

$$K_i \equiv \frac{C_{i,o}}{C_{i,w}}, where\ i = 1\ or\ 2 \tag{21}$$

The overall partition coefficient, for the total concentrations, is

$$K_T \equiv \frac{C_{T,o}}{C_{T,w}} = \frac{C_{1,o} + C_{2,o}}{C_{1,w} + C_{2,w}} \tag{22}$$

A simple mole balance, which is valid at equilibrium or at non-equilibrium, for each component leads to the following equations.

$$V_w^0 C_{i,w}^0 = V_w C_{i,w} + V_o C_{i,o}, where\ i = 1\ or\ 2 \tag{23}$$

If we assume that $V_w \approx V_w^0$ and $V_o \approx V_o^0$, then from Eqs. (21) and (23), we obtain, at equilibrium,

$$C_{i,w} = C_{i,w}^0 \left(\frac{WOR}{WOR + K_i}\right), i = 1\ or\ 2 \tag{24}$$

where

$$\mathrm{WOR} \equiv \frac{V_w^0}{V_o^0} \approx \frac{V_w}{V_o} \tag{25}$$

Moreover, the oil volume fraction, φ, is defined as

$$\varphi = \frac{V_o}{V_o + V_w} = \frac{1}{1 + WOR} \tag{26}$$

The mole fractions of component 1 and component 2 in the binary surfactant initially and at equilibrium are

$$a_{1,w}^0 = \frac{C_{1,w}^0}{C_{T,w}^0}, a_{2,w}^0 = 1 - a_{1,w}^0 \tag{27}$$

and

$$a_{1,w} = \frac{C_{1,w}}{C_{T,w}}, a_{2,w} = 1 - a_{!,w} \tag{28}$$

From Eqs. (24) to (27), we obtain the following.

$$a_{1,w} = \frac{a_{1,w}^0}{a_{1,w}^0 + a_{2,w}^0 \left(\frac{WOR + K_1}{WOR + K_2}\right)} \tag{29}$$

Hence, generally, the mole fraction of the component 1 in the equilibrium aqueous phase depends on the partition coefficients of both components and the WOR. In the limiting case where $K_1 = K_2$, $a_{1,w} = a_{1,w}^0$, and then the binary surfactant can be described by one "pseudo-component". As described by Eq. (29), when K_1 is greater than K_2, or when the component 1 partitions preferentially into the oil phase compared to the component 2, then $a_{1,w}$ is less than $a_{1,w}^0$, and varies with the WOR. This means that the aqueous phase is preferentially depleted with respect to the component 1. If component 1, with the higher partition coefficient, is also more surface-active or more efficient in decreasing the EIFT than the component 2, then as the extraction proceeds and the WOR decreases, the EIFT value may increase (see Section 6.3.).

Equations (22) and (24) imply that the overall partition coefficient is,

$$K_T = \frac{K_1 a_{1,w}^0 + K_2 a_{2,w}^0 \left(\frac{WOR + K_1}{WOR + K_2}\right)}{a_{1,w}^0 + a_{2,w}^0 \left(\frac{WOR + K_1}{WOR + K_2}\right)} \tag{30}$$

and it also depends on K_1, K_2 and the WOR. Only when K_1 and K_2 are the same, then Eq. (30) reduces to $K_T = K_1$. Hence, when K_T is observed to vary with the WOR, it may indicate the presence of preferential partitioning of the surfactant components from the aqueous phase to the oil phase.

6.4 Results and Discussion

6.4.1 Effect of the Mixing Mode on the Phase Behavior and the Interfacial Tension of Oil/Surfactant Aqueous Mixtures

After a crude oil sample was layered on top of a surfactant solution at a WOR of 0.99 (sample vials of A1|L, A1|R, B1|L, B1|R, C1|L, and C1|R in Figure 32a) the color of the bottom layer remained unchanged, even after 14 days, indicating little or no oil transfer. Hence, vigorous stirring is necessary to increase the rate of mass transfer of oil and surfactant components between the two phases, and for phase equilibrium to be reached within days or weeks. About 10 s after mixing with the three different modes of mixing described in Section 6.5.1, significant amounts of emulsions formed, spanning all or most of the mixtures (Figure 32b). For method A, an aqueous layer appeared at the bottom. Thus, the emulsion produced from the most gentle mixing method A, was less stable than those from the more vigorous mixing methods B and C. For method C, the total volume of the mixture increased after mixing (see Section 6.5.1), because a third black layer formed at the top. This layer, which was a foam containing air, oil, and aqueous solution, was stable for about five hours, after which it collapsed completely within one hour, with the total sample volume changing back to the initial volume.

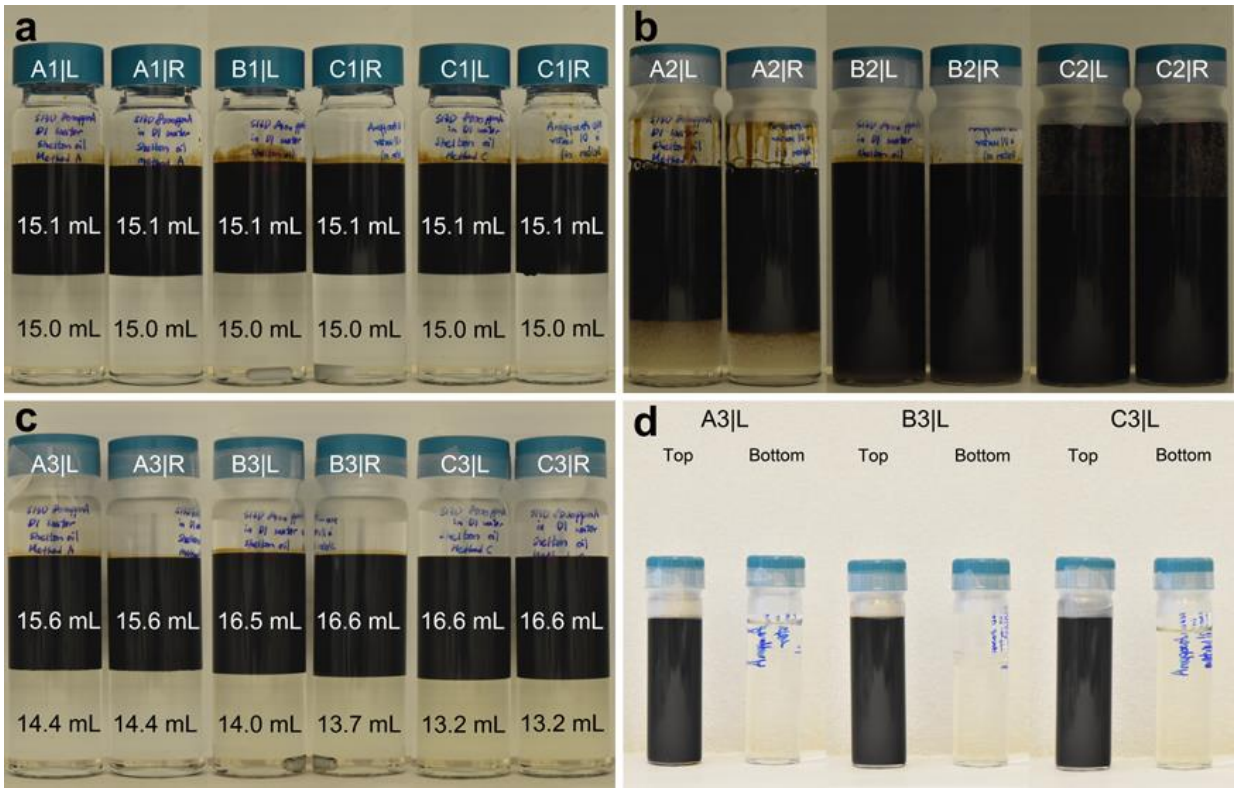

Figure 32. Photographs of mixtures of crude oil with aqueous S13D surfactant solution of 8,000 ppm in water before and after mixing and equilibration. (a) just after layering, each sample in duplicate, L or R (A1, B1 and C1); (b) 10 s after mixing with method A, B , or C (A2, B2, and C2); (c) 200 h after mixing (A3, B3, and C3); and (d) samples obtained from the top and the bottom layers of A3|L, B3|L, and C3|L.

At a time of 200 h after mixing (Figure 32c), the volume of the top oil-rich layer increased slightly by about 10%, compared to the initial volume, indicating that small amounts of the aqueous solution were transferred into the oil phase. This solution was either solubilized in an equilibrium oil phase into reverse micelles of the surfactant, some of which was inferred to have been transferred into the oil phase, or into a stable water-in-oil biphasic emulsion. The color of the bottom, water-rich layer for the mixtures with methods B and C (Figure 32c) was colored slightly brown, which was clearly different than the colorless water layer that existed before mixing. (Figure 32a). This suggests that some oil was transferred to the aqueous layer, and was probably solubilized into micelles, because most oil components are practically insoluble in water. The first inference is that methods B and C bring the samples closer to equilibrium than method A. Photographs of the layers of one of the replicates for each mode of mixing are shown in Figure 32d.

The total anionic surfactant concentrations of the bottom layers, $C_{1,w}$, after mixing at a WOR of 0.99 (Table 10) were essentially the same as those before mixing. The volumes of the aqueous layer, V_w, were lower than the initial volume, V_w^0, indicating substantial solubilization of water into the oil layer, apparently due to surfactant partitioning into the oil phase. The concentration of the surfactant in the oil phase were calculated from Eq. (23), and depended on the mixing method. The ratio, $C_{T,o}/C_{T,w}$ was the highest for method C, indicating that the mixture with method C is the closest to equilibrium. The partition coefficient was estimated to be 0.11. The EIFT values between the top and the bottom layers were similar to each other, because the total surfactant concentrations or mole fractions, and, hence, the surfactant compositions remained essentially the same.

Table 10.Volumes of the bottom layers, surfactant concentrations in the bottom layer, surfactant concentration ratios of the top and the bottom layers after mixing and premixed EIFTs for each of the three mixing modes for S13D water solutions with crude oil

Mixing mode	V_w (mL)	$C_{1,w}$ (ppm)	$\frac{C_{T,o}}{C_{T,w}}$	EIFT ($mN \cdot m^{-1}$)
Before Mixing	15.0	8,000 ± 1[a]	N/A	1.2 ± 0.1[b]
Method A	14.4	7,985 ± 100	0.04	1.0 ± 0.2
Method B	13.9	7,980 ± 100	0.06	0.9 ± 0.1
Method C	13.2	7,970 ± 100	0.11	0.9 ± 0.2

[a] This is $C_{1,w}^0$.
[b] This sample was not premixed with oil, and the un-pre-equilibrated EIFT is listed for the comparison purpose.

For brine solutions, the color of the aqueous layer also remained unchanged for 14 days after the oil was layered on top of it at the WOR of 0.95 (Figure 33a). About 10 s after mixing, the mixtures had formed emulsions throughout the sample volume, and no distinct layers were observed for some time, until a bottom layer formed. The formation of this layer took longer than what was required for water solutions, indicating that the generated emulsions were more stable in brine. For method C, a foam layer of air, water, and oil was also observed on top of the mixture. This foam layer collapsed after one hour, faster for the brine/oil system than for the water/oil system. At a time of 200 h after mixing, the bottom layers of the mixtures with methods A and B (Figure 33c) showed distinct changes in their color and the turbidity. The brown color indicated

that some amount of oil was transferred to the bottom brown aqueous layer. The transferred oil was either solubilized into micelles, or emulsified in water, because the layer turbidity suggested the presence of some dispersed oil droplets, hence an oil-in-water emulsion. For method C, a net volume increase (~2 mL) of the top layer and a similar volume decrease of the bottom aqueous layer were observed. This suggested that the amount of water transferred to the oil layer was larger than that of the oil transferred to the aqueous layer. Based on the color of the bottom layers of B3′ and C3′, the amount of oil transferred to the water layer was larger than that from the water solution (samples B3 and C3 in Figure 32).[134,135] Evidently, because of the higher salinity, more surfactant is transferred to the oil phase in the brine system than to the oil phase in the water system.

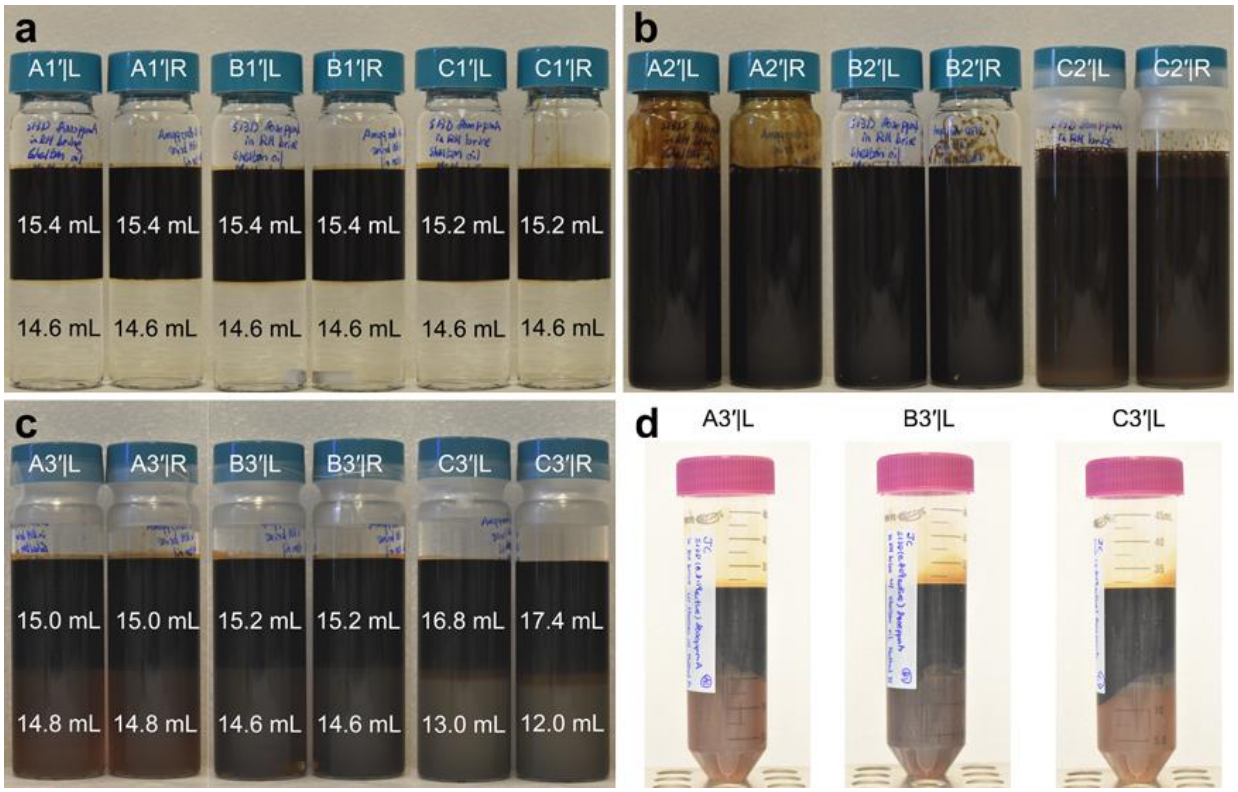

Figure 33. Photographs of mixtures of crude oil with aqueous S13D surfactant solution of 8,000 ppm in brine before and after mixing and equilibration. (a) just after layering, each sample in duplicate, L or R (A1′, B1′ and C1′); (b) 10 s after mixing with method A, B , or C (A2′, B2′, and C2′); (c) 200 h afer mixing (A3′, B3′, and C3′); and (d) samples obtained from the top and the bottom layers of A3′|L, B3′|L, and C3′|L.

The EIFT between the top oil layer and the bottom aqueous layer with method A was lower than that with method B. The premixed EIFT with method C could not be determined reliably,

because the boundary between the aqueous layer and the oil drop was not clearly visible due to the presence of large numbers of small oil droplets. These droplets were dispersed in the aqueous bottom layer and were driven toward the axis of rotation by the centripetal force. The dispersed emulsion droplets with method C were stable even one month after mixing. For this reason, centrifugation, as described in Section 6.5.1, was used to break the long-lived emulsions, and help obtain more reliable IFT values, with no interference from the small oil droplets. The EIFTs after centrifugation with method C were higher than those with methods A and B (Table 11), indicating that method C leads to phases that are closer to the equilibrium than methods A and B. This inference is consistent with the measured surfactant concentrations of the bottom layers after centrifugation.

Table 11. Comparison of the surfactant concentrations in the bottom layer, overall partition coefficients, and the premixed EIFTs among the three mixing modes for brine solutions at S13D concentration of 8,000 ppm at the WOR of 1.00.

Mixing Mode	$C_{T,w}$[a] (ppm)	$\frac{C_{T,o}}{C_{T,w}}$	EIFT	
			Before centrifugation ($\times 10^{-3}$ mN·m^{-1})	After centrifugation ($\times 10^{-3}$ mN·m^{-1})
Method A	8,000 ± 100	(< 0.009)[a]	21 ± 1	16 ± 1
Method B	7,900 ± 100	(< 0.021)[a]	205 ± 9	37 ± 2
Method C	4,300 ± 100	1.07	–[b]	387 ± 7

[a] The surfactant concentrations for methods A and B are probably not at equilibrium. The results with the method C are possibly at equilibrium.
[b] No IFT could be measured reliably, because the interface between the aqueous layer and the oil drop was not clearly visible due to the presence of small dispersed oil-in-water droplets.

The surfactant concentrations in the bottom layer were similar to the initial value (8,000 ppm) for the methods A and B. This implies little partitioning of the surfactant to the oil phase, and that the mixtures may not be at equilibrium. For method C, the surfactant concentration dropped the most, by about 46%, suggesting that the mixture was far closer to equilibrium than those with methods A and B. Our working hypothesis is that the results with the method C

correspond to the phase equilibrium of water, salts, oil, and surfactant. In addition, the premixed EIFT value with method C was higher than the un-pre-equilibrated EIFT by a factor of 28, while the EIFTs with methods A and B were close to the un-pre-equilibrated EIFT (14×10^{-3} mN·m^{-1}). These results suggest that, as more surfactant was transferred from the aqueous phase to the oil phase during mixing, the premixed EIFT increased. Hence, method A, which unfortunately is used quite often in industry, definitely produces phases quite far from the equilibrium, and is not recommended for producing pre-equilibrated phases. Method C was determined to be the most appropriate mixing method, among the three methods examined here, for producing phases at equilibrium, or closest to equilibrium, and for determining overall equilibrium IFTs. Also, the method C produces may be the most relevant to the middle and late stages of EOR processes in flows through the porous oil reservoirs.[136]

6.4.2 Effect of the Water-to-Oil Volume Ratio (WOR) on the Phase Behavior and Equilibrium Interfacial Tension

The phase behavior of mixtures of S13D brine solutions and oil was determined as a function of the WOR only with mixing method C, which leads to mixtures closest to equilibrium or at equilibrium, and with added centrifugation, which minimizes the effects of emulsions. Values of the WOR in the range from 2.33 to 0.43, or oil volume fractions of $0.3 \leq \varphi \leq 0.7$ were used, because they are typical conditions of laboratory-scale core-flood experiments. (Figure 34). When oil was layered at the top of the surfactant solution (Figure 34a), the color of the bottom layer remained unchanged for about 14 days. At a time of 200 h after mixing, two layers were observed, with no evidence of the formation of any third layer. The bottom layer was turbid and more intense brown (Figure 34b) the higher the WOR, indicating that more oil was transferred to the aqueous layer (see Section 6.2). Evidently, as the volume fraction, φ, of the oil increased, or as the WOR decreased, less surfactant remained in the aqueous layer, and less oil was solubilized in that layer. This inference was supported by the surfactant analysis data. Each mixture was centrifuged in order to remove long-lived emulsion droplets and determine the total surfactant concentration in the bottom aqueous layer.

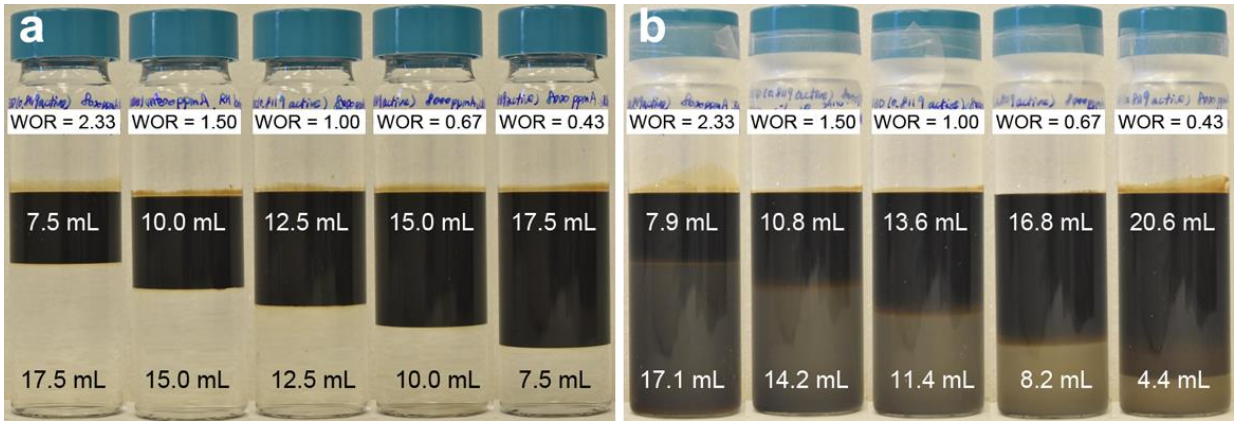

Figure 34. Phase behavior results of S13D 8,000 ppm in brine with crude oil mixtures (a) before shaking and (b) At the time of 200 h after using the mixing method C. For all mixtures two layers were observed.

At the WOR of 2.33, the total anionic surfactant concentration was 5,930 ppm and the corresponding premixed EIFT was 16×10^{-3} mN·m^{-1}, which is similar to the un-pre-equilibrated EIFT value of 14×10^{-3} mN·m^{-1} at 8,000 ppm (Table 12). When the WOR decreased from 2.33 to 0.43, the surfactant concentration ($C_{T,w}$) decreased, and the premixed EIFT value increased from 16×10^{-3} mN·m^{-1} to $1{,}100 \times 10^{-3}$ mN·m^{-1}. The results suggest that as the WOR decreased, or as the oil volume fraction, φ, increased, the amount of the surfactant that partitioned to the oil layer increased, as suggested by Eq. (30) in Section 6.2. This led to much higher EIFT values between the oil and the aqueous layer. Also, as the surfactant concentration in the bottom layer decreased, the amount of the solubilized oil decreased, because the surfactant concentration and the concentration of micelles in the bottom layer decreased. The concentrations in the oil, as calculated from Eq. (22) were quite high, ranging from 4.3 g·mL^{-1} to 2.2 g·mL^{-1}, and this leads to the ratios of $C_{T,o}/C_{T,w}$, or overall partition coefficients of 0.73 to 1.64 which are higher than the overall partition coefficients in water. The dependence of K_T on the WOR can be accounted for by Eq. (30), and suggests preferential partitioning of surfactant components into the oil phase.

Table 12. Surfactant concentrations in the bottom aqueous layers after centrifugation, surfactant concentrations in the oil layers, and overall partition coefficients as a function of the WOR, and comparison of the premixed EIFTs and the un-pre-equilibrated EIFTs of S13D solutions against crude oil at the concentrations of the premixed system's bottom layers.

WOR	$C_{T,w}$ (ppm)	$C_{T,w}$[a] ($g \cdot mL^{-1}$)	$C_{T,o}$[a] ($g \cdot mL^{-1}$)	$\frac{C_{T,o}}{C_{T,w}}$[b]	EIFT[c] ($\times 10^{-3}$ $mN \cdot m^{-1}$)	$EIFT_u$[d] ($\times 10^{-3}$ $mN \cdot m^{-1}$)
2.33	5,930 ± 102	5.9 ± 0.1	4.3 ± 0.1	0.73	16 ± 1	19 ± 1
1.50	5,154 ± 103	5.1 ± 0.1	4.1 ± 0.1	0.78	35 ± 1	14 ± 1
1.00	3,100 ± 103	3.1 ± 0.1	4.5 ± 0.1	1.50	283 ± 4	13 ± 1
0.67	2.250 ± 102	2.3 ± 0.1	3.7 ± 0.1	1.64	570 ± 7	9.5 ± 0.1
0.43	2,137 ± 103	2.2 ± 0.1	2.4 ± 0.1	1.10	1,100 ± 50	8.7 ± 0.1

[a] The volume of each layer was determined from the measured volumes of V_o and V_w after centrifugation.
[b] This ratio is probably the overall partition coefficient as described in Eq. (22).
[c] The EIFT between the top oil layer and the bottom aqueous layer from the corresponding premixed systems.
[d]The $EIFT_u$ is the un-pre-equilibrated EIFT between crude oil and the S13D brine solution at the surfactant concentration of the aqueous layer from the premixed mixtures after centrifugation.

The EIFT-WOR trend, as shown in Figure 35, is important for evaluating the surfactant formulations for the EOR applications. As the EOR process proceeds, the amount of oil that interacts with the injected surfactant solution increases, or the WOR decreases. Engineers designing oil recovery processes may need to have such information for better understanding the processes of the oil mobilization during the multiphase flow in the EOR processes. One may need to have low or ultralow IFT values at the initial stages of the process, which are related to the un-pre-equilibrated EIFT, and then seek was to maintain such low EIFT values at the later stages of an EOR processes.

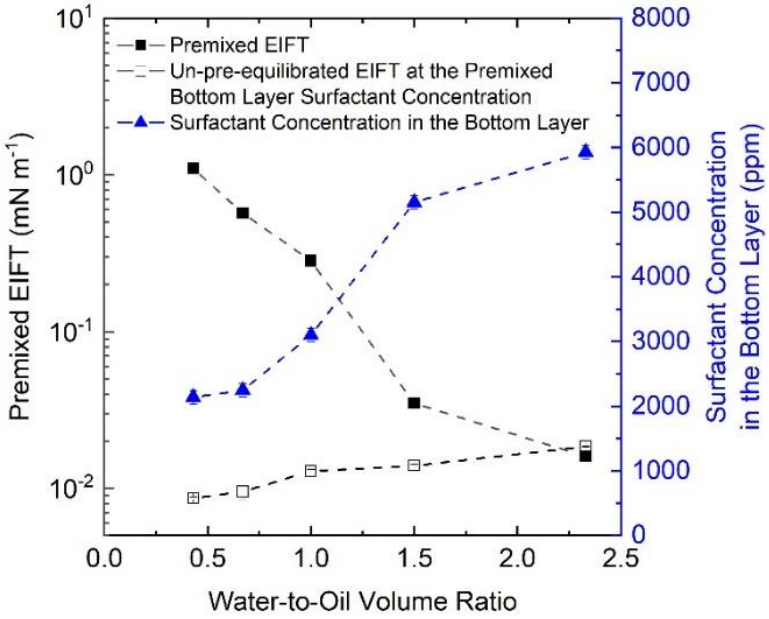

Figure 35. Premixed EIFT, the surfactant concentration in the bottom layer after premixing and the un-pre-equilibrated EIFT at the premixed bottom layer surfactant concentration vs. the water-to-oil volume ratio (WOR) for surfactant/brine/crude oil mixtures.

The significant increase in the EIFT with the WOR decrease was not due to the change in the total surfactant concentration, because the un-pre-equilibrated EIFTs at similar surfactant concentrations were much lower (Figure 35). Our hypothesis to explain these differences in the EIFTs is that the various surfactant components partitioned preferentially into the oil phase. With a model, such as the one in Section 6.2, one can understand the reasons for the changes of the EIFT with the WOR. As the total partitioning of the surfactant to the oil phase increases, a larger fraction of the more surface-active components transfer to the oil phase, and the "character" of the surfactant in the aqueous phase changes, thus producing quite different EIFT values. At a WOR of 1.0, the surfactant concentration in the bottom layer after premixing and centrifugation was 3,100 ppm and the corresponding premixed EIFT was 283 $\times 10^{-3}$ mN·m^{-1}, while the un-pre-equilibrated EIFT of S13D 3,100 ppm solution against the crude oil was 13 $\times 10^{-3}$ mN·m^{-1}.[35] This suggests that the mole fractions of the various surfactant components in the commercial surfactant mixture in the aqueous solution were altered during the premixing. The premixed EIFTs were higher than the corresponding un-pre-equilibrated EIFTs, indicating that the more effective tension-lowering surfactant components partitioned into the oil more than the less effective ones.

Thus the surfactant loss due to the partitioning into the oil phase can be significant and can significantly affect the IFT and the overall surfactant performance.

In order to determine the generality of the results, we also studied the phase behavior and the premixed EIFT values as a function of the WOR in a more limited study with a simple hydrocarbon, *n*-dodecane with which S13D is fully miscible at the conditions used. After the surfactant solution and *n*-dodecane mixtures were mixed with the method C and then centrifuged, there were two layers, an oil layer and an aqueous layer, and there was no evidence of the formation of a third phase in all mixtures. A thin white layer, which was observed between the aqueous and oil layers, was a collection of emulsion droplets, which were not removed by the centrifugation process (Figure 36).

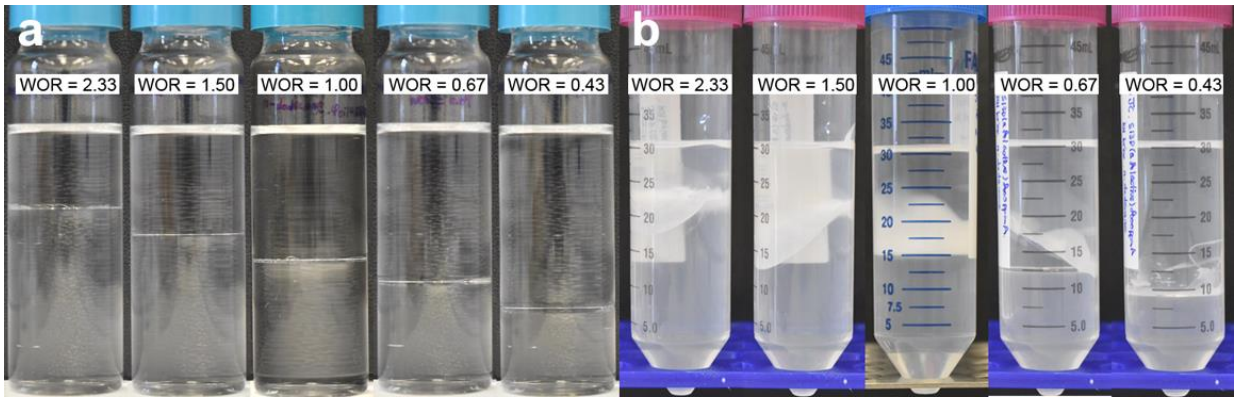

Figure 36. Phase behavior results of S13D 8,000 ppm in brine with *n*-dodecane mixtures, (a) before shaking, and (b) after centrifugation. The number of layers remained the same after centrifugation, and no evidence of a third layer was observed

As the WOR decreased, the surfactant concentration in the bottom layer decreased. (see Table 13). The concentration changes from those of the original surfactant solution, from 7,692 ppm to 6,656 ppm, were smaller than those with the crude oil, because, evidently, the partition coefficients were different. The concentrations in the oil phases were smaller, from 0.03 $g \cdot mL^{-1}$ to 2.0 $g \cdot mL^{-1}$, with the maximum observed at the WOR of 1.50. The overall partition coefficient, K_T, varied significantly with the WOR, from 0.003 to 0.28, suggesting preferential surfactant component partitioning also for *n*-dodecane. Nonetheless, the effect on the EIFT was weaker, with the EFIT ranging from 85 $\times 10^{-3}$ $mN \cdot m^{-1}$ to 178 $\times 10^{-3}$ $mN \cdot m^{-1}$ to 63 $\times 10^{-3}$ $mN \cdot m^{-1}$. Again, these

values were different from the un-pre-equilibrated EIFTs at the same total surfactant concentration in the aqueous phase (See also Figure 37).

Table 13. Surfactant concentrations in the bottom aqueous layers after centrifugation, surfactant concentrations in the *n*-dodecane layers, and overall partition coefficients as a function of the WOR, and comparison of the premixed EIFTs and the un-pre-equilibrated EIFTs of S13D solutions against *n*-dodecane at the concentrations of the premixed system's bottom layers.

WOR	$C_{T,w}$ (ppm)	$C_{T,w}$[a] ($g \cdot mL^{-1}$)	$C_{T,o}$[a] ($g \cdot mL^{-1}$)	$\frac{C_{T,o}}{C_{T,w}}$[b]	EIFT[c] ($\times 10^{-3}$ $mN \cdot m^{-1}$)	$EIFT_u$[d] ($\times 10^{-3}$ $mN \cdot m^{-1}$)
2.33	7,692 ± 101	7.7 ± 0.1	0.03 ± 0.01	0.003	85 ± 1	37 ± 1
1.50	6,831 ± 100	6.9 ± 0.1	2.0 ± 0.1	0.28	85 ± 1	36 ± 1
1.00	6,737 ± 99	6.8 ± 0.1	1.2 ± 0.1	0.18	178 ± 1	35 ± 1
0.67	6,768 ± 100	6.8 ± 0.1	0.8 ± 0.1	0.11	88 ± 1	36 ± 1
0.43	6,565 ± 103	6.6 ± 0.1	0.6 ± 0.1	0.09	63 ± 1	34 ± 1

[a] The volume of each layer was determined from the measured volumes of V_o and V_w after centrifugation.
[b] This ratio is probably the overall partition coefficient as described in Eq. (22).
[c] The EIFT between the top oil layer and the bottom aqueous layer from the corresponding premixed systems.
[d]The $EIFT_u$ is the un-pre-equilibrated EIFT between crude oil and the S13D brine solution at the surfactant concentration of the aqueous layer from the premixed mixtures after centrifugation.

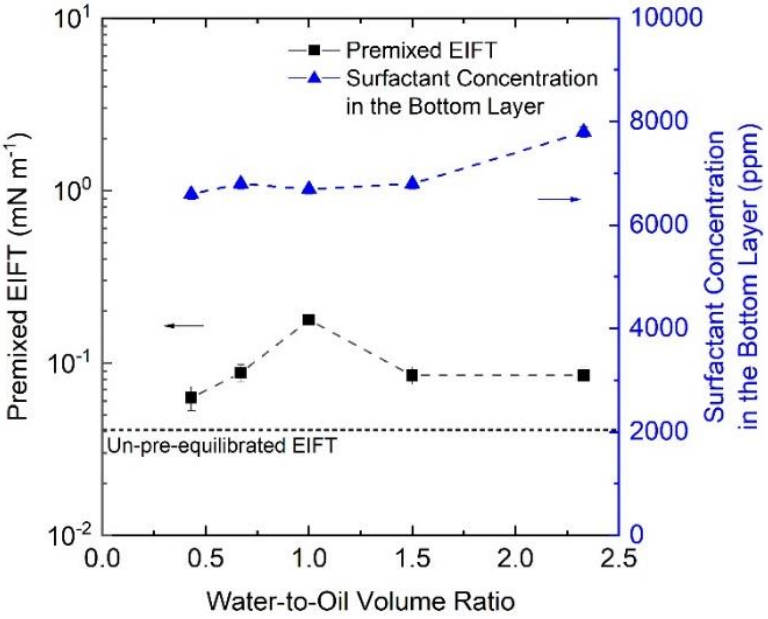

Figure 37. Premixed EIFT and the surfactant concentration in the bottom layer after premixing vs. the water-to-oil volume ratio (WOR) for surfactant/brine/*n*-dodecane mixtures. As the WOR decreased, the surfactant concentration in the bottom layer decreased slightly. However, the premixed EIFTs were slightly higher than un-pre-equilibrated EIFTs.

Moreover, the effect of premixing and the WOR was examined in the absence of any surfactant, as a control test. As expected, for all WOR values only two layers were present after pre-equilibration. The pre-equilibrated EIFT values between the top layer and the bottom layer of the mixtures were measured, and were quite similar to the un-pre-equilibrated EIFT values (see Figure 38 and Table 14). Hence the pre-equilibration with no surfactant had no effect on the EIFT. Thus, the tension reduction reported here are exclusively due to the surfactant.

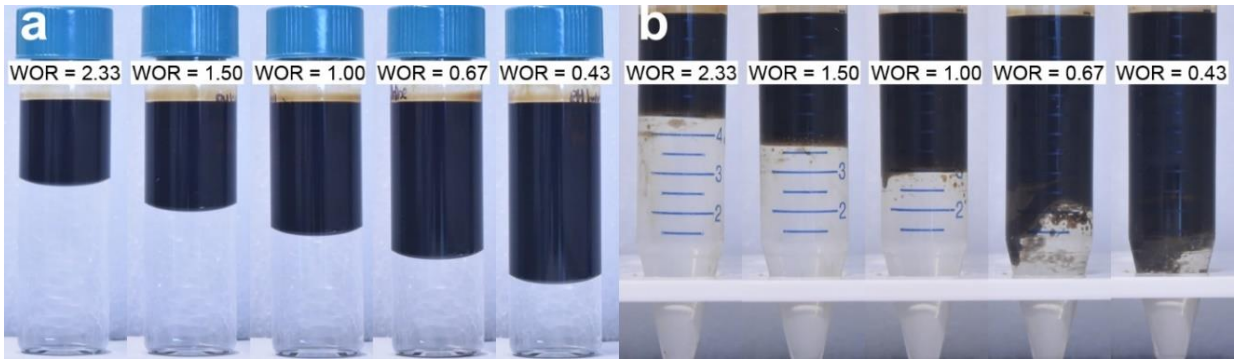

Figure 38. Phase behavior results of synthetic brine with crude oil mixtures, (a) before shaking, and (b) after centrifugation. Only two layers were observed, as expected.

Table 14. Un-pre-equilibrated EIFT and premixed EIFTs at the five water-to-oil volume ratio (WOR) for brine/oil mixtures. No anionic surfactant in the bottom layer after premixing was detected in the analyses

WOR	EIFT ($mN \cdot m^{-1}$)
~300	12.0 ± 0.1[a]
2.33	12.4 ± 0.7
1.50	14.2 ± 0.3
1.00	10.8 ± 0.1
0.67	15.9 ± 1.6
0.43	12.7 ± 1.1

[a] Un-pre-equilibrated EIFT

6.5 Conclusions

The premixed equilibrium interfacial tension (EIFT) values of a commercial anionic surfactant, S13D, were determined with three different mixing methods, in water and in a brine containing eight salts, with the water-to-oil volume ratios (WOR) ranging from 2.33 to 0.43, or oil volume fractions, φ, from 0.3 to 0.7. Among the mixing methods, (A) mild mixing, (B) magnetic stirring and (C) shaking vigorously by hand, the method C was proved to lead to phases much closer to the equilibrium than the other two methods, based on the phase volumes, surfactant concentrations, and IFT values. Using a centrifugation process can be quite helpful for better separation of phases, without interference of the effect of any long-lived emulsions on the assignment of equilibrium phases and on the IFT measurements. The pre-equilibrated EIFTs were different from the un-pre-equilibrated EIFTs. Such differences were inferred to be due to substantial and preferential surfactant component partitioning from the aqueous phase to the oil phase, thus changing the character of the two phases whose IFT was measured. Thus, there is no single EIFT value that fully characterizes the behavior and the performance of a surfactant/water/salt/oil system at a given surfactant concentration. Instead, one should determine

the range of EIFTs for a given oil, temperature, salinity, surfactant concentration, the WOR, and the degree of phase equilibration . Preferably, surfactant formulations should be sought to have low or ultralow EIFTs across a wide range of the total surfactant concentrations and WOR values. The effects of the WOR and of the mixing method should be carefully considered for general surfactant screenings in chemical EOR applications, for designing EOR processes, and for interpreting results of pilot tests and field applications. Finally, simpler surfactant mixtures, with fewer components, may be considered, so that preferential component partitioning effects on EIFTs may be avoided or minimized.

6.6 Experimental

6.6.1 Materials

6.6.1.1 Water and Brine

Purified water was produced by reverse osmosis and a Barnstead™ MicroPure™ Water Purification System with a mixed ion exchange resin. A synthetic brine was prepared by dissolving eight salts in 1 L of the purified water, which was also degassed, in the following order: 4.41 mg of manganese(II) chloride tetrahydrate ($MnCl_2 \cdot 4H_2O$); 322.0 mg of magnesium(II) chloride hexahydrate ($MgCl_2 \cdot 6H_2O$); 221.4 mg of barium chloride dihydrate ($BaCl_2 \cdot 2H_2O$); 10.6 mg of sodium sulfate decahydrate ($Na_2SO_4 \cdot 10H_2O$); 2292.3 mg of sodium bicarbonate ($NaHCO_3$); and 385.0 mg of calcium chloride dihydrate ($CaCl_2 \cdot 2H_2O$). The salt concentration was 9,700 ppm by weight, and the total equivalent normal concentration was about 0.15 N, and the pH at 24 °C was 8.0. Almost all of the salts were obtained from Fisher Chemical in certified ACS grade and used as received. Reagent grade $CaCl_2 \cdot 2H_2O$ was purchased from Fisher Science Education.

6.6.1.2 Crude Oil

The crude oil samples, kindly provided by the Pioneer Oil Company, were initially centrifuged at 2,000 rpm (with an average acceleration of 800 g) for 60 minutes to remove solid particles and water droplets, and then they were filtered through a 0.5 μm metal screen. The filtrates looked homogeneous, dark brown, translucent, and had a low viscosity (~10 cP) at 25 °C.

6.6.1.3 Surfactant

The commercial surfactant, PETROSTEP® S-13D HA or "S13D", was obtained from the Stepan Company (Northfield, IL). It is a clear viscous liquid, and it was used as received. S13D contains about 80% (by weight) anionic surfactant components ("80% active"). The composition of the remaining 20% has not been disclosed. The surfactant contains several single chain isopropoxylated sodium sulfate surfactant components,[28,84] and its average molecular weight is 1,032 $g \cdot mol^{-1}$. The weight or molar concentration values reported refer to the active surfactant., unless stated otherwise.

6.6.2 Methods

6.6.2.1 Phase Behavior Tests and Mixing Procedures

Borosilicate vials were first soaked in pure water for 24 h to leach any ionic impurities. Then, 15 mL of an aqueous surfactant solution in water or brine (ρ = 1.004 $g \cdot mL^{-1}$) was added to the clean borosilicate vials. Then, 15 mL of crude oil (ρ = 0.8868 $g \cdot mL^{-1}$) was gently layered on top of the aqueous phase with no agitation. The layers stayed as a mixture of two separate phases, and no discoloration of the aqueous phase or other change was observed after multiple days. This suggests that the diffusion rate of the components of the oil, surfactant, and aqueous solution between the two phases was slow; thus, mixing procedures were utilized to increase the rate of mass transfer.

Three different modes of mixing were applied individually to the layered oil-water mixtures, in order to determine which mode brings the mixtures closest to phase equilibrium: (A) "mild" mixing, (B) vigorous magnetic stirring, and (C) vigorously shaking by hand. In the mild mixing procedure (A), samples were inverted slowly, and then brought back to their original upright position five times, and the whole mixing process finished within 30 s. This procedure was used in order to allow some mixing and mass transfer, while minimizing the formation of long-lived emulsions, which may complicate the assignment of the number of equilibrium phases. In the magnetic stirring method (B), the mixture was stirred with a magnetic stirring bar for 10 minutes at 1,500 rpm. In the final method (C), the samples were vigorously shaken by hand for one minute, and then allowed to settle. All three methods produced emulsions after mixing. Method (C) also produced an additional black foam layer on top of the oil layer. This layer was

detected from its characteristic turbidity and color, and from the significant sample volume expansion, which indicated the presence of air bubbles in that layer. The mixtures separated into several layers, and were observed for up to 10 days, until the volume and the appearance of each layer reached a steady state. Photographs were taken as needed, usually at 10 s and every 24 h after mixing. A dark brown top layer was normally observed. It was inferred to be oil-rich and oil-continuous. The bottom layer normally looked turbid or opaque, and sometimes brown or gray in color. The turbidity or opaqueness was due to the light scattering by the dispersed oil-in-water droplets. A middle layer (not necessarily a middle phase) was also observed. To determine whether this layer was an oil/water emulsion or a separate middle-phase microemulsion phase, the whole oil-water mixture was transferred to a 45 mL conical tube, and the mixture was centrifuged for 90 minutes at ~12,000 rpm (at an average acceleration of 19,800 g), in order to accelerate any possible sedimentation or creaming, to concentrate any possible emulsion, and to possibly induce coalescence and faster separation of the dispersed droplets. After the centrifugation process, each of the resulting separate layers was sampled. The density of each layer was measured at 24 °C. Finally, the dynamic and the equilibrium IFT between the water-rich layer and the oil-rich layer was measured,[35] and the procedures for these experiments are reviewed briefly below.

6.6.2.2 Interfacial Tensiometry

Borosilicate vials were first soaked in pure water for 24 h to leach any ionic impurities. Then, 15 mL of an aqueous surfactant solution in water or brine (ρ = 1.004 g·mL^{-1}) was added to the clean borosilicate vials. Then, 15 mL of crude oil (ρ = 0.8868 g·mL^{-1}) was gently layered on top of the aqueous phase with no agitation. The layers stayed as a mixture of two separate phases, and no discoloration of the aqueous phase or other change was observed after multiple days. This suggests that the diffusion rate of the components of the oil, surfactant, and aqueous solution between the two phases was slow; thus, mixing procedures were utilized to increase the rate of mass transfer.

The interfacial tension values were determined with the spinning drop method (SDM) using the following equation.

$$\gamma = \frac{(\rho_1 - \rho_2)\omega^2 R^3}{4} f\left(\frac{L}{R}\right) \tag{31}$$

Here, ρ_1 and ρ_2 are the densities of the dense phase and the light phase, ω is the circular frequency ($\omega = 2\pi v$), v is the rotation frequency, and R and L are the maximum radius and the length of the drop; f(L/R) is a correction factor, which can be calculated rigorously from the solution of the Laplace-Young equation,[67] and it is smaller than 1.004 for L/R values greater than 8. In most cases this factor was ignored, because the L/R values were greater than 8.

The actual bubble or drop radius (R_{actual}) is smaller than the observed radius ($R_{observed}$) obtained from the captured image, due to light refraction in the cylindrical glass wall.[68]

$$R = R_{actual} \cong \frac{R_{observed}}{n_1} \tag{32}$$

Here, n_1 is the refractive index of the dense liquid; for water or brine, $n_1 = 1.33$.

The dynamic IFT (DIFT) was measured as a function of time at a fixed value of v, until the IFT value reached a steady state value (SIFT).[35] To test the stability of the SIFT, the rotation frequency was abruptly changed, varying the oil/water surface area and the instantaneous surface density of the adsorbed surfactant, and the DIFT and the SIFT were measured again. If the two SIFT values were the same, they were termed "the EIFT". The EIFTs of each premixed or pre-equilibrated system were compared to the EIFTs of the un-pre-equilibrated samples for the same oil, salinity, and surfactant at the same initial concentration.[35] In addition, the oil droplets were carefully monitored for any evidence of a third phase or a drop shape that might be inconsistent with the Laplace-Young equation and could suggest the presence of a third phase. Unless otherwise stated, all IFTs reported refer to "normally-shaped" drops and to samples where there was no evidence of a third phase. In certain cases, when the equilibrated bottom aqueous layer had some residual suspended oil droplets, these droplets were centrifuged upon spinning to the axis of the oil drop, and they often prevented accurate determination of the drop diameter. For this reason, the aqueous layers were centrifuged as needed to remove all or most of the suspended droplets prior to the measurements. The WOR for the conditions of a typical IFT measurement ranges from 500 to 1,500.

6.6.2.3 Two-phase Titration and Density Measurements

The total concentration of the anionic surfactant component in the aqueous solution sample was determined by the two-phase titration method.[137,138] A cationic surfactant was added to the sample aqueous solution, and this cationic surfactant binds with an anionic surfactant molecule in a 1:1 molar ratio. Then, the cationic-anionic surfactant complex was extracted into a chloroform phase. Based on the color change of the aqueous layer because of the added indicator, an equivalent point was determined. The following chemicals were used as received. Hyamine 1622 ($C_{27}(H_{42})ClNO_2$) is the cationic surfactant used, and it was purchased from the Rohm and Haas Company. Sulfuric acid and chloroform were purchased from Fisher Scientific. A stock solution of the dimidium bromide–disulfine blue indicator was purchased from the EMD Millipore Corporation. The densities of the liquid samples were measured at 24 °C with an Anton Paar DMA 5000 density meter. Each reported value is the average of five consecutive measurements.

7. RELATIONSHIP OF VARIOUS INTERFACIAL TENSIONS OF SURFACTANTS/BRINE/OIL FORMULATIONS TO OIL RECOVERY EFFICIENCY

7.1 Overview

Chemical enhanced oil recovery (cEOR) aims to increase the oil recovery of mature oil fields, using aqueous solutions of surfactants and polymers, to mobilize trapped oil and maintain production. The interfacial tensions (IFTs) between the aqueous solution, the oil phase, and other possible phases formed (e.g., "middle phase" microemulsion) are important for designing and assessing a chemical formulation. Ultralow ($<10^{-2}$ mN·m^{-1}) IFTs are needed to increase the capillary number and help mobilize trapped oil droplets. Despite this fact, phase behavior tests have received more attention than IFTs for designing and evaluating surfactant formulations that result in high oil recovery efficiencies. Five types of EIFTs have been identified along with robust protocols for determining them. These are: (I) the un-pre-equilibrated equilibrium IFT ($EIFT_{up}$); (II) the un-pre-equilibrated EIFTs in the presence of rock ($EIFT_{up,rock}$); (III) the pre-equilibrated EIFTs ($EIFT_{p}$) in the presence of oil; (IV) the pre-equilibrated EIFT in the presence of rock and oil ($EIFT_{p,rock}$); and (V) the effluent EIFT ($EIFT_{eff}$). The first one is the EIFT of the aqueous surfactant/brine solution against an oil drop without any pre-equilibration steps. The second one is the EIFT between an oil drop and the surfactant solution after pre-equilibration with a rock sample to account for adsorption losses. The third one is the EIFT between the pre-equilibrated water and the oil phases from surfactant/brine/oil mixtures. The fourth one is the EIFT between the pre-equilibrated water and the oil phases from surfactant/brine/oil/rock mixtures. The fifth one is the EIFT from an effluent sample mixture of a laboratory-scale core flood test. Among the five types of EIFTs, the fifth one was found to be the most important for the highest oil recovery performance in core flood tests, because it captures the most important surfactant partition processes, the partitioning to the oil phase and the partitioning by adsorption on the rock surface. Among three surfactant formulations tested with core flood experiments, the one with the lowest $EIFT_{p,rock}$ (~0.01 mN·m^{-1}) had the highest oil recovery ratio (78%), and the one with the highest $EIFT_{p,rock}$ (~0.2 mN·m^{-1}) had the lowest oil recovery ratio (55%). The other EIFTs correlated less with the oil recovery performance. Identifying surfactant formulations that have low or ultralow

EIFTs, especially ultralow $EIFT_{p,rock}$'s, are critical for screening formulations appropriate for core flood tests and target field applications, and for predicting oil recovery performance.

7.2 Introduction

Mature oil reservoirs provide potential hydrocarbon resources in the United States and other countries because more than 50% of the original-oil-in-place (OOIP) often remains unrecovered after primary and secondary oil recovery processes, leaving this remaining-oil-in-place (ROIP) as stranded oil.[139] A key challenge is to mobilize the unrecovered oil droplets trapped during secondary oil recovery in the porous reservoir rock due to high interfacial tension (IFT) between the oil droplets and the surrounding brine. High IFTs result in poor sweep efficiency, limited droplet mobilization, and low oil recovery efficiency. Oil recovery rates can be improved by lowering the IFTs between the oil and aqueous phases in the reservoir, thus lowering the pressure drop needed to mobilize the oil. Several techniques such as gas injection, steam injection, and chemical injection processes have been implemented.[2] This work focuses on effective ways of lowering IFT values by introducing surfactants and polymers into the aqueous solutions.

When IFT values are reduced to below 10^{-1} $mN \cdot m^{-1}$, the mobilization of trapped oil droplets is enhanced, and EOR performance improves. Thus, it is important to have low ($< 10^{-1}$ $mN \cdot m^{-1}$) or ultralow ($< 10^{-2}$ $mN \cdot m^{-1}$) IFTs between the oil and the aqueous phases during waterflooding.[28,43,140–143] A surfactant formulation is a mixture of one or more surfactant molecules in a brine. To improve the efficiency and economics of an EOR process, a critical step involves evaluating and optimizing the compositions of such formulations for the reservoir conditions.[95,98] The evaluation of surfactant formulations at the laboratory scale usually consists of: (a) phase behavior tests of aqueous surfactant formulations and oil mixtures; (b) measurements or estimations of IFTs between oil and aqueous or microemulsion phases; and (c) laboratory-scale core flood tests to estimate EOR efficiencies, and to relate them to the phase and IFT behavior.[2,7] While steps (a) and (b) include only water and oil phases, step (c) and further testing (e.g., pilot field tests) include reservoir rock surfaces and their interactions with oil, water, and surfactant. One of the major concerns of the interactions between reservoir rock surfaces and multiphase liquid flows is the adsorption losses of injected surfactants and polymers. These losses can impact the oil mobilization ability of the injected liquid solutions.[144–152] In this paper, the IFT behavior

and the phase behavior are determined at laboratory-scale, and their correlations with laboratory-scale core flood test results are evaluated.

After Winsor's pioneering work,[142,153,154] oil/water phase behavior tests, and their evaluations, have been the major focus of surfactant formulation development and selection before core flood tests.[18,23,24,155,156] The IFT values between oil and aqueous phases are usually estimated based on phase behavior results, including water and oil solubilization, and surfactant structure,[132] or are not reported. Usually, determining reliable IFT values in a robust way is a challenge, mainly due to time effects on the IFT and the effects of multicomponent nature of the surfactant, the oil, and the brine. Thus, for a given chemical composition during injection, it is difficult or impossible to determine a single IFT value that fully represents the dynamics of cEOR recovery, because the composition changes during the flow and interactions with the oil and the rock. Moreover, for most industrial synthetic methods, the resulting commercial surfactants are mixtures of numerous components. A distinguishing feature of this work is a focus on the rigorous measurements of IFTs using newly defined protocols, which are designed to mimic reservoir conditions to a varying extent.

The absolute and relative concentrations of the various surfactant components in the aqueous phase change upon flow in a porous reservoir and contact with the oil and the rock, because of: (a) overall and preferential partitioning of surfactants between the oil and the aqueous phases and (b) surfactant losses due to adsorption on reservoir rock surfaces.[37,157,158] If a middle-phase microemulsion forms during an oil recovery process, then the number of relevant IFTs at each location increases from one, the IFT between the oil and the aqueous phase, to three, one between the oil phase and the aqueous phase, a second one between the oil phase and the microemulsion phase, and a third one between the aqueous phase and the microemulsion phase. In this work, only simple two-phase, oil/water systems were examined for determining relevant IFTs for estimating EOR efficiency, because no middle phase microemulsion phases formed for the laboratory and core flood conditions used.

A broad range of dynamic and equilibrium IFT values for a formulation used for EOR applications was found, as reported previously.[35,37] In this article, we define five types of IFTs, and focus on EIFTs: (I) the un-pre-equilibrated equilibrium IFT ($EIFT_{up}$); (II) the un-pre-equilibrated equilibrium IFT in the presence of rock ($EIFT_{up,rock}$); (III) the pre-equilibrated equilibrium IFT ($EIFT_{p}$) with oil; (IV) the pre-equilibrated equilibrium IFT in the presence of rock

and oil ($EIFT_{p,rock}$); and (V) the "effluent" equilibrium IFT ($EIFT_{eff}$). Types I and III were studied previously.[35,37] The $EIFT_{up}$, type I, is the equilibrium interfacial tension (EIFT) between a surfactant brine solution and a drop of oil.[35] These two phases are contacted for the first time at the beginning of the tensiometry experiment.[35] For determining the $EIFT_{up,rock}$, type II, a surfactant brine solution is pre-equilibrated with core material in the absence of oil. Then, the $EIFT_{up,rock}$ is determined between the pre-equilibrated surfactant brine solution and an oil drop. The $EIFT_{p}$, type III, is defined as the equilibrium IFT between an oil and an aqueous phase after they have pre-equilibrated in the absence of rock.[37] The $EIFT_{p,rock}$, type IV, is the EIFT between an oil and an aqueous phase after they have pre-equilibrated with rock. Finally, an $EIFT_{eff}$, type V, is defined as that between an oil and an aqueous layer produced after a laboratory-scale core flood experiment. The EIFTs of type III, IV, and V depend on the volume ratio of the aqueous and oil phases, because the amounts of the partitioned surfactant components depend on the volume of each phase.[37] Because IFTs are not measured directly during recovery processes, the EIFTs of Type IV and type V are probably the ones are the most similar to them.

The relationships of these five types of EIFTs to certain laboratory-scale oil recovery test results are examined for several surfactant formulations of two commercial surfactants and a co-solvent. The several types of EIFTs and the oil recovery efficiencies are evaluated, to determine their possible correlations. The type IV, $EIFT_{p,rock}$, data correlate best with the oil recovery efficiency data of laboratory scale core flood experiments. These studies can help improve the evaluation and design of surfactants and surfactant formulations, and minimize the time and resources needed for laboratory and core flood studies prior to field tests.

7.3 Results and Discussion

7.3.1 Phase behavior of surfactant/co-surfactant in brine

The 123-15S and A-6 surfactants and the co-solvent, L4-2, in 11 different ratios (Table 15), were mixed with the synthetic brine. After 5 min of magnetic stirring, formulations 1-9 were clear homogeneous single-phase solutions; formulations 10 and 11 were biphasic. Formulations 1-6 became clear solutions without showing any turbidity at any time as the surfactant dissolution proceeded. Formulations 7-9 were turbid initially, and later became clear colorless solutions. The turbidity was inferred to be due to suspended A-6 droplets because the solubility of the A-6 alone

in the synthetic brine is lower than the concentrations used in the mixtures. The subsequent solution clarification is probably due to the solubilization of the suspended A-6 into the mixed micelles assumed to be formed by the other two surfactants. Formulations 10 and 11 remained turbid and white after 24 h.

Table 15. Surfactant compositions and phase behavior results

Surfactant Formulation	123-15S : A-6 : L4-2 ratio	Total surfactant concentration (ppm)	Salinity (ppm)	Visual observations results
1	10 : 0 : 0	8,000	9,400	clear, colorless, one phase
2	10 : 0 : 1	8,000	9,400	clear, colorless, one phase
3	10 : 0 : 2	8,000	9,400	clear, colorless, one phase
4	9 : 1 : 0	8,000	9,400	clear, colorless, one phase
5	9 : 1 : 1	8,000	9,400	clear, colorless, one phase
6	9 : 1 : 2	8,000	9,400	clear, colorless, one phase
7	8 : 2 : 0	8,000	9,400	clear, colorless, one phase
8	8 : 2 : 1	8,000	9,400	clear, colorless, one phase
9	8 : 2 : 2	8,000	9,400	clear, colorless, one phase
10	6 : 4 : 0	12,000	9,400	turbid, white, two phases
11	6 : 4 : 1.8	12,000	9,400	turbid, white, two phases

7.3.2 Phase behavior and interfacial tensions of surfactant brine solutions with crude oil

Each of the eleven formulations in Table 15 was mixed with crude oil at a water-to-oil volume ratio of 1.00.[35] After vigorous mixing by hand for a minute and subsequent 100 h of equilibration, each mixture had two distinct layers; no evidence of any other phase was found. In Figure 39, photographs of surfactant formulations 8, 10, and 11 are shown. At 10 s after shaking

vigorously by hand, each mixture looked black with a dark brown foam-like layer on top (Figures 39A-2, 39B-2, and 39C-2). The dark brown foam formation was indicated by the increase in the total volume, which was due to entrained air in the top foam-oil layer (Figures 39A-1, 39B-1, and 39C-1). At 100 h after shaking, the foam-oil layer had disappeared as the foam broke, and there was no net volume change. Each mixture then consisted of two distinct liquid layers: a black, oil-rich layer on the top, and a turbid and brown aqueous layer at the bottom (Figures 39A-3, 39B-3, and 39C-3). The color change of the bottom layer indicated that some oil had been transferred to the aqueous layer, either as solubilized material or as emulsion droplets. The top layer volume increased slightly for all three cases, because evidently some surfactant partitioned into the oil phase and solubilized more water than the oil that was solubilized in the water phase. After centrifugation, two layers were seen in each mixture, again with no evidence of a third phase (Figures 39A-4, 39B-4, and 39C-4). Centrifugation removed by creaming many oil droplets from the aqueous layer. These droplets tended to interfere with the IFT measurements in the spinning drop apparatus, and sometimes made it impossible to obtain reliable IFT measurements.

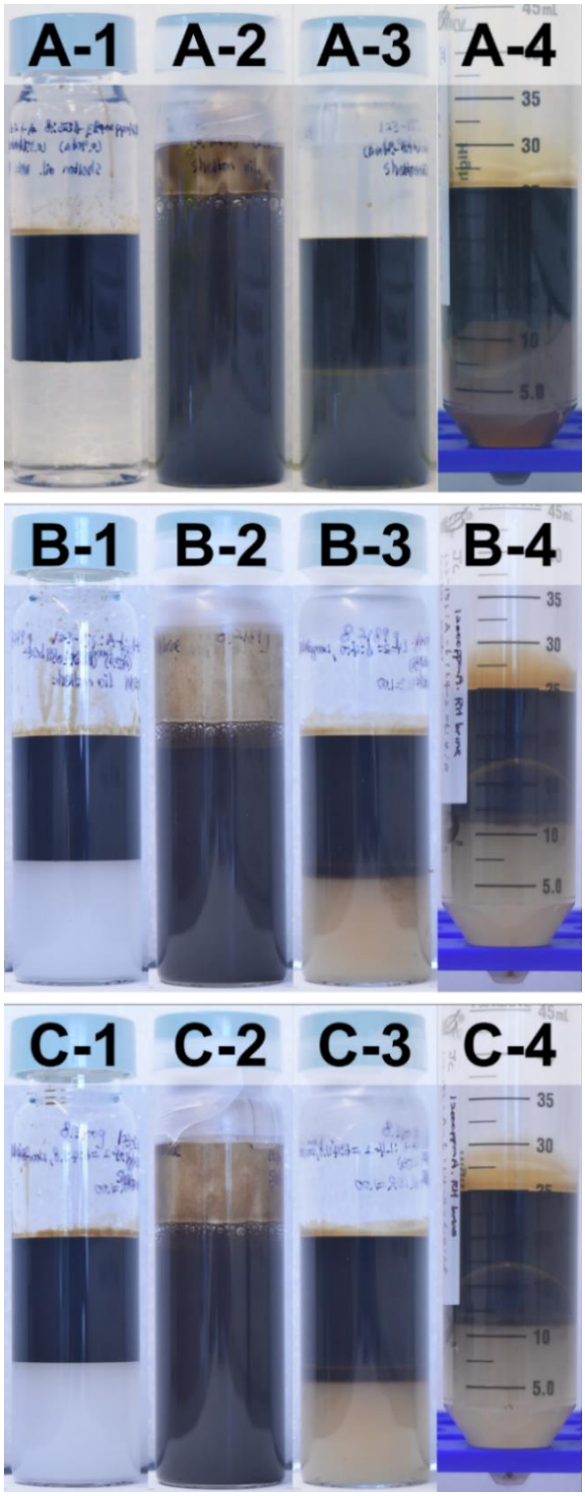

Figure. 39. Phase behavior test results of the three mixtures of crude oil and surfactant brine solutions at different points in time. These times are: (i) just after layering (A-1, B-1, and C-1); (ii) 10 s after shaking (A-2, B-2, and C-2); (iii) 100 h after shaking (A-3, B-3, and C-3); and (iv) after centrifugation of mixtures (A-4, B-4, and C-4). The surfactant solutions are for formulations 8 (A-1, A-2, A-3, and A-4), 10 (B-1, B-2, B-3, and B-4), and 11 (C-1, C-2, C-3, and C-4) from Table 15.

The un-pre-equilibrated EIFTs ($EIFT_{up}$), pre-equilibrated EIFTs ($EIFT_p$), and the surfactant concentrations in the bottom aqueous layers were determined as a function of surfactant to co-solvent mass ratio (Table 15). Prior to the pre-equilibration, five formulations (1, 4, 7, 10, and 11) had ultralow $EIFT_{up}$ values. The $EIFT_{up}$ values for the other solutions could not be determined, because the DIFT continued to decrease as the injected oil drop emulsified spontaneously, and formed many small droplets; thus, no steady IFT value was reached. Nonetheless, these observations suggest that the EIFT values were so low, probably lower than $\sim 10^{-4}$ $mN \cdot m^{-1}$, and were that the most likely reason of the spontaneous emulsification of the injected oil droplets.

Table 16. Equilibrium interfacial tensions (EIFT) for surfactant/oil/brine mixtures before ($EIFT_{up}$) and after ($EIFT_p$) pre-equilibration

Surfactant formulation	Before pre-equilibration	After pre-equilibration	
	$EIFT_{up}$ ($\times 10^{-3}$ mN m^{-1})	$EIFT_p$ ($\times 10^{-3}$ mN m^{-1})	Surfactant conc. in the aq. layer (ppm)
1	2 [a]	220 ± 10	1,200 ± 100
2	[b]	300 ± 10	590 ± 99
3	[b]	90 ± 5	800 ± 99
4	2 [a]	80 ± 5	1,980 ± 103
5	[b]	27 ± 7	1,860 ± 100
6	[b]	20 ± 5	1,840 ± 100
7	2 [a]	12 ± 2	700 ± 103
8	[b]	2.7 ± 0.1	1,840 ± 102
9	[b]	70 ± 8	1,580 ± 98
10	3.2 ± 0.1	14 ± 0.1	5,400 ± 96
11	2.0 ± 0.1	22 ± 0.1	3,500 ± 93

[a] The interface was not stable for a sufficiently long time to do area perturbation tests after the IFT reached a steady-state value. [b] The interfacial tension values were not measurable in the spinning drop apparatus, because the injected oil drops broke up spontaneously.

After the pre-equilibration and centrifugation, each $EIFT_p$ was higher than the $EIFT_{up}$. This change was probably due to the surfactant partitioning from the aqueous phase to the oil phase.[37] In addition, by comparing the $EIFT_p$ values of the surfactant formulations 1 (123-15S:A-6:L4-2 = 10:0:0), 4 (9:1:0), and 7 (8:2:0), it was observed that the $EIFT_p$ decreased from 220×10^{-3} $mN \cdot m^{-1}$ to 80×10^{-3} $mN \cdot m^{-1}$, and to 12×10^{-3} $mN \cdot m^{-1}$ when the A-6 ratio was increased from 10:0 to 8:2. A similar trend was observed among the surfactant formulations 2 (10:0:1), 5 (9:1:1), and 8 (8:2:1). The addition of a co-solvent, L4-2, had a similar EIFT reduction trend. For example, the $EIFT_p$ was reduced from 80×10^{-3} $mN \cdot m^{-1}$ to 27×10^{-3} $mN \cdot m^{-1}$, and then to 20×10^{-3} $mN \cdot m^{-1}$ when the 123-15S:A-6:L4-2 ratio was shifted first from 9:1:0 to 9:1:1 and then to 9:1:2. To test the effect of the interaction between the surfactant/brine/oil mixtures and the Berea Sandstone samples on the IFT, the surfactant formulations 8, 10, and 11 were chosen, because the $EIFT_p$ values remained low after the pre-equilibration.

7.3.3 Phase behavior and interfacial tensions of surfactant/brine/oil/rock mixtures

Laboratory-scale pre-equilibration tests of surfactant/brine/oil/rock were done to examine the effect of liquid mixture/rock interaction on their phase behavior and EIFTs. At 10 s after shaking by hand (Figure 40b), all mixtures were black with a foam layer on top, and with the volume increases indicating entrainment of some air and oil in this layer. Most of the added ground sandstone had settled at 100 h after shaking (Figure 40C), and two distinct liquid layers were observed in each sample with no net volume changes. After centrifugation (Figure 40D), most of the small emulsion droplets suspended in the bottom layers were removed by creaming, and the layers became clear. Similar to surfactant/brine/oil mixture cases, no evidence of third layer formation was observed. In addition, the color of the aqueous layers was less intense than those from the surfactant/brine/oil mixture cases (Figures 39 A-4, B-4, and C-4). These differences indicate that the oil component concentrations were different.

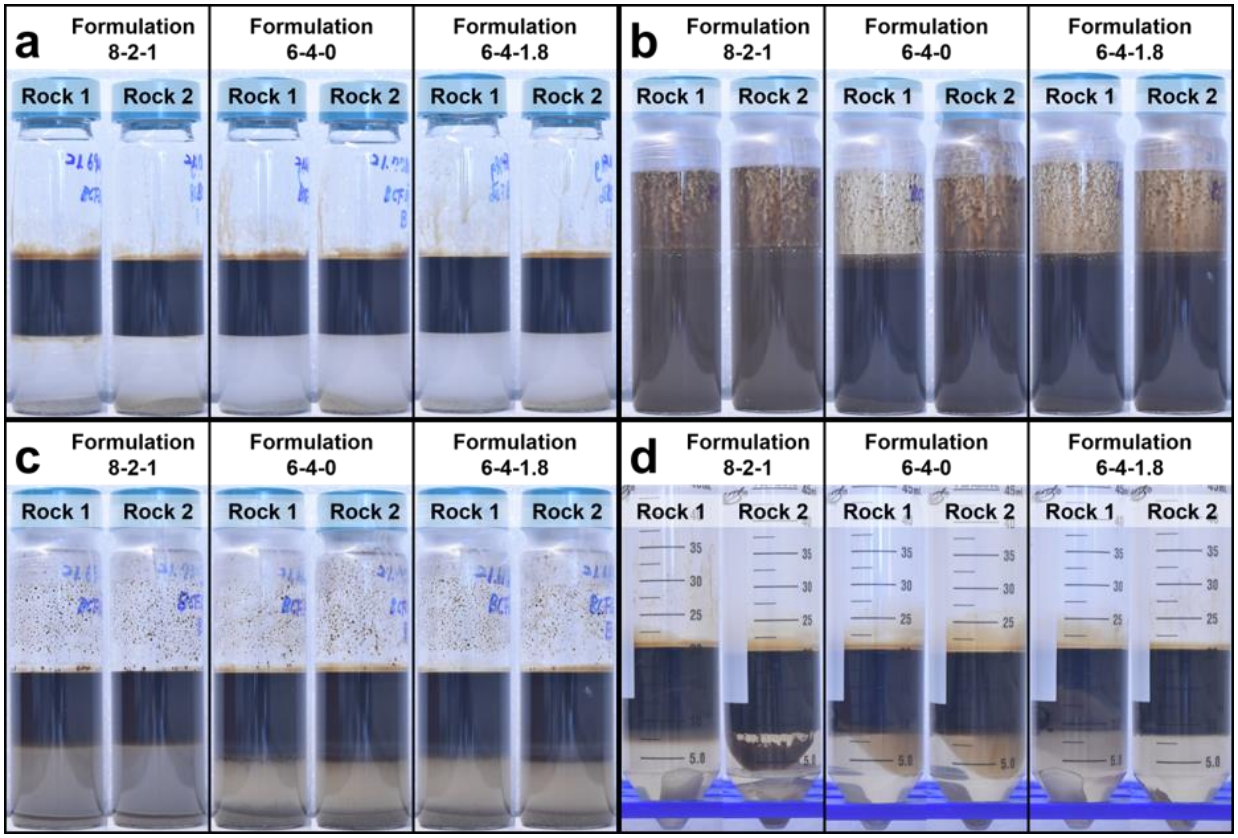

Figure. 40. Phase behavior test results of crude oil, surfactant brine solutions (Surfactant formulations 8, 10, and 11 where 123-15S:A-6:L4-2; their ratios were 8:2:1, 6:4:0, and 6:4:1.8, respectively from Table 15), and ground Berea sandstone samples (Rock 1 and 2): (a) mixture just layered, (b) 10 s after shaking by hand, (c) 100 h after shaking, and (d) after centrifugation. All mixtures had two distinct layers after centrifugation, and the no third layer was observed.

The $EIFT_{up}$ and the EIFT from the surfactant/brine/rock mixtures ($EIFT_{up,rock}$), and the EIFT from the surfactant/brine/rock/oil mixtures ($EIFT_{p,rock}$) were compared to examine the contribution of the surfactant adsorption to the IFT. With no surfactant adsorption on the rock surface, all three formulations had ultralow or low EIFT values ($EIFT_{up}$, Table 16). Based on the two-phase titration results, it was found that about a third of the total surfactant was adsorbed for formulations 10 and 11, and little was adsorbed for formulation 8 (Table 17). The EIFT values between the equilibrated surfactant solution and the crude oil remained in the ultralow range. By contrast, the $EIFT_{p,rock}$ values of formulations 8 and 10 were much higher than the $EIFT_{up,rock}$ values and the $EIFT_p$ values (see Table 16). These results indicate that the surfactant adsorption on the rock sample surfaces shifted the EIFTs to even higher values than the $EIFT_p$'s. The surfactant adsorption losses were significant. For formulation 11, the surfactant concentrations for

the two rock samples after pre-equilibration with rock and oil were about 400 ppm, lower than those after pre-equilibration with oil only (Table 16), but the $EIFT_{p,rock}$ values were as low as the $EIFT_p$ values. Among the three formulations, formulation 11 had low or ultralow EIFT values in all cases, showing the potential for maintaining low IFT values after surfactant losses due to the partitioning into the oil phase and due to the adsorption to the rock.

Table 17. Comparison of the EIFTs and surfactant concentrations in the aqueous layers for three surfactant formulations with Berea Sandstone rock samples.

Surfactant Formulation	Rock	After pre-equilibration of surfactant/brine/rock			After pre-equilibration of surfactant/brine/rock/oil	
		$EIFT_{up,rock}$ ($\times 10^{-3}$ $mN \cdot m^{-1}$)	Surfactant conc. in the aq. layer (ppm)	Adsorbed surfactant (mg surf. $\cdot g\ rock^{-1}$)	$EIFT_{p,rock}$ ($\times 10^{-3}$ $mN \cdot m^{-1}$)	Surfactant conc. in the aq. layer (ppm)
8	1	~2.2[a]	11,720 ± 130	1.4 ± 0.7	70 ± 65	170 ± 10
8	2	5.6 ± 0.2	11,497 ± 490	2.6 ± 2.3	400 ± 220	490 ± 60
10	1	7.7 ± 0.2	8,300 ± 120	18.5 ± 0.6	56 ± 25	1,400 ± 300
10	2	2.4 ± 0.2	7,700 ± 220	21.6 ± 1.1	43 ± 30	340 ± 200
11	1	4.8 ± 0.1	8,000 ± 80	20.3 ± 0.4	8.2 ± 4.9	420 ± 90
11	2	5 ± 1	7,600 ± 90	22.3 ± 0.5	16 ± 13	470 ± 170

[a] The interfacial tension values were not measurable in the spinning drop apparatus, because the injected oil drops broke up spontaneously.

7.3.4 Core flood experiments

Core flood tests with formulations 8, 10, and 11 were done to test how the EIFT values correlate with the oil recovery performance of these formulations, for which the oil recovery rates from the initial water flooding (IWF) were 33%. After injection of the SP and P solutions, the tertiary oil recovery was substantial. About 55% of the residual oil was produced with formulation 8, and about 73% and 78% was produced with formulations 10 and 11 (Table 18).

Table 18. Core flood experiment results with Berea sandstone for surfactant formulations 8, 10, and 11 (Table 16).

Surfactant formulation	Original Oil-in-Place (mL)	Remaining Oil After Initial Water Flooding (mL)	Oil Recovered From EOR process (mL)	%ROIP	%OOIP
8	41	27	15	55	71
10	40	27	20	73	82
11	40	26	20	78	86

Photographs of the core materials after the core flood tests showed that formulations 10 and 11 did mobilize residual oil throughout the core material. Little amounts of oil remained anywhere in the core, and no color inhomogeneities due to residual oil were seen in photographs of the sectioned cores (Figure 41). The dark triangular area at the right end of the core material for formulation 8 indicates regions of higher residual oil. Hence, the oil mobilization sweep efficiency was reduced, either because the surfactant solution failed to mobilize oil at the later stages of the core flood or because there was some core inhomogeneity (i.e., at region X in the Figure 41a) that disrupted the flow. Nonetheless, the oil recovery was quite high at the portion of the core that was apparently accessible.

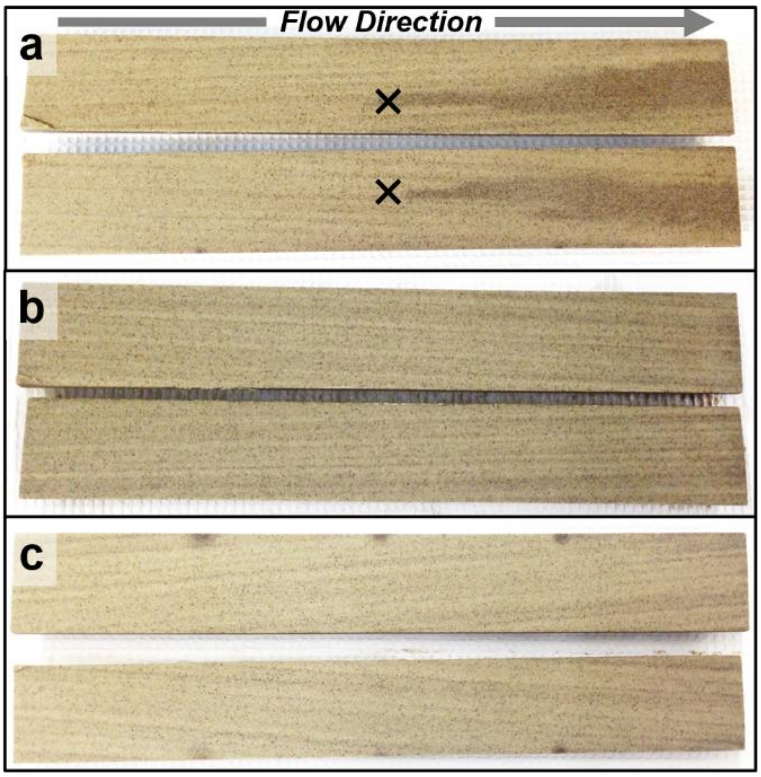

Figure 41. Photograph of the core cut in half in the direction parallel to the multiphase flow after the core flood test for surfactant formulations (a) 8, (b) 10, and (c) 11. The core flood experiment with the surfactant formulation 8, the core showed a dark triangular area on at the end that indicated poor mobilization and a potential bypass of the oil by surfactant brine solution during the test.

Formulations 8, 10, and 11 had ultralow $EIFT_{up}$ values and low $EIFT_p$ values at a water-to-oil ratio of 1.00 (Table 16). In contrast, the $EIFT_{p,rock}$ for formulation 8 was higher than that of the other two formulations (Figure 42). These results suggest that the surfactant concentrations were reduced significantly due to adsorption losses, and the surfactant compositions were probably changed. These changes could lead to weaker oil mobilization at the later stages of the core flood test. The $EIFT_{p,rock}$'s of formulation 10 and 11 were similar to the $EIFT_p$'s, indicating that the surfactant adsorption on the rock surface did not affect significantly the EIFTs. Thus, the behavior of the pre-equilibrated surfactant/brine/oil/rock mixtures may not represent well the *in situ* behavior of the aqueous/oil system at the later stages of the core flood test. The mass transfer rates of the various surfactant and oil components among water, oil, and rock during the core flood tests could be significantly different from those during the laboratory-scale phase behavior tests. Whereas all the $EIFT_{up}$ values were ultralow, the $EIFT_p$'s and $EIFT_p$,rock's were higher than the $EIFT_{up}$'s, suggesting that the surfactant partitioning into the oil phases affected significantly the

EIFT. Thus, $EIFT_{p,rock}$ is better indicator for the surfactant evaluation over the $EIFT_{up}$ or $EIFT_p$, because the pre-equilibration of the surfactant/brine/oil/rock embraces the interaction and the mass transfer among aqueous phases, oil phases, and the rock surfaces, while the $EIFT_p$ covers only those of aqueous and oil phases. Therefore, it is critical to determine directly the more relevant IFTs and the surfactant concentrations in the effluent samples of core flood tests.

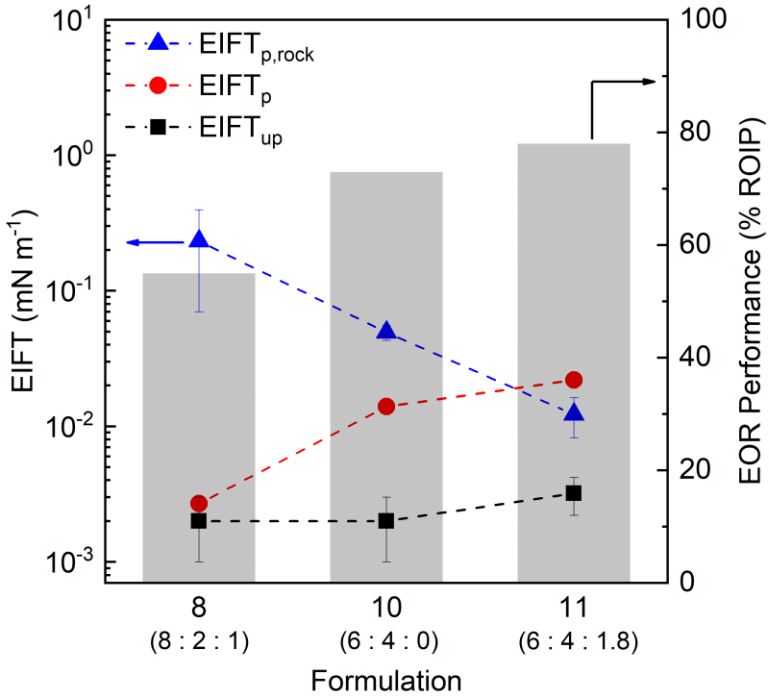

Figure 42. The $EIFT_{up}$, $EIFT_p$, $EIFT_{p,rock}$ and the EOR performance (%ROIP) of formulations 8, 10, and 11. Each $EIFT_{p,rock}$ value is the average of the $EIFT_{p,rock}$ values determined for the two core samples. Whereas all the $EIFT_{up}$ values were ultralow, the $EIFT_p$'s and $EIFT_{p,rock}$'s were higher than the $EIFT_{up}$'s, suggesting that the surfactant partitioning into the oil phases affected significantly the EIFT.

7.3.5 Core flood effluent analyses and interfacial tensions

No evidence of the formation of third phases or third layers was observed in any of the effluent samples. The amount of the produced oil per vial since the beginning of the surfactant polymer solution injection increased rapidly to the range of 20 to 50% of the normalized pore volume (PV) of the core material, and then decreased slowly (Figure 43b). After most of the oil was produced, the aqueous layers looked brown and turbid. These results indicate that the

surfactant-containing aqueous phases had exited the core after most of the oil was produced. Hence, an oil bank was probably formed in front of the injected surfactant polymer slug.

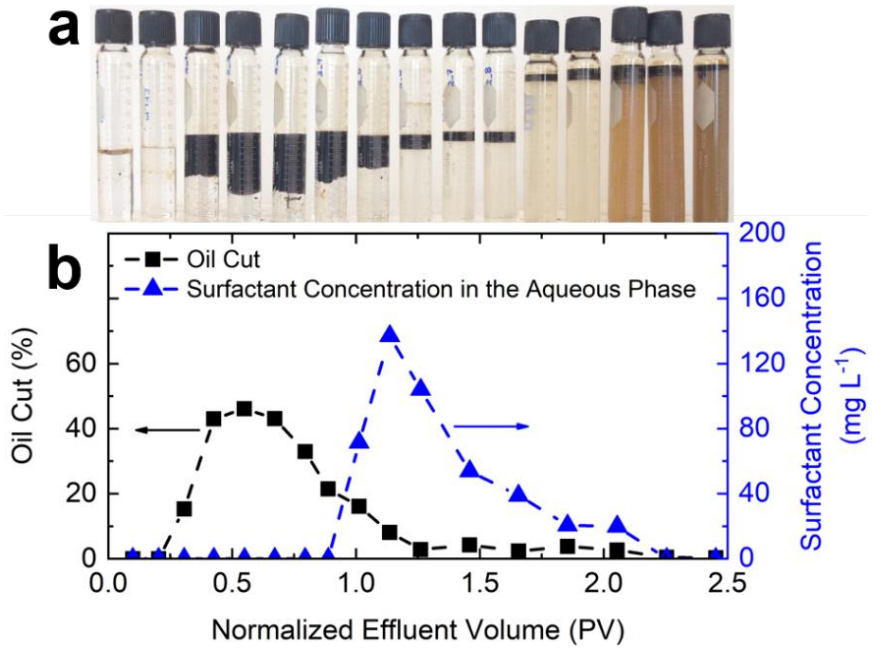

Figure 43. (a) Photographs of the effluent sample vials; and (b) oil cuts and surfactant concentrations in aqueous phases of the effluent samples vs. normalized effluent volume, for formulation 10. Similar trends were observed for the other two core floods with formulations 8 and 11.

The $EIFT_{eff}$ trend of formulations 10 and 11 was significantly different from that of formulation 8. For formulations 10 and 11, the $EIFT_{eff}$ values with the Oil_1, which was produced earlier than the Oil_2, were much higher than those with the Oil_2 (Figures 44b and 44c). For example, at around 1.0 PV with formulation 10 (Figure 44b and Table 19), the $EIFT_{eff}$ with Oil_1 was 3.0 $mN \cdot m^{-1}$, and that with Oil_2 was 0.069 $mN \cdot m^{-1}$. These differences suggest that the concentrations of the various surfactant components in the two oil samples were significantly different, due to their preferential partitioning to rock and oil during the core flood tests.[37] Similar trends were observed for formulation 11 (Figures 44c and 44f). However, for formulation 8 (Figures 44a and 44d), the $EIFT_{eff}$'s were similar and close to those with Oil_1. These trends were observed, even though the surfactant concentrations in the effluent aqueous layers were quite higher (Figure 44a, blue line) than those for the other two formulations (Figures 44b, and 44c, blue lines). These results suggest that the surfactant components that contribute most to the IFT reduction had higher

adsorption losses in the early stages of the core flood tests than the less surface-active components. Thus, even though the total surfactant concentrations were higher than those for the other two cases in the aqueous effluents, the oil mobilization was less effective, and more oil drops remained at the later stage of the core flood tests (Figure 41a).

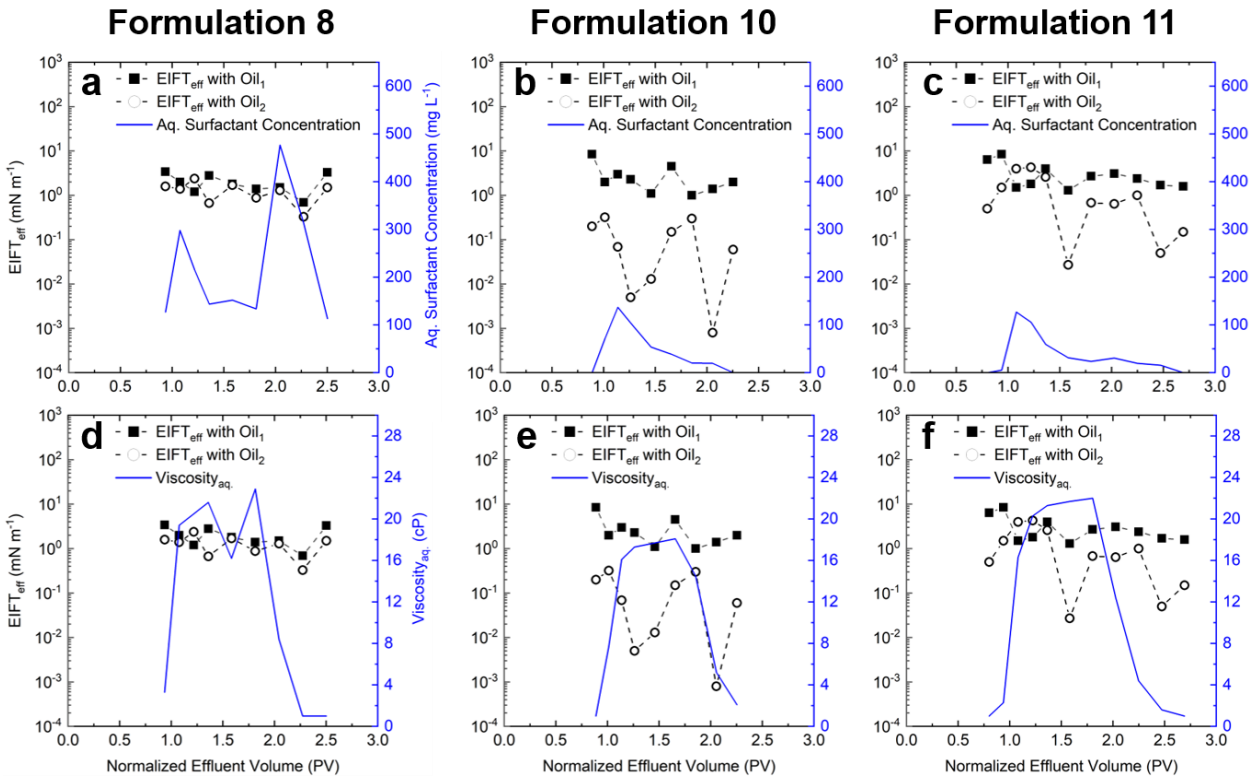

Figure 44. PV dependence of the EIFT$_{eff}$'s between the effluent aqueous samples and the first (Oil$_1$, -■-) or the second (Oil$_2$, -○-) effluent oil samples, and the surfactant concentrations (a-c) and the viscosities (d-f) of the effluent aqueous samples.

Table 19. Solution properties and interfacial tensions ($EIFT_{eff}$) between the produced oil samples and the effluent aqueous layers.

Formulation Used in Core Flood Tests	Aqueous phase	Polymer conc. of effluent (ppm)	Viscosity (cP)	Surfact. Conc'n in Aqueous Phases ($mg\ L^{-1}$)		$EIFT_{eff}$ with Oil_1 ($mN \cdot m^{-1}$)	$EIFT_{eff}$ with Oil_2 ($mN \cdot m^{-1}$)
				123-15S	A-6		
8	Sample 7	272	3.3	127	-*	3.4 ± 0.1	1.6 ± 0.1
8	Sample 8	507	19.4	298	117	2.0 ± 0.1	1.4 ± 0.1
8	Sample 9	596	20.5	215	86	1.2 ± 0.1	2.4 ± 0.1
8	Sample 10	637	21.6	144	64	2.8 ± 0.1	0.67 ± 0.05
8	Sample 11	646	16.2	152	60	1.8 ± 0.1	1.7 ± 0.1
8	Sample 12	594	22.9	134	56	1.4 ± 0.1	0.88 ± 0.05
8	Sample 13	470	8.4	477	263	1.5 ± 0.1	1.3 ± 0.1
8	Sample 14	265	1.0	313	217	0.7 ± 0.1	0.33 ± 0.01
8	Sample 15	6	1.0	113	96	3.3 ± 0.1	1.5 ± 0.1
10	Sample 8	-	1.0	-	-	8.5 ± 0.2	0.20 ± 0.01
10	Sample 9	593	7.7	72	-	2.0 ± 0.1	0.32 ± 0.02
10	Sample 10	763	16.1	137	-	3.0 ± 0.1	0.069 ± 0.001
10	Sample 11	770	17.3	104	-	2.3 ± 0.1	0.0050 ± 0.0001
10	Sample 12	783	17.7	54	-	1.1 ± 0.1	0.013 ± 0.001
10	Sample 13	781	18.1	39	-	4.5 ± 0.2	0.15 ± 0.01
10	Sample 14	775	14.5	21	-	1.0 ± 0.1	0.30 ± 0.01
10	Sample 15	591	5.2	20	-	1.4 ± 0.1	0.0008 ± 0.0001
10	Sample 16	364	2.1	-	-	2.0 ± 0.1	0.06 ± 0.01
11	Sample 6	-	1.0	-	-	6.4 ± 0.2	0.50 ± 0.01
11	Sample 7	112	2.3	5.3	-	8.5 ± 0.7	1.5 ± 0.1
11	Sample 8	550	16.3	127	-	1.5 ± 0.1	4.0 ± 0.1

Table 19 continued

11	Sample 9	609	20.3	106	-	1.8 ± 0.1	4.3 ± 0.1
11	Sample 10	620	21.3	59	-	4.0 ± 0.2	2.6 ± 0.1
11	Sample 11	550	21.7	32	-	1.3 ± 0.1	0.027 ± 0.001
11	Sample 12	608	22.0	24	-	2.7 ± 0.1	0.68 ± 0.03
11	Sample 13	585	12.4	31	-	3.1 ± 0.2	0.64 ± 0.01
11	Sample 14	392	4.4	20	-	2.4 ± 0.1	1.0 ± 0.1
11	Sample 15	181	1.6	16	-	1.7 ± 0.1	0.05 ± 0.01
11	Sample 16	-	1.0	-	-	1.6 ± 0.1	0.15 ± 0.01

* The chemical concentration was lower than the detection limit of the apparatus used. The detection limit was 1 ppm for polymer concentrations and 1 mg L^{-1} for surfactant component concentrations.

7.4 Conclusions

Five different types of equilibrium interfacial tensions (EIFTs) were defined to test the ones that are more significant factors for oil recovery efficiency. The goal was to examine the effect of surfactant partitioning into the oil phase and adsorption on the rock surfaces to the ability of the remaining surfactant to affect the interfacial tension (IFT) between the oil and aqueous phases. The behavior of eleven surfactant formulations, composed of commercial surfactants (123-15S and A-6) and a co-solvent (L4-2) in a synthetic brine with eight salts were compared. These surfactant formulations were chosen because they had ultralow (< 10^{-2} mN·m^{-1}) EIFT values before any pre-equilibration. When each formulation was pre-equilibrated with crude oil in a 1:1 volume ratio, one formulation, with the 8:2:1 ratio of 123-15S:A-6:L4-2, maintained ultralow EIFT. Eight formulations, with ratios 10:0:2, 9:1:0, 9:1:1, 9:1:2, 8:2:0, 8:2:2, 6:4:0, and 6:4:1.8, had low EIFT values (between 10^{-2} mN·m^{-1} and 10^{-1} mN·m^{-1}). The EIFT increases were evidently due to the preferential partitioning of the various surfactant components into the oil phase. When each of these formulations that had the lowest EIFT after the pre-equilibration with oil was pre-equilibrated also with Berea sandstone in the absence of oil, the EIFT was similar to those with no

pre-equilibration. Although these results were probably affected by the high mass ratio of the surfactant to the rock, there was significant surfactant loss ranging from 3% to 33%. When the three formulations were pre-equilibrated with crude oil and rock, only one of them had a low EIFT value between the pre-equilibrated oil and aqueous phase.

The laboratory-scale oil recovery performance was inversely correlated to the EIFT values after pre-equilibration with both oil and rock. Moreover, the surfactant formulations that recovered the least amount of oil from the core flood test had non-ultralow effluent EIFTs. The other two formulations showed at least one ultralow effluent EIFT. These results suggest that if a surfactant formulation has ultralow IFTs throughout the recovery process, a continuous oil mobilization may occur, and oil recovery performance in core flood tests is high. The EIFTs after pre-equilibration of the surfactant solution with rock, and oil appear to be the best indicators, or predictors, of good EOR performance, and hence may provide a reliable measure for screening surfactant formulations. Therefore, establishing the importance of the several types of EIFTs, and the development of robust protocols measuring them, may complement certain conventional surfactant formulation evaluation methods prior to core flood tests, which in the past relied primarily on phase behavior tests.

7.5 Experimental

7.5.1 Materials

A synthetic brine was prepared with pure water and salts sodium chloride (NaCl), sodium bicarbonate ($NaHCO_3$), calcium chloride dihydrate ($CaCl_2 \cdot 2H_2O$), magnesium (II) chloride hexahydrate ($MgCl_2 \cdot 6H_2O$), barium chloride dihydrate ($BaCl_2 \cdot 2H_2O$), potassium chloride (KCl), sodium sulfate decahydrate ($Na_2SO_4 \cdot 10H_2O$), and manganese (II) chloride tetrahydrate ($MnCl_2 \cdot 4H_2O$), as previously.[35] The proprietary commercial alkylpropyleneoxide extended sulfonate surfactant, ALFOTERRA® 123-15S 90 (123-15S), was obtained from Sasol Chemicals (USA) LLC (Houston, TX). The proprietary commercial alkylxylene sulfonate surfactant PETROSTEP® A-6 (A-6) was obtained from the Stepan Company (Northfield, IL). Both surfactants were yellow or amber, viscous liquids and were used as received. The proprietary commercial co-solvent, SURFONIC® L4-2 (L4-2) was a clear, colorless liquid obtained from Huntsman International LLC (The Woodlands, TX) and was used as received. The first surfactant,

123-15S, contains about 90 wt% of several single-chain isopropoxylated alkyl sodium sulfate surfactant components. The second surfactant, A-6, contains about 56 wt% of alkyl xylene sodium sulfate components. The co-solvent is a mixture of ethylene glycol adducts of *n*-butanol. The detailed compositions of the surfactants and the co-solvent are not available. A partially hydrolyzed polyacrylamide, FLOPAAM^{TM} 3330S, was obtained from SNF (Andrézieux-Bouthéon, France) and used as received to increase the viscosity of the surfactant brine solutions. The polymer average molecular weight is 8×10^6 g·mole^{-1}, and the anionic content is about 25-30%. Starch and CdI_2 were purchased from Sigma-Aldrich, and they were used as received. The 5.25% sodium hypochlorite solution was purchased from Champion Packaging & Distribution (Woodridge, IL) and used as received. Commercially available Berea sandstone cylindrical core materials (30 cm in length and 3.8 cm in diameter) were purchased from Cleveland Quarries (Vermilion, OH), and they were used for laboratory-scale core flood experiments. The Berea sandstone contained on average ~93% SiO_2, ~4% Al_2O_3 (~4%), less than 1% of FeO, and less than 0.5% of Fe_2O_3, MgO, and CaO. The average permeability was 200 mD, and the average porosity was 20%.

7.5.2 Specific surface areas of Berea Sandstone

A Quantachrome Nova 2200e Surface Area & Pore Size Analyzer was used to determine surface areas from the amounts of N_2 adsorbed on the sample surface of the solid particles. For each measurement, 1 g of particulate crushed Berea Sandstone^{TM} was first heated at 150 °C under vacuum (< 10^{-2} mmHg) to remove any volatile residual materials. The surface area was determined from N_2 physisorption data using the multipoint Brunauer–Emmett–Teller (BET) isotherm. At each N_2 pressure point from 5×10^{-3} atm to 1 atm, the adsorption equilibrium was reached within 5 min. The specific surface area was about 0.7 $m^2 \cdot g^{-1}$ to 1.0 $m^2 \cdot g^{-1}$ for all particle size ranges tested (Table 19). These results suggest that the surfactant adsorption behavior on the ground Berea Sandstone sample could represent that of the Berea Sandstone core material used for the core flood tests.

Table 20. Specific Surface Area of Berea Sandstone samples

Sample number	Particle Size Range (μm)	Specific Surface Area ($m^2 \cdot g^{-1}$)
1	10 – 100	0.77 ± 0.1
2	10 – 100	0.81± 0.1
3	10 – 250	0.84 ± 0.2
4	10 – 250	0.92 ± 0.3
5	10 – 250	0.93 ± 0.3
6	500 – 5,000	1.01 ± 0.1
7	500 – 5,000	1.01 ± 0.1

7.5.3 Phase behavior tests and equilibrium interfacial tension (EIFT) measurements

Borosilicate vials were soaked in purified water to remove any residual impurities. Phase behavior tests were done by mixing 12 mL of an aqueous surfactant solution in the synthetic brine (ρ = 1.004 $g \cdot mL^{-1}$) with 12 mL of crude oil (ρ = 0.887 $g \cdot mL^{-1}$) by vigorously shaking by hand. The mixture was centrifuged for 1.5 h at 12,000 rpm (at an average acceleration of 19,800 g) to accelerate the phase separation process and the particle or droplet sedimentation, creaming, and coalescence. More details of the cleaning procedures and the phase behavior protocols were described in our previous work.[37] Surfactant/brine/oil/rock mixtures were prepared by mixing 2 g of crushed Berea sandstone sample with a mixture of oil/brine/surfactant. The mixture was equilibrated for 100 h and was centrifuged. After centrifugation, each of the resulting liquid layers was sampled, and its density was determined at 24 °C with an Anton Paar DMA 5000 density meter. The un-pre-equilibrated equilibrium interfacial tension ($EIFT_{up}$) and the pre-equilibrated equilibrium interfacial tension ($EIFT_p$) were determined as described in our previous work using Dataphysics SVT 20 spinning drop tensiometer.[34,35,37]

7.5.4 Equilibration of surfactant/brine with Berea rock particles and EIFT between the surfactant solution and crude oil

The surfactant brine solution was mixed with ground Berea Sandstone at a solution volume to rock mass ratio of 5:1. To determine the adsorption isotherm, five surfactant concentrations were tested: 12,000 ppm, 6,000 ppm, 3,000 ppm, 1,500 ppm, and 750 ppm. For each surfactant concentration, three surfactant formulations, which were composed of two commercial surfactants (123-15S and A-6) and one commercial co-solvent (L4-2), were used. The ratio of the 123-15S, A-6, and L4-2 of formulations 8, 10, and 11 were 8:2:1, 6:4:0, and 6:4:1.8, respectively. Each experiment was repeated with a second rock sample. Each mixture was shaken vigorously by hand for 1 min at room temperature and was stored for 100 h to ensure equilibration. Then, the mixture was centrifuged at 12,000 rpm (at an average of 19,800 g) for 20 min at 24 °C. The EIFT between the supernatant clear liquid solution and a drop of oil was defined as the $EIFT_{up,rock}$. The surfactant concentration in the remaining aqueous layer was determined by the two-phase titration method. As the initial concentration increased from 750 ppm to 12,000 ppm the amount of adsorbed surfactant increased from 2 mg of surfactant / g of rock to 20 mg of surfactant / g of rock for formulations 10 and 11. However, for formulation 11, the amount of adsorbed surfactant remained below 2 mg of surfactant / g of rock (Figure 45).

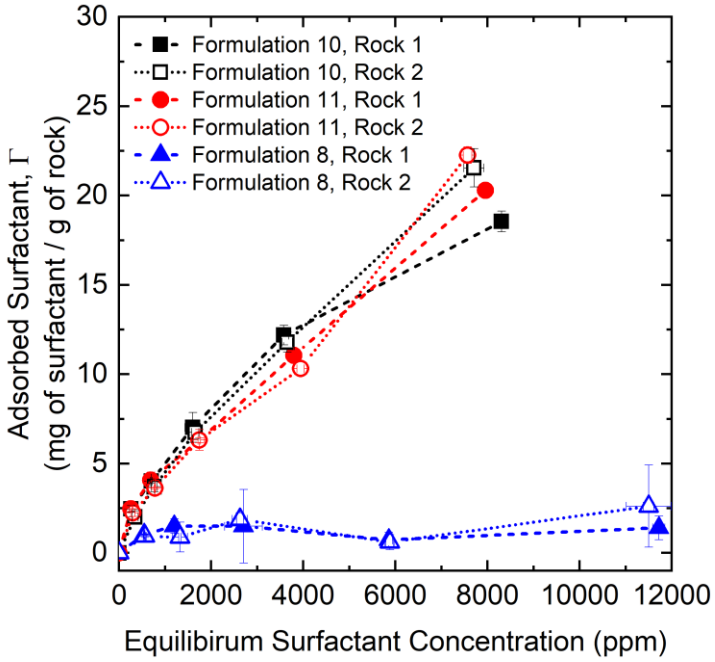

Figure 45. The adsorption isotherms of formulations 8, 10, and 11.

7.5.5 Core flood tests with Berea sandstone

Cylindrical Berea Sandstone unsaturated core materials were first dried for 8 h in an oven at 110 ℃ and weighed. The dried core was placed inside a vacuum chamber for 1 h. A synthetic brine was introduced under vacuum to fully saturate the core materials. The saturated core material was removed from the vacuum chamber and then weighed. The difference between the saturated and unsaturated core masses was the liquid mass inside. From this, the core pore volume (PV) was estimated.

The core material was placed inside a Phoenix Hassler-type core holder, which had three junction points connected to pressure transducers at equal distances. The ends of each core were capped with metal injection pistons with the same diameter as that of the core material. The pistons filters were used to dispense the injected surfactant-polymer formulations evenly across the cross-sectional area of the core and minimize the effect of pressure fluctuations during the core flood experiments. An "overburden pressure" of 400 psi was applied for the core holder and the encased core material. The pressure difference along the core was determined by monitoring the injection and production pressure, and along the three junctions. Then, the core holder was placed inside a standard mechanical convection oven (Blue M 146 series, purchased from Thermal Product Solutions ,New Columbia, PA) at 24 ℃. Then brine was injected, at a flow rate of 0.25 $mL \cdot min^{-1}$, or 0.5 $mL \cdot min^{-1}$, or 1.0 $mL \cdot min^{-1}$, or 1.25 $mL \cdot min^{-1}$. The volume of the produced brine was measured at each flow rate to determine the brine permeability of the core. About two pore volumes of crude oil were injected to fully displace the brine. The oil-saturated core was sealed and stored for two weeks, after which it was flooded by synthetic brine, to displace the oil and simulate a typical secondary oil recovery process. This process is the "initial water flooding"(IWF) stage. The effluent liquid was sequentially collected in centrifuge vials (15 mL graduated glass). The IWF continued until the "oil cut," or the percent oil volume of the later effluent sample, fell below 1%. After the IWF stage was completed, a surfactant-polymer solution (SP) was injected, followed by a polymer solution (P), and then a brine solution, to simulate a tertiary recovery process. The brine was injected to recover any residual oil mobilized by the SP and P solutions. The brine injection is referred to as the "extended water flooding" (EWF) stage. Throughout the tertiary recovery process, the effluent liquid was collected using the same methods as that of the IWF. Vials of effluent sample were divided into three groups based on when they were collected and the injection time of each solution. These groups were the SP, P, and EWF phases. The effluent

sample vials were centrifuged for 30 min at 1,800 rpm (at an average acceleration of 550 g) at 43 ℃ to facilitate phase separation, and then photographs of the sample vials were obtained.

7.5.6 Aqueous surfactant polymer sample analyses

The surfactant concentrations of aqueous samples were determined using high performance liquid chromatography (HPLC), or the two-phase titration method for anionic surfactant content, or both.[37]. For HPLC, a Thermo Ultimate 3000 UHPLC system equipped with a charged aerosol detector (CAD), and an Acclaim™ Surfactant Plus HPLC Column, which was packed with 3 µm silica particles was used. For determining surfactant concentrations in a surfactant solution or a surfactant polymer solution with the HPLC, a 500 µL of aqueous solution was diluted 1:1 with a 1 wt% aqueous bleach solution. Each diluted sample was incubated at 35 ℃ overnight to degrade any polymer and to reduce the sample viscosity.[159] Then the sample was passed through a 0.2 µm polyethersulfone syringe filter. A filtered sample of 10 µL was injected onto the column and eluted at a rate of 1 $mL \cdot min^{-1}$ at 30 ℃. The elution was done in two stages. The first stage was an isocratic elution stage for 13 min at 10 vol% of 0.1 M aqueous ammonium acetate, 30 vol% acetonitrile, and 60 vol% water. The second stage was a gradient elution stage. The eluent composition was linearly changed over 10 min from 30 vol% acetonitrile and 60 vol% water to 90 vol% acetonitrile and 0 vol% water, while the volume percent of 0.1 M aqueous ammonium acetate was kept constant at 10%. The 123-15S and A-6 surfactants eluted at around 13.4 min and 17.8 min, respectively. The co-solvent was weakly retained, and its peak overlapped with those of salts and other weakly retained species (Figure 46).

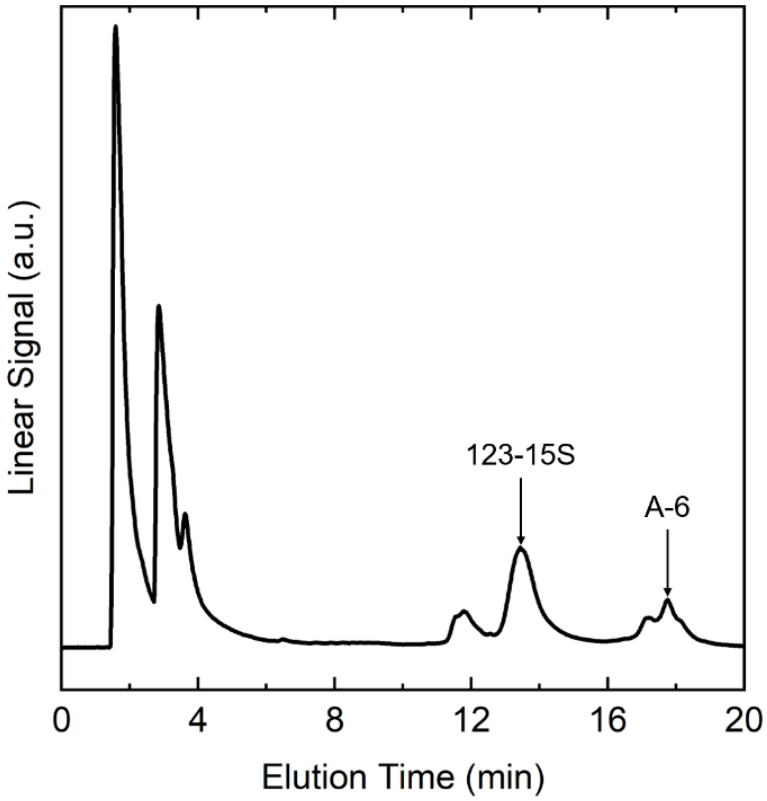

Figure 46. Chromatogram (black) of a solution containing 123-15S (peak at 13.4 min) and A-6 (peak at 17.8 min). The peak width for 123-15S and A-6 are attributed to the polydisperse nature of each commercial surfactant. L4-2 typically eluted with other weakly retained material at 2.6 min.

The polymer concentrations in the aqueous layers of effluent samples were determined from the absorbances, at a wavelength of 581 nm, of a complex formed selectively by the polyacrylamide polymer with a cadmium iodide (CdI_2)-starch solution.[160] To generate this complex, the following procedure was used. First a buffer solution was prepared by dissolving 25 g of sodium acetate trihydrate, 110 mL of glacial acetic acid, and 0.75 g of hydrated aluminum sulfate in 800 mL DI water. The pH of the solution was adjusted to 3.5 by adding acetic acid, and DI water was added until the mixture volume reached 1 L. Then a CdI_2-starch stock solution was prepared as follows. First, 11 g of CdI_2 (Sigma-Aldrich) was dissolved in 400 g of DI water, and the solution was boiled for 15 min. The mixture was cooled to room temperature, and DI water was added for a total solution mass of 800 g. Then, 2.5 g of starch (Sigma-Aldrich) was added slowly with gentle magnetic stirring. The mixture was boiled for 5 min and was again cooled to room temperature. Then, the mixture was filtered through two Whatman No. 42 filter papers with

the assistance of vacuum. DI water was added to the filtrate to have the total mass of the solution be 1,000 g.

For each sample analysis, 1 mL of an aqueous surfactant/polymer sample was first mixed, with 5 mL of the buffer solution and 29 mL of DI water. Then, 1 mL of saturated bromine water (RICCA Chemical Company) was added to the mixture, and it was allowed to react for 15 min. Then, 5 mL of 1 wt% sodium formate solution (Sigma-Aldrich) was added, and it was allowed to react for 5 min. Afterwards, 3 mL of the starch-CdI_2 stock solution was added. The resulting solution had a deep purple color only when the sample contained polymer. Then, 1 mL of each sample was transferred to a 1 cm path length cuvette. The absorbance values at 581 nm were measured with a ThermoScientific Genesys 30 spectrophotometer. The polymer concentration of each sample was determined by calibration. The absorbances were proportional to the polymer concentrations (Figure 47). The specific absorptivity was $(372 \pm 5) \times 10^{-5}$ cm^{-1} ppm^{-1}.

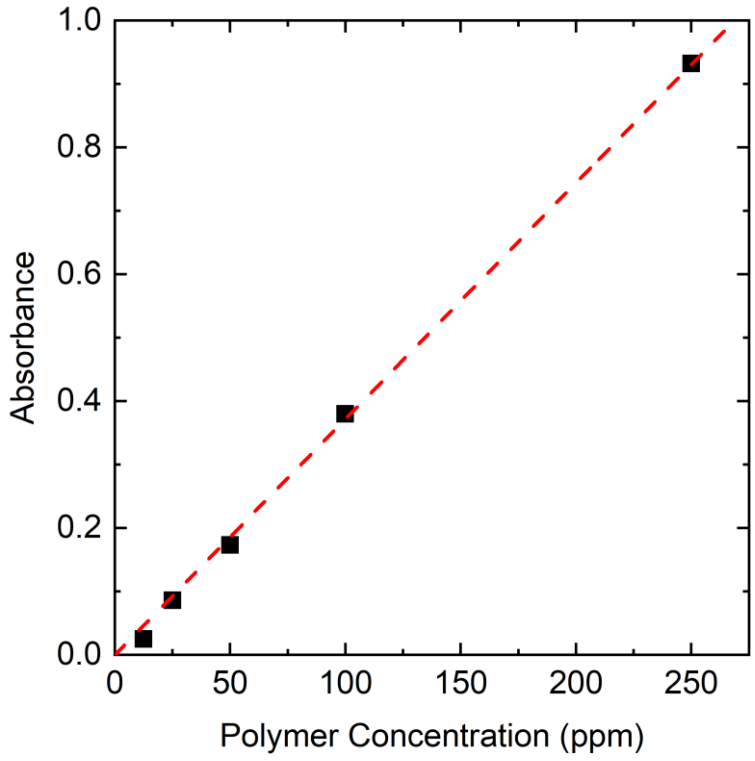

Figure 47. Calibration curve for determining polymer concentration, in ppm by weight, in aqueous surfactant polymer samples from the absorbances at 581 nm. The dashed line is the linear fit to the data. The slope is $(372 \pm 5) \times 10^{-5}$ $cm^{-1} \cdot ppm^{-1}$.

7.5.7 Sample selection procedure for the effluent EIFT ($EIFT_{eff}$) measurements

The equilibrium interfacial tension values between the oil and aqueous phases of effluent samples that were produced during core flood tests were determined. The effluent sample vials that were sequentially collected after the initial water flooding (IWF) were divided into two groups so that the total oil layer volume of each group should be larger than 3 mL. The oil layers were separated from the aqueous layers and mixed in single vial for each vial group (Figure 48); the resulting two oil sample vials are named "Oil_1 "and "Oil_{p2}". The $EIFT_{eff}$ was determined between one of the two oil samples and an aqueous layer of one of several effluent sample vials with the protocol described in Section 2.2.

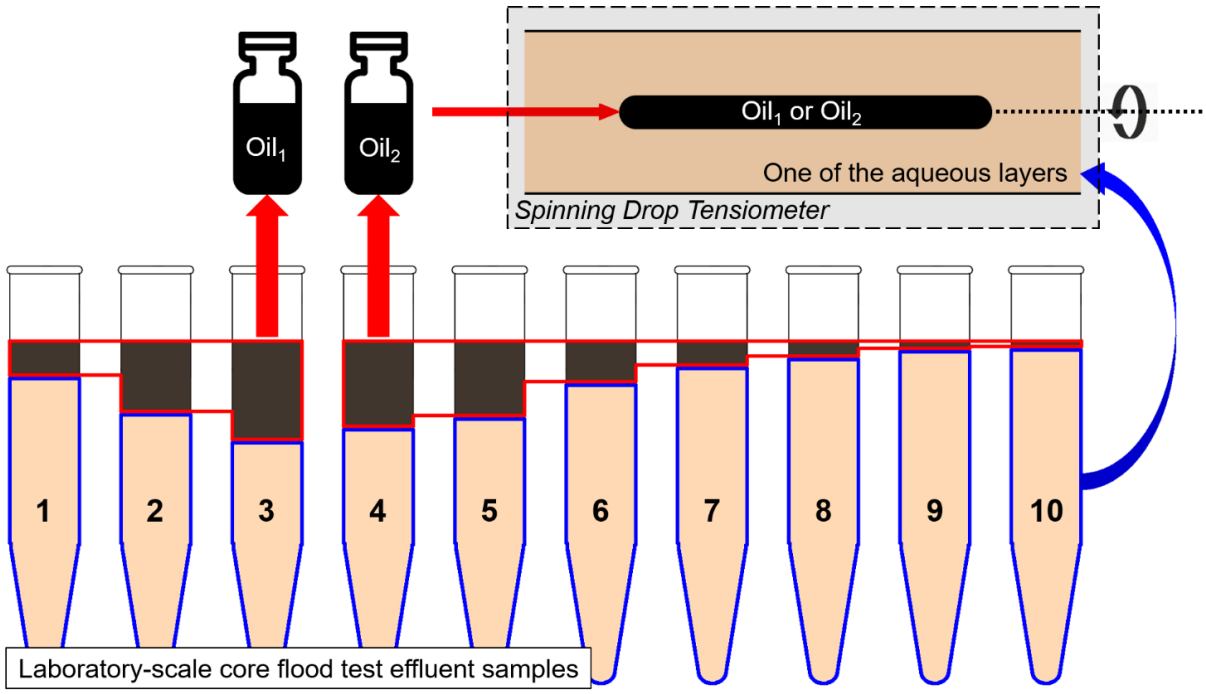

Figure. 48. Schematic diagram for determining the effluent EIFT ($EIFT_{eff}$) from the laboratory-scale core flood effluent samples. The Oil_1 sample is a mixture of the oil layers from effluent samples that are produced earlier than the Oil_2 sample. The $EIFT_{eff}$'s were measured between one of the produced aqueous layers from the effluent samples and Oil_1 or Oil_2.

8. SOME PRELIMINARY RESULTS AND SOME RECOMMENDATIONS FOR FUTURE RESEARCH

8.1 Interfacial tensions for pre-equilibrated systems involving microemulsion phases

The robust protocols for evaluating phase behavior of surfactant, brine, and oil mixtures are critical, because the phase behavior results determine the number of relevant interfacial tensions of the mixtures. If a mixture has two phases, an oil-rich phase and a water-rich phase, one interfacial tension can be defined from the mixture, and this case was a major focus so far. When a mixture has three phases at equilibrium, an oil-rich phase, a water-rich phase, and a microemulsion phase, three interfacial tensions can be defined: (i) the one between the oil-rich phase and the microemulsion phase, (ii) the one between the water-rich phase and the microemulsion phase, and (iii) the one between the oil-rich phase and the water-rich phase. The microemulsion phase may sometimes present after pre-equilibration of the aqueous surfactant solution with the oil. The discovery and characterization of middle phase microemulsion phases, when they do form, have been reported since the 1950s.[7,17,43,153] Reliable EIFT measurements involving microemulsion phases are difficult when they are very low,10^{-2} to 10^{-4} $mN \cdot m^{-1}$, or when the microemulsion phase is very viscous or highly non-Newtonian. Moreover, if the IFT dynamics involves mechanisms other than surfactant adsorption, the available tensiometry techniques may have to be fine-tuned to properly extract equilibrium values. In such cases, the area perturbation tests may not provide reliable EIFTs. In addition, the interpretation of DIFT measurements from the drop shapes may be affected by the formation of possible layers of a third microemulsion phase between the oil and water phases.

8.2 Use of equilibrium and dynamic surface tension behavior for detecting critical micelle/aggregation concentration

A double-chain cationic surfactant, didodecyldimethylammonium bromide (DDAB), is known to form stable or metastable aggregates such as unilamellar vesicles, or multilamellar liposomes, and other bilayer structures. Such aggregates can be utilized for stabilizing solid particles from agglomeration and sedimentation.[161] In some reports there is indirect EST evidence and some hypotheses that DDAB forms also micelles at some small concentration range, lower than that for forming vesicles (Table 21); however, such EST trends were inconsistent. Here, the

robust tensiometry protocol for determining ESTs with area perturbations were applied to DDAB in water and in 10 mM sodium bromide (NaBr), to help establish ESTs and possibly identify evidence of a critical micelle concentration (CMC) or a critical aggregation concentration (CAC) values.

Table 21. Reported transition concentrations of DDAB in water and tensiometry methods used

Transition Concentration (mM)	Tensiometry Method
0.036 [162]	Drop Weight
0.75 [163]	-
0.80 [164]	Wilhelmy Plate
0.045 (CMC), 0.70 (CAC) [165]	Du Noüy Ring

The CMC and CAC values may be estimated from EST curves as the total surfactant concentration changes. In Figure 49, two schematic diagrams are presented (i) when a surfactant has only one transition concentration, CMC or CAC, or (ii) when a surfactant has two transition concentrations, CMC and CAC. To identify the potential DDAB concentration range that forms micelles and vesicles, robust determination of EST is necessary to identify the changes in the EST curve slopes. When DDAB concentrations were below 0.2 mM, the steady state surface tensions (SST) that were established within one hour and were stable against area perturbations shifted to a lower value at long timescale (e.g., ~ 20 h, see Figure 50).

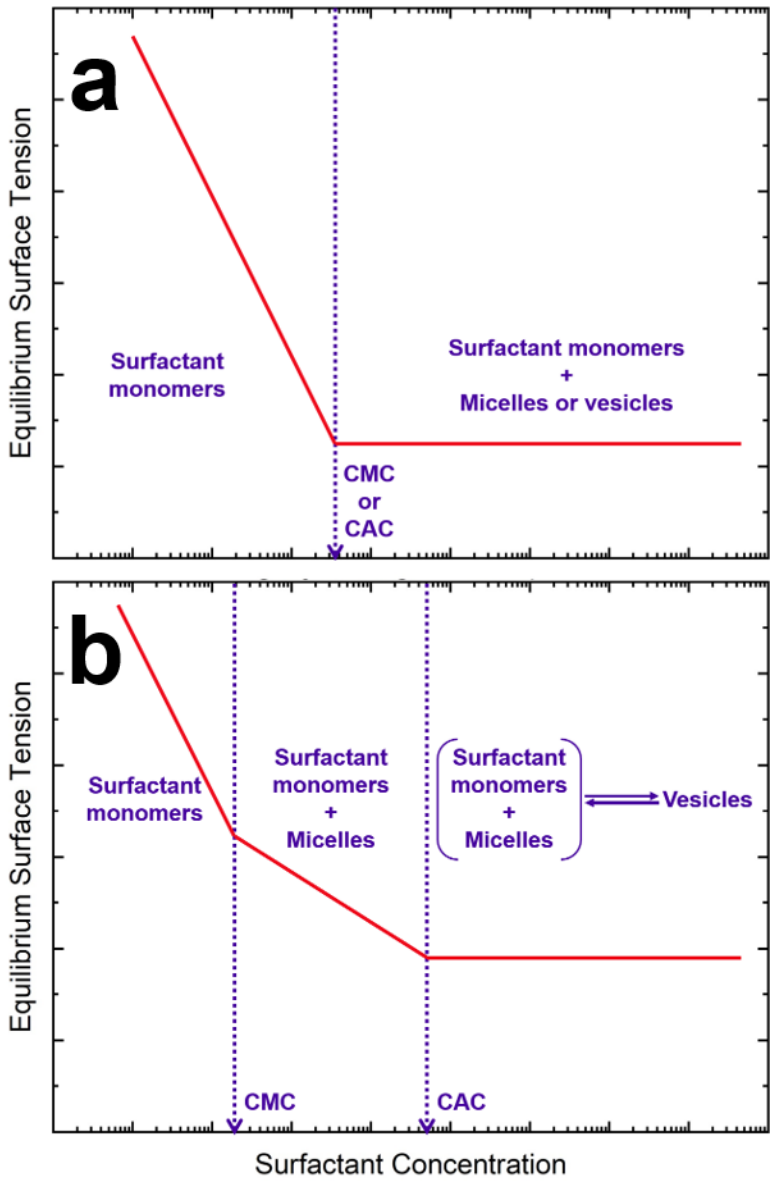

Figure 49. Schematic diagram of equilibrium surface tension (EST) curves with (a) one transition concentration, such as a CMC or CAC, and (b) two transition concentrations, one CMC and one CAC.

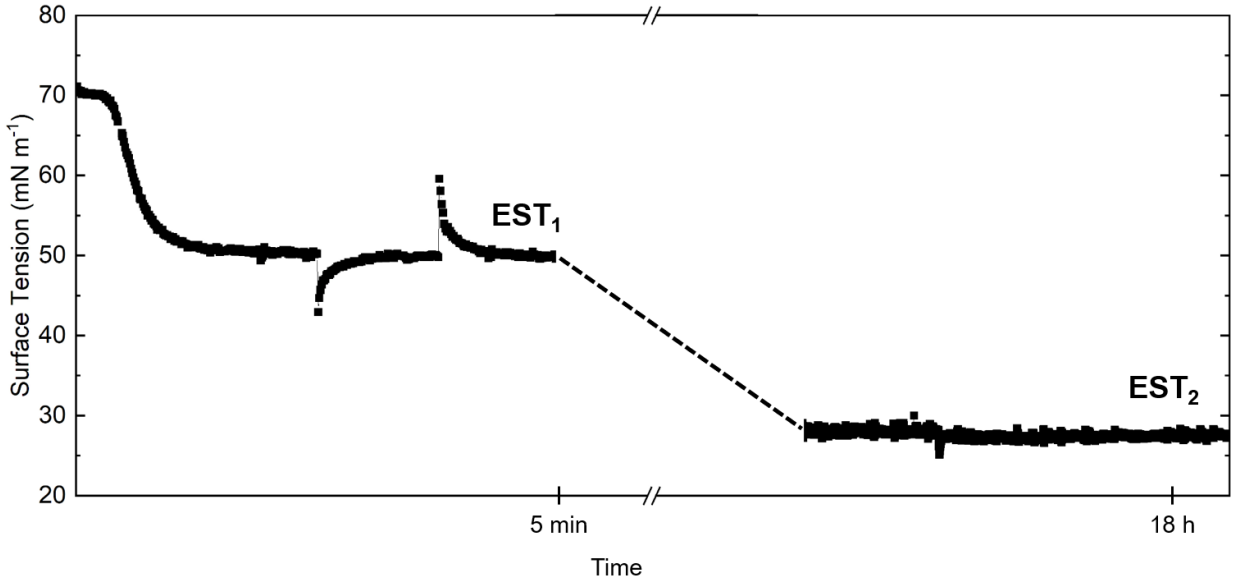

Figure 50. Dynamic surface tension of 10^{-2} mM DDAB in water at a long timescale, such as ~20 h. The first apparent EST (EST_1, ~50 $mN \cdot m^{-1}$) was established within one hour; the second apparent EST (EST_2, ~28 $mN \cdot m^{-1}$) appeared after about 20 h of continuous tension measurement.

As the DDAB concentration decreased, the DST shifted from the first apparent EST_1, determined from the stability of the steady state value against area perturbation, to a second lower apparent EST_2 (Figure 51). A similar behavior was observed with a 10 mM NaBr solution. Both apparent ESTs were stable against the area perturbations used, suggesting that the adsorbed surfactant layers on the air/water interfaces were soluble monolayers. It is not entirely clear which of the two apparent ESTs is the true stable equilibrium EST, and which one is the metastable EST. It is likely that the EST_2 is the stable EST. No proof of CMC can be reliably obtained from the available data. The EST-concentration profile looks like the curve in Figure X1a if the EST_2 data are used, and as the curve in Figure X1b if the EST_1 data are used. The nature of the monolayers of states 1 and 2 is unclear, and requires further studies, perhaps with methods that can directly probe the adsorbed layer structure and surface density.

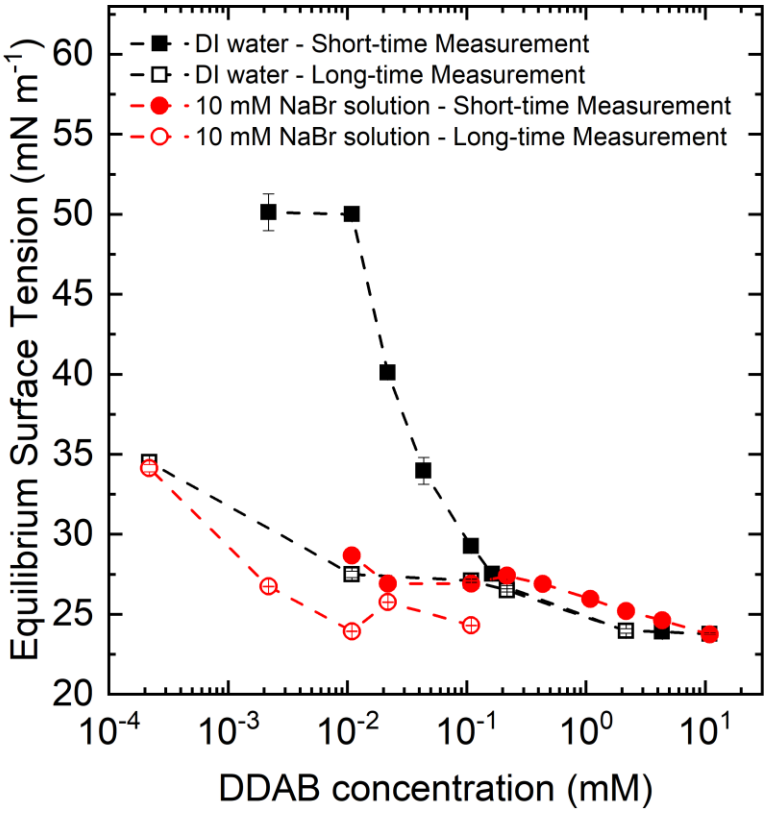

Figure 51. Equilibrium surface tensions of DDAB in water and 10 mM NaBr solution.

REFERENCES

(1) Uren, L. C.; Fahmy, E. H. Factors Influencing the Recovery of Petroleum from Unconsloidated Sands by Water-Flooding. *Trans. AIME* **1927**, *77* (1), 318–335.

(2) Sheng, J. J. *Modern Chemical Enhanced Oil Recovery: Theory and Practice*; Gulf Professional Publishing, 2010.

(3) Mungan, N. Role of Wettability and Interfacial Tension in Water Flooding. *Soc. Pet. Eng. J.* **1964**, *4* (2), 115–123.

(4) Taber, J. J. Dynamic and Static Forces Required To Remove a Discontinuous Oil Phase from Porous Media Containing Both Oil and Water. *Soc. Pet. Eng. J.* **1969**, *9* (1), 3–12.

(5) Foster, W. R. A Low-Tension Waterflooding Process. *J. Pet. Technol.* **1973**, *25* (2), 205–210.

(6) Stegemeier, G. L. Relationship of Trapped Oil Saturation to Petrophysical Properties of Porous Media. In *SPE Improved Oil Recovery Symposium*; Society of Petroleum Engineers, 1974; pp 225–238.

(7) Reed, R. L.; Healy, R. N. Some Physicochemical Aspects of Microemulsion Flooding: A Review. In *Improved Oil Recovery by Surfactant and Polymer Flooding*; Shah, D. O., Schechter, R. S., Eds.; Academic Press: New York, 1977; pp 383–437.

(8) Bourrel, M.; Schechter, R. S. *Microemulsions and Related Systems: Formulation, Solvency, and Physical Properties*; Marcel Dekker, Inc.: New York, 1988.

(9) Melrose, J. C.; Brandner, C. F. Role of Capillary Forces In Detennining Microscopic Displacement Efficiency For Oil Recovery By Waterflooding. *J. Can. Pet. Technol.* **1974**, *13* (4), 54–62.

(10) Gupta, S. P.; Trushenski, S. P. Micellar Flooding - Compositional Effects on Oil Displacement. *Soc. Pet. Eng. J.* **1979**, *19* (2), 116–128.

(11) Oh, S.; Slattery, J. C. Interfacial Tension Required for Significant Displacement of Residual Oil. *Soc. Pet. Eng. J.* **1979**, *19* (2), 83–96.

(12) Pope, G. A. The Application of Fractional Flow Theory to Enhanced Oil Recovery. *Soc. Pet. Eng. J.* **1980**, *20* (03), 191–205.

(13) Morrow, N. R.; Chatzis, I.; Taber, J. J. Entrapment and Mobilization of Residual Oil in Bead Packs. *SPE Reserv. Eng.* **1988**, *3* (3), 927–934.

(14) Amaefule, J. O.; Handy, L. L. The Effect of Intetfacial Tensions on Relative Oil / Water Penneabilities of Consolidated Porous Media. *Soc. Pet. Eng. J.* **1982**, *22* (03), 371–381.

(15) Hill, H. J.; Reisberg, J.; Stegemeier, G. L. Aqueous Surfactant Systems for Oil Recovery. *J. Pet. Technol.* **1973**, *25* (2), 186–194.

(16) Cayias, J. L.; Schechter, R. S.; Wade, W. H. The Utilization of Petroleum Sulfonates for Producing Low Interfacial Tensions between Hydrocarbons and Water. *J. Colloid Interface Sci.* **1977**, *59* (1), 31–38.

(17) Healy, R. N.; Reed, R. L.; Stenmark, D. G. Multiphase Microemulsion Systems. *Soc. Pet. Eng. J.* **1976**, *16* (3), 147–160.

(18) Salager, J. L.; Forgiarini, A. M.; Bullón, J. How to Attain Ultralow Interfacial Tension and Three-Phase Behavior with Surfactant Formulation for Enhanced Oil Recovery: A Review. Part 1. Optimum Formulation for Simple Surfactant-Oil-Water Ternary Systems. *J. Surfactants Deterg.* **2013**, *16* (4), 449–472.

(19) Nelson, R. C.; Pope, G. A. Phase Relationships in Chemical Flooding. *Soc. Pet. Eng. J.* **1978**, *18* (5).

(20) Aveyard, R.; Binks, B. P.; Clark, S.; Mead, J. Interfacial Tension Minima in Oil-Water-Surfactant Systems. Behavior of Alkane-Aqueous Sodium Chloride Systems Containing Aerosol OT. *J. Chem. Soc., Faraday Trans. 1* **1986**, *82* (1), 125–142.

(21) Goel, S. K. Phase Behavior and Detergency Study of Lauryl Alcohol Ethoxylates with High Ethylene Oxide Content. *J. Surfactants Deterg.* **2000**, *3* (2), 221–227.

(22) Tongcumpou, C.; Acosta, E. J.; Quencer, L. B.; Joseph, A. F.; Scamehorn, J. F.; Sabatini, D. A.; Yanumet, N.; Chavadej, S. Microemulsion Formation and Detergency with Oily Soils: III. Performance and Mechanisms. *J. Surfactants Deterg.* **2005**, *8* (2), 147–156.

(23) Levitt, D. B.; Jackson, A. C.; Heinson, C.; Britton, L. N.; Malik, T.; Dwarakanath, V.; Pope, G. A. Identification and Evaluation of High-Performance EOR Surfactants. *SPE Reserv. Eval. Eng.* **2009**, *12* (2), 243–253.

(24) Flaaten, A. K.; Nguyen, Q. P.; Pope, G. A.; Zhang, J. A Systematic Laboratory Approach to Low-Cost, High-Performance Chemical Flooding. *SPE Reserv. Eval. Eng.* **2009**, *12* (5), 713–723.

(25) Mohammadi, H.; Delshad, M.; Pope, G. A. Mechanistic Modeling of Alkaline / Surfactant / Polymer Floods. *SPE Reserv. Eval. Eng.* **2009**, *12* (4), 518–527.

(26) Scriven, L. E. Equilibrium Bicontinuous Structure. *Nature* **1976**, *263* (5573), 123–125.

(27) De Gennes, P. G.; Taupin, C. Microemulsions and the Flexibility of Oil/Water Interfaces. *J. Phys. Chem.* **1982**, *86* (13), 2294–2304.

(28) Hirasaki, G. J.; Miller, C. A.; Puerto, M. C. Recent Advances in Surfactant EOR. *Soc. Pet. Eng. J.* **2011**, *16* (4), 889–907.

(29) Solairaj, S.; Britton, C.; Lu, J.; Kim, D. H.; Weerasooriya, U.; Pope, G. A. New Correlation to Predict the Optimum Surfactant Structure for EOR. In *SPE Improved Oil Recovery Symposium*; 2013; pp 2–11.

(30) Huh, C.; Reed, R. L. A Method for Estimating Interfacial Tensions and Contact Angles from Sessile and Pendant Drop Shapes. *J. Colloid Interface Sci.* **1983**, *91* (2), 472–484.

(31) Liu, S.; Zhang, D.; Yan, W.; Puerto, M. C.; Hirasaki, G. J.; Miller, C. A. Favorable Attributes of Alkaline-Surfactant-Polymer Flooding. *Soc. Pet. Eng. J.* **2008**, *13* (1), 5–16.

(32) ShamsiJazeyi, H.; Verduzco, R.; Hirasaki, G. J. Reducing Adsorption of Anionic Surfactant for Enhanced Oil Recovery: Part II. Applied Aspects. *Colloids Surfaces A Physicochem. Eng. Asp.* **2014**, *453* (1), 168–175.

(33) Nagarajan, R.; Ruckenstein, E. Theory of Surfactant Self-Assembly: A Predictive Molecular Thermodynamic Approach. *Langmuir* **1991**, *7* (12), 2934–2969.

(34) Chung, J.; Boudouris, B. W.; Franses, E. I. Accurate Determination of the Equilibrium Surface Tension Values with Area Perturbation Tests. *J. Vis. Exp.* **2019**, No. 150, e59818.

(35) Chung, J.; Boudouris, B. W.; Franses, E. I. Surface Tension Behavior of Aqueous Solutions of a Propoxylated Surfactant and Interfacial Tension Behavior against a Crude Oil. *Colloids Surfaces A Physicochem. Eng. Asp.* **2018**, *537*, 163–172.

(36) Chung, J.; Yang, Y.-J.; Tang, H.; Santagata, M.; Franses, E. I.; Boudouris, B. W. Phase and Rheological Behavior of Aqueous Mixtures of an Isopropoxylated Surfactant. *Colloids Surfaces A Physicochem. Eng. Asp.* **2018**, *554* (May), 60–73.

(37) Chung, J.; Boudouris, B. W.; Franses, E. I. Effects of the Water-Oil Volume Ratio and Premixing or Pre-Equilibration on the Interfacial Tension and Phase Behavior of Biphasic Mixtures. *Colloids Surfaces A Physicochem. Eng. Asp.* **2019**, *571* (January), 55–63.

(38) Maerker, J. M.; Gale, W. W. Surfactant Flood Process Design for Loudon. *SPE Eeservoir Eng.* **1992**, *7* (1), 36–44.

(39) Barnes, J. R.; Dirkzwager, H.; Smit, J. R.; Smit, J. P.; On, A.; Reinaldo Navarrete, C.; Ellison, B.; Buijse, M. A. Application of Internal Olefin Sulfonates and Other Surfactants to EOR . Part 1 : Structure - Performance Relationships for Selection at Different Reservoir Conditions. *Soc. Pet. Eng.* **2010**, 1–16.

(40) Tagavifar, M.; Jang, S. H.; Chang, L.; Mohanty, K.; Pope, G. A. Controlling the Composition, Phase Volume, and Viscosity of Microemulsions with Cosolvent. *Fuel* **2018**, *211*, 214–222.

(41) Gogarty, W. B.; Meabon, H. P.; Milton, H. W. Mobility Control Design for Miscible-Type Waterfloods Using Micellar Solutions. *J. Pet. Technol.* **1970**, *22* (02), 141–147.

(42) Gogarty, W. B.; Davis, J. A. J. Field Experience with the Maraflood Process. In *SPE Improved Oil Recovery Symposium*; Society of Petroleum Engineers: Tulsa, Oklahoma, 1972; pp 377–394.

(43) Healy, R. N.; Reed, R. L.; Carpenter Jr., C. W. A Laboratory Study of Microemulsion Flooding. *Soc. Pet. Eng. J.* **1975**, *259*, 87–100.

(44) Unsal, E.; Broens, M.; Armstrong, R. T. Pore Scale Dynamics of Microemulsion Formation. *Langmuir* **2016**, *32* (28), 7096–7108.

(45) Defay, R.; Bellemans, A.; Prigogine, I. *Surface Tension and Adsorption*; Longmans, 1966.

(46) Padday, J. F. Theory of Surface Tension. *Surf. Colloid Sci.* **1969**, *1*, 101–151.

(47) Adamson, S. W. *Physical Chemistry of Surfaces*, 5th Editio.; Wiley: New York, 1990.

(48) Davis, H. T.; Scriven, L. E. Stress and Strucutre in Fluid Interfaces. In *Advances in Chemical Physics*; Prigogine, I., Rice, S., Eds.; John Wiley & Sons, 1982; pp 357–454.

(49) Boyce, J. F.; Schurch, S.; Rotenberg, Y.; Neumann, A. W. The Measurement of Surface and Interfacial Tension by the Axisymmetric Drop Technique. *Colloids and Surfaces* **1984**, *9*, 307–317.

(50) Río, O. I.; Neumann, A. W. Axisymmetric Drop Shape Analysis: Computational Methods for the Measurement of Interfacial Properties from the Shape and Dimensions of Pendant and Sessile Drops. *J. Colloid Interface Sci.* **1997**, *196* (2), 136–147.

(51) Cayias, J. L.; Schechter, R. S.; Wade, W. H. The Measurement of Low Interfacial Tension via the Spinning Drop Technique. *J. Colloid Interface Sci.* **1975**, *8*, 234–247.

(52) Seeto, Y.; Puig, J. E.; Scriven, L. E.; Davis, H. T. Interfacial Tensions in Systems of Three Liquid Phases. *J. Colloid Interface Sci.* **1983**, *96* (2), 360–372.

(53) Coltharp, K. A.; Franses, E. I. Equilibrium and Dynamic Surface Tension Behavior of Aqueous Soaps: Sodium Octanoate and Sodium Dodecanoate (Sodium Laurate). *Colloids Surfaces A Physicochem. Eng. Asp.* **1996**, *108* (2–3), 225–242.

(54) Vonnegut, B. Rotating Bubble Method for the Determination of Surface and Interfacial Tensions. *Rev. Sci. Instrum.* **1942**, *13* (1), 6–9.

(55) Hjelmeland, O. S.; Larrondo, L. E. Experimental Investigation of the Effects of Temperature, Pressure, and Crude Oil Composition on Interfacial Properties. *SPE Reserv. Eng.* **1986**, *1* (4), 321–328.

(56) Kékicheff, P.; Grabielle-Madelmont, C.; Ollivon, M. Phase Diagram of Sodium Dodecyl Sulfate-Water System. 1. A Calorimetric Study. *J. Colloid Interface Sci.* **1989**, *131* (1), 112–132.

(57) Chang, K.; Macosko, C. W.; Morse, D. C. Ultralow Interfacial Tensions of Polymer/Polymer Interfaces with Diblock Copolymer Surfactants. *Macromolecules* **2007**, *40* (10), 3819–3830.

(58) Shah, D. O.; Schechter, R. S. *Improved Oil Recovery by Surfactant and Polymer Flooding*; Academic Press Inc.: New York, 1977.

(59) Hiemenz, P. C.; Rajagopalan, R. *Principles of Colloid and Surface Chemistry*, 3rd ed.; Marcel Dekker, Inc.: New York, 1997.

(60) Doe, P. H.; El-Emary, M.; Wade, W. H.; Schechter, R. S. Surfactants for Producing Low Interfacial Tensions: II. Linear Alkylbenzenesulfonates with Additional Alkyl Substituents. *J. Am. Oil Chem. Soc.* **1978**, *55* (5), 505–512.

(61) Miller, R.; Lunkenheimer, K. On the Determination of Equilibrium Surface Tension Values of Surfactant Solutions. *Colloid Polym. Sci.* **1983**, *261* (7), 585–590.

(62) Miller, R.; Lunkenheimer, K. Adsorption Kinetics Measurements of Some Nonionic Surfactants. *Colloid Polym. Sci.* **1986**, *264* (4), 357–361.

(63) Lunkenheimer, K.; Miller, R. Properties of Homologous Series of Surface-Chemically Pure Surfactants at the Water-Air Interface Part I: Equilibrium Properties. *Abhandlungen der Akad. der Wissenschaften der DDR, abteilung Math. Naturwissenschaften, Tech.* **1986**, No. N1, 113–112.

(64) Franses, E. I.; Basaran, O. A.; Chang, C.-H. Techniques to Measure Dynamic Surface Tension. *Curr. Opin. Colloid Interface Sci.* **1996**, *1* (2), 296–303.

(65) Hua, X. Y.; Rosen, M. J. Dynamic Surface Tension of Aqueous Surfactant Solutions 1. Basic Parameters. *J. Colloid Interface Sci.* **1988**, *124* (2), 652–659.

(66) Rotenberg, Y.; Boruvka, L.; Neumann, A. W. Determination of Surface Tension and Contact Angle from the Shapes of Axisymmetric Fluid Interfaces. *J. Colloid Interface Sci.* **1983**, *93* (1), 169–183.

(67) Princen, H. M.; Zia, I. Y. Z.; Mason, S. G. Measurement of Interfacial Tension from the Shape of a Rotating Drop. *J. Colloid Interface Sci.* **1967**, *23* (1), 99–107.

(68) Puig, J. E.; Seeto, Y.; Pesheck, C. V.; Scriven, L. E. Optical Analysis of the Spinning Drop. *J. Colloid Interface Sci.* **1992**, *148* (2), 459–468.

(69) Lin, S.-Y.; Mckeigue, K.; Maldarelli, C. Diffusion-Controlled Surfactant Adsorption Studied by Pendant Drop Digitization. *AIChE J.* **1990**, *36* (12), 1785–1795.

(70) Moody, C. A.; Field, J. A. Perfluorinated Surfactants and the Environmental Implications of Their Use in Fire-Fighting Foams. *Environ. Sci. Technol.* **2000**, *34* (18), 3864–3870.

(71) Buckley, J. S. Chemistry of the Crude Oil/Brine Interface. In *Proceedings of the 3rd International Symposium on Evaluation of Reservoir Wettability and Its Effect on Oil Recovery*; University of Wyoming: Laramie, 1994; pp 33–38.

(72) Reisberg, J.; Doscher, T. M. Interfacial Phenomena in Crude Oil-Water Systems. *Producers monthly*. 1956, pp 43–50.

(73) Hawkins, B. F.; Taylor, K. C.; Islam, M. R. Dynamic Interfacial Tension In Surfactant Enhanced Alkaline Flooding. *J. Can. Pet. Technol.* **1990**, *29* (1), 50–55.

(74) Hirasaki, G. J.; Zhang, D. L. Surface Chemistry of Oil Recovery From Fractured , Oil-Wet , Carbonate Formations. *Soc. Pet. Eng. J.* **2004**, *9* (2), 151–162.

(75) McCaffery, F. G. Interfacial Tensions and Aging Behaviour of Some Crude Oils Against Caustic Solutions. *J. Can. Pet. Technol.* **1976**, *15* (3), 71–74.

(76) Nasr-El-Din, H. A.; Taylor, K. C. Dynamic Interfacial Tension of Crude Oil / Alkali / Surfactant , Systems. *Colloids and Surfaces* **1992**, *66* (1), 23–37.

(77) Freer, E. M.; Svitova, T.; Radke, C. J. The Role of Interfacial Rheology in Reservoir Mixed Wettability. *J. Pet. Sci. Eng.* **2003**, *39* (1–2), 137–158.

(78) Harkins, W. D.; Zollman, H. Interfacial Tension and Emulsification. I. the Effects of Bases, Salts, and Acids upon the Interfacial Tension between Aqueous Sodium Ol,Eate Solutions and Benzene. *J. Am. Chem. Soc.* **1926**, *48* (1), 69–80.

(79) Chang, C. H.; Franses, E. I. Adsorption Dynamics of Surfactants at the Air/Water Interface: A Critical Review of Mathematical Models, Data, and Mechanisms. *Colloids Surfaces A Physicochem. Eng. Asp.* **1995**, *100* (C), 1–45.

(80) Stebe, K. J.; Lin, S.-Y.; Maldarelli, C. Remobilizing Surfactant Retarded Fluid Particle Interfaces . I . Stress-Free Conditions at the Interfaces of Micellar Solutions of Surfactants with Fast Sorption Kinetics. *Phys. Fluids A Fluid Dyn.* **1991**, *3* (1), 3–20.

(81) Hines, J. D. The Preparation of Surface Chemically Pure Sodiumn-Dodecyl Sulfate by Foam Fractionation. *J. Colloid Interface Sci.* **1996**, *180* (2), 488–492.

(82) Gurkov, T. D.; Dimitrova, D. T.; Marinova, K. G.; Bilke-Crause, C.; Gerber, C.; Ivanov, I. B. Ionic Surfactants on Fluid Interfaces: Determination of the Adsorption; Role of the Salt and the Type of the Hydrophobic Phase. *Colloids Surfaces A Physicochem. Eng. Asp.* **2005**, *261* (1–3), 29–38.

(83) Kostarelos, K.; Lenschow, S. R.; Stylianou, M. A.; de Blanc, P. C.; Mygind, M. M.; Christensen, A. G. Jet A Fuel Recovery Using Micellar Flooding: Design and Implementation. *Sci. Total Environ.* **2015**, *563–564*, 890–898.

(84) Gregersen, C. S.; Kazempour, M.; Alvarado, V. ASP Design for the Minnelusa Formation under Low-Salinity Conditions: Impacts of Anhydrite on ASP Performance. *Fuel* **2013**, *105*, 368–382.

(85) Dong, J.; Chen, S.; Corti, D. S.; Franses, E. I.; Zhao, Y.; Ng, H. T.; Hanson, E. Effect of Triton X-100 on the Stability of Aqueous Dispersions of Copper Phthalocyanine Pigment Nanoparticles. *J. Colloid Interface Sci.* **2011**, *362* (1), 33–41.

(86) Garti, N.; Libster, D.; Aserin, A. Lipid Polymorphism in Lyotropic Liquid Crystals for Triggered Release of Bioactives. *Food Funct.* **2012**, *3* (7), 700.

(87) Hegmann, T.; Qi, H.; Marx, V. M. Nanoparticles in Liquid Crystals: Synthesis, Self-Assembly, Defect Formation and Potential Applications. *J. Inorg. Organomet. Polym. Mater.* **2007**, *17* (3), 483–508.

(88) Yang, Y.-J.; Corti, D. S.; Franses, E. I. Use of Close-Packed Vesicular Dispersions to Stabilize Colloidal Particle Dispersions against Sedimentation. *Langmuir* **2015**, *31* (32), 8802–8808.

(89) Dellinger, T. M.; Braun, P. V. Lyotropic Liquid Crystals as Nanoreactors for Nanoparticle Synthesis. *Chem. Mater.* **2004**, *16* (11), 2201–2207.

(90) Guo, C.; Wang, J.; Cao, F.; Lee, R. J.; Zhai, G. Lyotropic Liquid Crystal Systems in Drug Delivery. *Drug Discov. Today* **2010**, *15* (23–24), 1032–1040.

(91) Alexandridis, P.; Olsson, U.; Lindman, B. A Record Nine Different Phases (Four Cubic, Two Hexagonal, and One Lamellar Lyotropic Liquid Crystalline and Two Micellar Solutions) in a Ternary Isothermal System of an Amphiphilic Block Copolymer and Selective Solvents (Water and Oil). *Langmuir* **1998**, *14* (10), 2627–2638.

(92) Mezzenga, R.; Meyer, C.; Servais, C.; Romoscanu, A. I.; Sagalowicz, L.; Hayward, R. C. Shear Rheology of Lyotropic Liquid Crystals: A Case Study. *Langmuir* **2005**, *21* (8), 3322–3333.

(93) Laughlin, R. G. *The Aqueous Phase Behavior of Surfactants*; Academic Press: London, 1996.

(94) Pillai, V.; Shah, D. O. *Dynamic Properties of Interfaces and Association Structures*; American Oil Chemists' Society, 1996.

(95) Negin, C.; Ali, S.; Xie, Q. Most Common Surfactants Employed in Chemical Enhanced Oil Recovery. *Petroleum* **2017**, *3* (2), 197–211.

(96) Wu, Y.; Iglauer, S.; Shuler, P.; Tang, Y.; Goddard III, W. A. Branched Alkyl Alcohol Propoxylated Sulfate Surfactants for Improved Oil Recovery. *Tenside, Surfactants, Deterg.* **2010**, *47* (3), 152–161.

(97) Rosen, M. J.; Wang, H.; Shen, P.; Zhu, Y. Ultralow Interfacial Tension for Enhanced Oil Recovery at Very Low Surfactant Concentrations. *Langmuir* **2005**, *21* (9), 3749–3756.

(98) Iglauer, S.; Wu, Y.; Shuler, P.; Tang, Y.; Goddard III, W. A. New Surfactant Classes for Enhanced Oil Recovery and Their Tertiary Oil Recovery Potential. *J. Pet. Sci. Eng.* **2010**, *71* (1–2), 23–29.

(99) Liu, Q.; Dong, M.; Ma, S.; Tu, Y. Surfactant Enhanced Alkaline Flooding for Western Canadian Heavy Oil Recovery. *Colloids Surfaces A Physicochem. Eng. Asp.* **2007**, *293* (1–3), 63–71.

(100) Nguyen, T. T.; Youssef, N. H.; McInerney, M. J.; Sabatini, D. A. Rhamnolipid Biosurfactant Mixtures for Environmental Remediation. *Water Res.* **2008**, *42* (6–7), 1735–1743.

(101) Do, L. D.; Withayyapayanon, A.; Harwell, J. H.; Sabatini, D. A. Environmentally Friendly Vegetable Oil Microemulsions Using Extended Surfactants and Linkers. *J. Surfactants Deterg.* **2009**, *12* (2), 91–99.

(102) Klaus, A.; Tiddy, G. J. T.; Touraud, D.; Schramm, A.; Stühler, G.; Drechsler, M.; Kunz, W. Phase Behavior of an Extended Surfactant in Water and a Detailed Characterization of the Dilute and Semidilute Phases. *Langmuir* **2010**, *26* (8), 5435–5443.

(103) Klaus, A.; Tiddy, G. J. T.; Touraud, D.; Schramm, A.; Stühler, G.; Kunz, W. Phase Behavior of an Extended Surfactant in Water and a Detailed Characterization of the Concentrated Phases. *Langmuir* **2010**, *26* (22), 16871–16883.

(104) Charoensaeng, A.; Sabatini, D. A.; Khaodhiar, S. Solubilization and Adsolubilization of Polar and Nonpolar Organic Solutes by Linker Molecules and Extended Surfactants. *J. Surfactants Deterg.* **2009**, *12* (3), 209–217.

(105) Kékicheff, P. Phase Diagram of Sodium Dodecyl Sulfate-Water System. 2. Complementary Isoplethal and Isothermal Phase Studies. *J. Colloid Interface Sci.* **1989**, *131* (1), 133–152.

(106) Tanford, C. *The Hydrophobic Effect: Formation of Micelles and Biological Membranes*, 2nd ed.; J. Wiley., 1980.

(107) Kuperkar, K.; Abezgauz, L.; Prasad, K.; Bahadur, P. Formation and Growth of Micelles in Dilute Aqueous CTAB Solutions in the Presence of NaNO3 and NaClO3. *J. Surfactants Deterg.* **2010**, *13* (3), 293–303.

(108) Joshi, J. V.; Aswal, V. K.; Goyal, P. S. Combined SANS and SAXS Studies on Alkali Metal Dodecyl Sulphate Micelles. *J. Phys. Condens. Matter* **2007**, *19* (19), 196219.

(109) Shanks, P. C.; Franses, E. I. Estimation of Micellization Parameters of Aqueous Sodium Dodecyl Sulfate from Conductivity Data. *J. Phys. Chem.* **1992**, *96* (4), 1794–1805.

(110) Weingärtner, H. An Introduction to Aqueous Electrolyte Solutions. *ChemPhysChem* **2008**, *9* (10), 1482–1482.

(111) Millero, F. J. The Partial Molal Volume of Ions in Various Solvents. *J. Phys. Chem.* **1969**, *73* (7), 2417–2420.

(112) Haynes, W. M. CRC Handbook of Chemistry and Physics. Taylor & Francis 2016.

(113) Zemb, T.; Charpin, P. Micellar Structure from Comparison of X-Ray and Neutron Small-Angle Scattering. *J. Phys.* **1985**, *46* (2), 249–256.

(114) Goyal, P. S.; Aswal, V. K. Combined SANS and SAXS in Studies of Nanoparticles with Core-Shell Structure. *Indian J. Pure Appl. Phys.* **2006**, *44* (10), 724–728.

(115) Aswal, V. K.; Goyal, P. S.; De, S.; Bhattacharya, S.; Amenitsch, H.; Bernstorff, S. Small-Angle X-Ray Scattering from Micellar Solutions of Gemini Surfactants. *Chem. Phys. Lett.* **2000**, *329* (5), 336–340.

(116) Lipfert, J.; Columbus, L.; Chu, V. B.; Lesley, S. A.; Doniach, S. Size and Shape of Detergent Micelles Determined by Small-Angle X-Ray Scattering. *J. Phys. Chem. B* **2007**, *111* (43), 12427–12438.

(117) Oliver, R. C.; Lipfert, J.; Fox, D. A.; Lo, R. H.; Doniach, S.; Columbus, L. Dependence of Micelle Size and Shape on Detergent Alkyl Chain Length and Head Group. *PLoS One* **2013**, *8* (5), e62488.

(118) Kulkarni, C. V.; Wachter, W.; Iglesias-Salto, G.; Engelskirchen, S.; Ahualli, S. Monoolein: A Magic Lipid? *Phys. Chem. Chem. Phys.* **2011**, *13* (8), 3004–3021.

(119) Qiu, H.; Caffrey, M. The Phase Diagram of the Monoolein/Water System: Metastability and Equilibrium Aspects. *Biomaterials* **2000**, *21* (3), 223–234.

(120) Boldon, L.; Laliberte, F.; Liu, L. Review of the Fundamental Theories behind Small Angle X-Ray Scattering, Molecular Dynamics Simulations, and Relevant Integrated Application. *Nano Rev.* **2015**, *6* (1), 25661.

(121) Us'yarov, O. G. Small-Angle X-Ray Scattering in Sodium Dodecyl Sulfate Solutions and Micelle Clustering. *Colloid J.* **2016**, *78* (5), 698–704.

(122) Hyde, S. T. Microstructure of Bicontinuous Surfactant Aggregates. *J. Phys. Chem.* **1989**, *93* (4), 1458–1464.

(123) Kang, K. C.; Linga, P.; Park, K. nam; Choi, S. J.; Lee, J. D. Seawater Desalination by Gas Hydrate Process and Removal Characteristics of Dissolved Ions (Na+, K+, Mg2+, Ca2+, B3+, Cl-, SO42-). *Desalination* **2014**, *353*, 84–90.

(124) Marcus, Y. Ionic Radii in Aqueous Solutions. *Chem. Rev.* **1988**, *88* (8), 1475–1498.

(125) Pathak, A. K. Conductance and Bulk Vertical Detachment Energy of Hydrated Sulphate and Oxalate Dianions: A Theoretical Study. *Mol. Phys.* **2014**, *112* (11), 1548–1552.

(126) Mueller, S.; Llewellin, E. W.; Mader, H. M. The Rheology of Suspensions of Solid Particles. *Proc. R. Soc. London A Math. Phys. Eng. Sci.* **2010**, *466* (2116), 1201–1228.

(127) Montalvo, G.; Valiente, M.; Rodenas, E. Rheological Properties of the L Phase and the Hexagonal, Lamellar, and Cubic Liquid Crystals of the CTAB/Benzyl Alcohol/Water System. *Langmuir* **1996**, *12* (21), 5202–5208.

(128) Dhinojwala, A.; Granick, S. Relaxation Time of Confined Aqueous Films under Shear. *J. Am. Chem. Soc.* **1997**, *119* (1), 241–242.

(129) Wu, Y.; Shuler, P.; Blanco, M.; Tang, Y.; Goddard III, W. A. A Study of Branched Alcohol Propoxylate Sulfate Surfactants for Improved Oil Recovery; Society of Petroleum Engineers, 2005.

(130) Puerto, M. C.; Hirasaki, G. J.; Miller, C. A.; Barnes, J. R. Surfactant Systems for EOR in High- Temperature , High-Salinity Environments. *Soc. Pet. Eng. J.* **2012**, 11–19.

(131) Puerto, M. C.; Hirasaki, G. J.; Miller, C. A.; Reznik, C.; Dubey, S.; Barnes, J. R. Effects of Hardness and Cosurfactant on Phase Behavior of Alcohol-Free Alkyl Propoxylated Sulfate Systems. *SPE Improv. Oil Recover. Symp.* **2014**, No. April 2014, 1–23.

(132) Huh, C. Interfacial Tensions and Solubilizing Ability of a Microemulsion Phase That Coexists with Oil and Brine. *J. Colloid Interface Sci.* **1979**, *71* (2), 408–426.

(133) Franses, E. I. *Thermodynamics with Chemical Engineering Applications*; Cambridge University Press, 2014.

(134) Tucker, E. E.; Christian, S. D. Solubilization of Benzene by Aqueous Sodium Octylsulfate: Effect of Added Sodium Chloride. *J. Colloid Interface Sci.* **1985**, *104* (2), 562–568.

(135) Bai, G.; Brusseau, M. L.; Miller, R. M. Influence of Cation Type, Ionic Strength, and PH on Solubilization and Mobilization of Residual Hydrocarbon by a Biosurfactant. *J. Contam. Hydrol.* **1998**, *30* (3–4), 265–279.

(136) Yutkin, M. P.; Lee, J. Y.; Mishra, H.; Radke, C. J.; Patzek, T. W. Bulk and Surface Aqueous Speciation of Calcite: Implications for Low-Salinity Waterflooding of Carbonate Reservoirs. *Soc. Pet. Eng. J.* **2018**, *23* (01), 84–101.

(137) Reid, V. W.; Longman, G. F.; Heinerth, E. Determination of Anionic-Active Detergents by Two-Phase Titration. *Tenside* **1967**, 292–304.

(138) Li, Z.; Rosen, M. J. Two-Phase Mixed Indicator Method for the Determination of Zwitterionic Surfactants. *Anal. Chem.* **1981**, *53* (9), 1516–1519.

(139) Energy Information Administration. *Assumptions to Annual Energy Outlook 2020: Oil and Gas Supply Module*; 2020.

(140) Healy, R. N.; Reed, R. L. Physsicochemical Aspects of Microemulsion Flooding. *Soc. Pet. Eng. J.* **1974**, *257*, 491–501.

(141) Anderson, D. R.; Bidner, M. S.; Davis, H. T.; Manning, C. D.; Scriven, L. E. Interfacial Tension and Phase Behavior in Surfactant-Brine-Oil Systems. In *Society of Petroleum Engineers of AIME*; Tulsa, Oklahoma, 1976; pp 189–200.

(142) Salager, J. L.; Morgan, J. C.; Schechter, R. S.; Wade, W. H.; Vasquez, E. Optimum Formulation of Surfactant/Water/Oil Systems for Minimum Interfacial Tension or Phase Behavior. *Soc. Pet. Eng. J.* **1979**, 107–115.

(143) Guo, H.; Li, Y.; Kong, D.; Ma, R.; Li, B.; Wang, F. Lessons Learned From Alkali/Surfactant/Polymer-Flooding Field Tests in China. *SPE Reserv. Eval. Eng.* **2019**, *22* (01), 78–99.

(144) Somasundaran, P.; Hanna, H. S. Adsorption of Sulfonates on Reservoir Rocks. *Soc. Pet. Eng. J.* **1979**, *19* (04), 221–232.

(145) Kwok, W.; Nasr-El-Din, H. A.; Hayes, R. E.; Sethi, D. Static and Dynamic Adsorption of a Non-Ionic Surfactant on Berea Sandstone. *Colloids Surfaces A Physicochem. Eng. Asp.* **1993**, *78*, 193–209.

(146) Paria, S.; Khilar, K. C. A Review on Experimental Studies of Surfactant Adsorption at the Hydrophilic Solid–Water Interface. *Adv. Colloid Interface Sci.* **2004**, *110* (3), 75–95.

(147) Curbelo, F. D. S.; Santanna, V. C.; Neto, E. L. B.; Dutra, T. V.; Dantas, T. N. C.; Neto, A. A. D.; Garnica, A. I. C. Adsorption of Nonionic Surfactants in Sandstones. *Colloids Surfaces A Physicochem. Eng. Asp.* **2007**, *293* (1), 1–4.

(148) Lv, W.; Bazin, B.; Ma, D.; Liu, Q.; Han, D.; Wu, K. Static and Dynamic Adsorption of Anionic and Amphoteric Surfactants with and without the Presence of Alkali. *J. Pet. Sci. Eng.* **2011**, *77* (2), 209–218.

(149) Bera, A.; Kumar, T.; Ojha, K.; Mandal, A. Adsorption of Surfactants on Sand Surface in Enhanced Oil Recovery: Isotherms, Kinetics and Thermodynamic Studies. *Appl. Surf. Sci.* **2013**, *284*, 87–99.

(150) Azam, M. R.; Tan, I. M.; Ismail, L.; Mushtaq, M.; Nadeem, M.; Sagir, M. Static Adsorption of Anionic Surfactant onto Crushed Berea Sandstone. *J. Pet. Explor. Prod. Technol.* **2013**, *3* (3), 195–201.

(151) ShamsiJazeyi, H.; Verduzco, R.; Hirasaki, G. J. Reducing Adsorption of Anionic Surfactant for Enhanced Oil Recovery: Part I. Competitive Adsorption Mechanism. *Colloids Surfaces A Physicochem. Eng. Asp.* **2014**, *453* (1), 162–167.

(152) Saxena, N.; Kumar, A.; Mandal, A. Adsorption Analysis of Natural Anionic Surfactant for Enhanced Oil Recovery: The Role of Mineralogy, Salinity, Alkalinity and Nanoparticles. *J. Pet. Sci. Eng.* **2019**, *173*, 1264–1283.

(153) Winsor, P. A. Binary and Multicomponent Solutions of Amphiphilic Compounds. Solubilization and the Formation, Structure, and Theoretical Significance of Liquid Crystalline Solutions. *Chem. Rev.* **1968**, *68* (1), 1–40.

(154) Wade, W. H.; Morgan, J. C.; Schechter, R. S.; Jacobson, J. K.; Salager, J. L. Interfacial Tension and Phase Behavior of Surfactant Systems. *Soc. Pet. Eng. J.* **1978**, *18* (4), 242–252.

(155) Dean, R. M. Selection and Evaluation of Surfactants for Field Pilots, University of Texas at Austin, 2011.

(156) Sharma, A.; Azizi-Yarand, A.; Clayton, B.; Baker, G.; Mckinney, P.; Britton, C.; Delshad, M.; Pope, G. The Design and Execution of an Alkaline/Surfactant/Polymer Pilot Test. *SPE Reserv. Eval. Eng.* **2013**, *16* (04), 423–431.

(157) Novosad, J.; Maini, B.; Batycky, J. A Study of Surfactant Flooding at High Salinity and Hardness. *J. Am. Oil Chem. Soc.* **1982**, *59* (10), 833A-839A.

(158) Al-Murayri, M. T.; Al-Qattan, A.; Kamal, D. S.; Winoto, W.; Li, Z.; Britton, C.; Delshad, M. A Practical and Economically Feasible Surfactant EOR Strategy: Impact of Injection Water Ions on Surfactant Utilization. *SPE Kuwait Oil & Gas Show and Conference*. Society of Petroleum Engineers: Mishref, Kuwait 2019, p 22.

(159) Solairaj, S. New Method of Predicting Optimum Surfactant Structure for EOR, University of Texas at Austin, 2011.

(160) Scoggins, M. W.; Miller, J. W. Determination of Water-Soluble Polymers Containing Primary Amide Groups Using the Starch-Triiodide Method. *Soc. Pet. Eng. J.* **1979**, *19* (03), 151–154.

(161) Yang, Y.-J.; Kelkar, A. V.; Zhu, X.; Bai, G.; Ng, H. T.; Corti, D. S.; Franses, E. I. Effect of Sodium Dodecylsulfate Monomers and Micelles on the Stability of Aqueous Dispersions of Titanium Dioxide Pigment Nanoparticles against Agglomeration and Sedimentation. *J. Colloid Interface Sci.* **2015**, *450*, 434–445.

(162) Svitova, T. F.; Smirnova, Y. P.; Pisarev, S. A.; Berezina, N. A. Self-Assembly in Double-Tailed Surfactants in Dilute Aqueous Solutions. *Colloids Surfaces A Physicochem. Eng. Asp.* **1995**, *98* (1), 107–115.

(163) Soltero, J. F. A.; Bautista, F.; Pecina, E.; Puig, J. E.; Manero, O.; Proverbio, Z.; Schulz, P. C. Rheological Behavior in the Didodecyldimethylammonium Bromide/Water System. *Colloid Polym. Sci.* **2000**, *278* (1), 37–47.

(164) Biswal, N. R.; Paria, S. Interfacial and Wetting Behavior of Natural–Synthetic Mixed Surfactant Systems. *RSC Adv.* **2014**, *4* (18), 9182–9188.

(165) Grillo, I.; Penfold, J.; Tucker, I.; Cousin, F. Spontaneous Formation of Nanovesicles in Mixtures of Nonionic and Dialkyl Chain Cationic Surfactants Studied by Surface Tension and SANS. *Langmuir* **2009**, *25* (7), 3932–3943.

VITA

Jaeyub Chung

Education

Ph.D., Chemical Engineering *Fall 2020*

Purdue University, West Lafayette, IN, USA

Advisors: Professors Bryan W. Boudouris and Elias I. Franses

Thesis: "Interfacial Tension and Phase Behavior of Oil/Aqueous Systems with Applications to Enhanced Oil Recovery"

Graduate Student, Chemical Engineering *Fall 2010 – Spring 2013*

Georgia Institute of Technology, Atlanta, GA, USA

Advisors: Professors David S. Sholl and Sankar Nair

Research Theme: "Molecular Adsorption and Transport of Alcohols in Metal-organic Frameworks (MOFs) with Applications to Biofuel Purification"

B.S., Chemical and Biological Engineering, cum laude *March 2010*

Seoul National University, Seoul, Republic of Korea

Undergraduate Advisor: Dr. Kyusoon Shin

Research Experience

Graduate Research Assistant *August 2015 – present*

Purdue University, West Lafayette, IN, USA

Graduate Research Assistant *August 2010 – May 2013*

Georgia Institute of Technology, Atlanta, GA, USA

Full-time Researcher Internship *January 2013 – March 2013*

Korea Institute of Science and Technology (KIST), Seoul, Republic of Korea

Undergraduate Researcher *January 2009 – August 2010*

Seoul National University, Seoul, Republic of Korea

Selected Honors and Awards

- Best Poster Presentation Award, GSO Symposium, *Purdue University* *2020*
- Doh Wonsuk Memorial Award, *Korean Institute of Chemical Engineers* *2019*
- Outstanding Poster Presentation Award, Notre Dame-Purdue Symposium on Soft Matter & Polymers and Poster Session, *University of Notre Dame and Purdue University* *2019*
- Best Poster Presentation Award, GSO Symposium, *Purdue University* *2019*
- Outstanding Poster Presentation Award, Notre Dame-Purdue Symposium on Soft Matter & Polymers and Poster Session, *University of Notre Dame and Purdue University* *2018*
- Best Poster Presentation Award, GSO Symposium, *Purdue University* *2018*
- Outstanding Performance on the Oral Qualifying Examination, *Georgia Tech* *2011*
- National Science& Technology Scholarship, *Republic of Korea* *2006-2010*

Grant Writing Experience

2. DOE Office of Fossil Energy. Advanced Technologies for enhanced oil recovery. 5 years, $8.8M 2019 (Bryan W. Boudouris, PI) *Not Funded*

1. Pioneer Oil. 1 year $100,000. Development of Aqueous Surfactant Formulations for Low Temperature Chemical Waterflooding for Various Oil Reservoirs of the Illinois Basin 2018 (Bryan W. Boudouris and Elias I. Franses, co-PI) *Funded*

Affiliations and Leadership

Manager, Soft-material Seminar Series Group at Purdue University *May 2019 – December 2020*

- Organized weekly meetings and seminars for ~50 researchers in five research groups for promoting interdisciplinary research projects and discussions

President, Korean Chemical Engineer Association at Purdue University *May 2017 – August 2018*

- Coordinated students and faculties for organizing events on safety, and community outreach

Mentor, Purdue University

- Michael Steinerd, SURF Program *May 2017 – August 2017*
- Anthony Maquet, Undergraduate Research Program *September 2018 – December 2019*

Teaching Assistant, Purdue University

- Teaching Assistant, Separation Process (CHE 30600) *Fall 2016*
- Teaching Assistant, Design and Analysis of Processing Systems (CHE45000) *Spring 2018*

Volunteer, Hanbit Pediatric Cancer Patient Group, Republic of Korea *May 2003 – August 2010*

- Helped childhood cancer patients and their families to maintain optimistic attitudes and provided mental support by sharing personal experience.

Presentations

1. "Surface Tension Behavior of Aqueous Solutions of a Propoxylated Surfactant and Interfacial Tension Behavior Against an Un-Preequilibrated Crude Oil." **Chung, J.**; Boudouris, B.W.; Franses, E.I. *Notre Dame–Purdue Symposium on Soft Matter & Polymers and Poster Session, West Lafayette, IN, USA*. September 2017. (Poster presentation)

2. "Surface Tension Behavior of Aqueous Solutions of a Propoxylated Surfactant and Interfacial Tension Behavior Against an Un-Preequilibrated Crude Oil." **Chung, J.**; Boudouris, B.W.; Franses, E.I. *AIChE Annual Meeting 2017, Minneapolis, MN, USA*. November 2017.

3. "Interfacial Tension and Phase Behavior of Pre-Equilibrated mixtures of Aqueous Solutions of an Isopropoxylated Surfactant and Crude Oil." **Chung, J.**; Boudouris, B.W.; Franses, E.I. *Purdue University GSO Symposium, West Lafayette, IN, USA*. August 2018.

4. "Interfacial Tension and Phase Behavior of Pre-Equilibrated mixtures of Aqueous Solutions of an Isopropoxylated Surfactant and Crude Oil." **Chung, J.**; Boudouris, B.W.; Franses, E.I. *5th Annual Notre Dame–Purdue Symposium on Soft Matter & Polymers and Poster Session, Notre Dame, IN, USA*. October 2018. (Poster presentation)

5. "Phase and Rheological Behavior of Aqueous Mixtures of an Isopropoxylated Surfactant." **Chung, J.**; Yang, Y.-J.; Tang, H.; Santagata, M.; Franses, E.I.; Boudouris, B.W. *AIChE Annual Meeting 2018, Pittsburgh, PA, USA*. November 2018. (Presenter: Elias I. Franses)

6. "Interfacial Tension and Phase Behavior of Pre-Equilibrated mixtures of Aqueous Solutions of an Isopropoxylated Surfactant and Crude Oil." **Chung, J.**; Boudouris, B.W.; Franses, E.I. *AIChE Annual Meeting 2018, Pittsburgh, PA, USA*. November 2018.

7. “Phase Behavior and Interfacial Tension of Pre-Equilibrated Mixtures of Aqueous Solutions of a Commercial Surfactant and Crude Oil.” **Chung, J.**; Boudouris, B.W.; Franses, E.I. 2019 Spring *Purdue Process Safety and Assurance Center(P2SAC) Conferences , West Lafayette, IN, USA*. May 2019. (Poster presentation)

8. “Use of Equilibrium and Dynamic Surface Tension Behavior for Detecting Critical Micelle/Aggregation Concentration For a Double-chain Cationic Surfactant.” **Chung, J.**; Hsieh, A.-H.; Corti, D.S.; Franses, E.I. *93rd ACS Colloid & Surface Science Symposium, Atlanta GA, USA*, June 2019.

9. “A New Surfactant Evaluation Protocol Based on Interfacial Tension, Phase Behavior, and Laboratory-scale Core-flood Tests for Chemical Enhanced Oil Recovery (cEOR) Applications.” **Chung, J.**; Holtsclaw, J.; Everett, T.A.; Henderson, T.; Boudouris, B.W.; Franses, E.I. *AIChE Annual Meeting 2019, Orlando, FL, USA*. November 2019.

10. “Effluent Analyses and Interfacial Tension Measurements for Laboratory-scale Coreflood Oil Recovery Experiments.” **Chung, J.**; Everett, T.A.; Henderson, T.; Holtsclaw, J.; Boudouris, B.W.; Franses, E.I. *AIChE Annual Meeting 2019, Orlando, FL, USA*. November 2019.

11. “Mechanisms of Surfactant Adsorption and Interfacial Tension Lowering for Enhanced Oil Recovery (EOR) Applications.” **Chung, J.**; Boudouris, B.W.; Franses, E.I. *APS March Meeting, Denver, CO, USA*. March 2020.

12. “Relationship of interfacial tensions of oil/water interfaces to oil recovery efficiency.” **Chung, J.**; Boudouris, B.W.; Franses, E.I. *Purdue University GSO Symposium, West Lafayette, IN, USA*. August 2020.

PUBLICATIONS

1. **Chung, J.**; Boudouris, B.W.; Franses, E.I., Surface tension behavior of aqueous solutions of a propoxylated surfactant and interfacial tension behavior against a crude oil. *Colloids and Surfaces A: Physicochemical and Engineering Aspects* **2018**, *537*, 163-172.
2. **Chung, J.**; Yang, Y.-J.; Tang, H.; Santagata, M.; Franses, E.I.; Boudouris, B.W., Phase and rheological behavior of aqueous mixtures of an isopropoxylated surfactant. *Colloids and Surfaces A: Physicochemical and Engineering Aspects* **2018**, *554*, 60-73.
3. **Chung, J.**; Boudouris, B.W.; Franses, E.I., Effects of the Water-Oil Volume Ratio and Premixing or Pre-equilibration on the Interfacial Tension and Phase Behavior of Biphasic Mixtures. *Colloids and Surfaces A: Physicochemical and Engineering Aspects* **2019**, *571*, 55-63.
4. **Chung, J.**; Boudouris, B.W.; Franses, E.I., Accurate Determination of the Equilibrium Surface Tension Values with Area Perturbation Tests. *Journal of Visualized Experiments* **2019**, *150*, e59818.
5. **Chung, J.**; Khot, A.; Savoie, B.M.; Boudouris, B.W., 100th Anniversary of Macromolecular Science Viewpoint: Recent Advances and Opportunities for Mixed Ion and Charge Conducting Polymers. *ACS Macro Letters* **2020**, *9*, 646-655.